Swiss Journal of Palaeontology (2026) 145: 213–249 | DOI 10.3897/sjp.145.180388

Research Article

Topical collection: A window into the Pliocene Record of South Caucasus

Systematics and palaeoneurology of a new Pliocene raccoon dog (Canidae, *Nyctereutes*) from Jradzor (Armenia)

Saverio Bartolini-Lucenti[1,2], Marie Meyer[3], Samuele Frosali[1], Joan Madurell-Malapeira[1,4], Wenhui Liu[5], Loïc Costeur[6], Damien Becker[7,8], Davit Vasilyan[7,8]

1 *Dipartimento di Scienze della Terra, Paleo[Fab]Lab, Università degli Studi di Firenze, Via La Pira 4, I-50121 Firenze, Italy*
2 *Institut Català de Paleontologia Miquel Crusafont (ICP-CERCA), Universitat Autònoma de Barcelona, Edifici ICTA-ICP, c/ Columnes s/n, Campus de la UAB, 08193 Cerdanyola del Vallès, Barcelona, Spain*
3 *Ecole Nationale Vétérinaire de Toulouse, 23 Chemin des Capelles, 31076 Toulouse Cedex 03, France*
4 *Department of Geology, Universitat Autònoma de Barcelona, Campus de la UAB, 08193 Cerdanyola del Vallès, Barcelona, Spain*
5 *National Museum of China, 16 East Chang'an Avenue, 100006 Beijing, China*
6 *Naturhistorisches Museum Basel, Augustinergasse 2, 4001 Basel, Switzerland*
7 *JURASSICA Museum, Route de Fontenais 21, 2900 Porrentruy, Switzerland*
8 *Department of Geosciences, University of Fribourg, Chemin du Musée 6, 1700 Fribourg, Switzerland*

https://zoobank.org/D237D907-CAEC-4E44-B999-FE48C2CCD70D

Corresponding author: Saverio Bartolini-Lucenti (saverio.bartolinilucenti@unifi.it)

Academic editor: Olivier Maridet ♦ **Received** 11 September 2025 ♦ **Accepted** 25 November 2025 ♦ **Published** 24 February 2026

Abstract

We describe a new fossil raccoon dog from the Late Pliocene site of Jradzor, Armenia, a key site to understand biogeographic connections and dispersal between Asia, Europe, and Africa. The specimens analysed here for the first time exhibit a mosaic of primitive and derived cranial and dental traits, distinguishing them from known taxa such as *Nyctereutes tingi* (e.g. elongated cranium, reduced subangular lobe), *N. sinensis* (e.g. molar proportions, sulcal pattern), and *N. megamastoides* (e.g. absence of squared M1 morphology). Virtual reconstruction of the endocranium reveals a unique sulcal and gyral pattern, including a parenthesis-shaped *gyrus sigmoideus* and a deeply developed *sulcus pseudosylvius*, placing it morphologically closer to Canini than extant Vulpini. Considering these features, we propose to ascribe it to a new *Nyctereutes* species. Morphometric and geometric morphometric analyses support its taxonomic distinctiveness and suggest ecological and behavioural affinities with jackal-like canids. Notably, the relative development of the rostral portion of the cerebrum implies a social structure more complex than that of extant *Nyctereutes*, suggesting the possibility of seasonal pack formation. Additionally, we reassess several neuroanatomical traits previously considered diagnostic, such as the cerebellar vermis and *sulcus endomarginalis*, revealing greater variability within *Nyctereutes* and challenging previous phylogenetic assumptions. These findings underscore the Pliocene diversification of the genus and highlight the Caucasus as a pivotal region in canid evolution. The erection of a new *Nyctereutes* species enriches our understanding of canid paleobiology and provides new perspectives on the evolutionary trajectories of hypocarnivorous canids.

Keywords

Canid evolution, Caucasus paleobiogeography, endocast morphology, Late Pliocene, virtual paleoneurology

Introduction

The living raccoon dogs and their phylogenetic affinities

Today, raccoon dogs are classified under the genus *Nyctereutes* Temminck, 1838, which is usually considered monospecific. *Nyctereutes procyonoides* (Gray, 1834) is a small canid characterised by short legs and tail compared to its body length and by its fur pattern, especially the facial mask, which bears resemblance to that of the true raccoon (genus *Procyon* Storr, 1780). According to their geographic distribution, raccoon dogs have been divided into six subspecies (Ward and Wurster-Hill 1990). In recent years, much evidence (chromosomal, molecular, and morphological) has revealed the peculiarity of the Japanese populations of raccoon dogs compared to the continental populations (Ward et al. 1987; Wada and Imai 1991; Wada et al. 1991; Kim et al. 2013). Consequently, some authors (Kim et al. 2015) have even proposed the inclusion of the population from Japan in a separate species, *Nyctereutes viverrinus* Temminck, 1838 (further divided into the nominal subspecies *N. v. viverrinus* from the islands of Honshu, Kyushu and Shikoku and *N. v. albus* from Hokkaido). Moving up from the subspecific level, the confusion and debate on the taxonomy and the relationship of the genus *Nyctereutes* with other canids remains open. Berta (1988), who performed one of the first cladistic analyses on living and fossil species of Canidae, found that *Nyctereutes* groups with the South American canids *Cerdocyon* Hamilton Smith, 1839, *Atelocynus* Cabrera, 1940, and *Speothos* Lund, 1839. Similar results were reported by Tedford et al. (1995), in which *Speothos* and *Atelocyon* cluster together as a sister group of the clade that includes *Cerdocyon* and *Nyctereutes*. Berta (1988) and Tedford et al. (1995) considered that the strong affinity of the latter two genera lay in features such as the presence of a developed subangular lobe in the mandible (a shared character with *Speothos*, *Urocyon* and *Otocyon* Müller, 1836), the expansion of the angular process (as in other South American taxa), the development of the scars of the *m. pterygoideus medialis* on the lingual side of the angular process (as in *Atelocynus* and *Speothos*), and the low-crowned canines (comparable to those of *Urocyon* and *Otocyon*). Tedford et al. (2009) erected the subtribe Cerdocyonina within the tribe Canini, including all the South American canids and the Eurasian raccoon dog. Molecular phylogenetic studies (Wayne et al. 1997; Bardeleben et al. 2005; Lindblad-Toh et al. 2005; Wayne and Ostrander 2007; Chen and Zhang 2012; Zhao et al. 2016; Zrzavý et al. 2018) have revealed a different pattern of affinities: *Nyctereutes* separates from the monophyletic clade of South American canids and roots at the base or within the group of foxes, close to the bat-eared fox, *Otocyon* (Lindblad-Toh et al. 2005). The position of *Nyctereutes* near the base of the tribe Vulpini implies that these morphologies retained by both the former and *Cerdocyon* (as well as other taxa) simply constitute convergent adaptations. Homoplasies may represent a source of confusion that can blur the actual affinities between species (inter alios Hennig 1966; Wiley et al. 1991; Poe and Wiens 2000; Simões et al. 2017), as revealed by previously cited molecular data.

The extant raccoon dog is an opportunistic feeder with cranial and dental adaptations for processing a highly varied diet (Ward and Wurster-Hill 1990). Its main adaptations lie in numerous cranial and dentognathic features that improve efficiency in the chewing process while feeding (Gaspard 1964; Penrose et al. 2016, 2020).

Palaeontological record of raccoon dogs in Eurasia and Africa

Despite the reduced specific diversity, at least ten different species were previously described (Bates 1937; Soria and Aguirre 1976; Ficcarelli et al. 1984; Tedford and Qiu 1991; Geraads et al. 2010; Werdelin and Dehghani 2011; Bartolini-Lucenti et al. 2018; Savvidou and Kostopoulos 2025). Among the attributed records of *Nyctereutes*, the oldest occurrence appears to be in Morocco, at the site of Lissasfa (Casablanca) (Fig. 1). Geraads (2011) described a small maxillary fragment with a partially preserved P4 and M1, with an estimated age of 6.0–5.5 Ma. The author discussed the resemblance with younger *Nyctereutes*, noting nonetheless some peculiarities, e.g. a small-sized P4 protocone or an enlarged P3 alveolus (Geraads 2011). Besides this uncertain record, the earliest widely accepted record is that of the early Early Pliocene *Nyctereutes tingi* Tedford & Qiu, 1991, from localities of the Yushe Basin (Shanxi, China) and the Zanda Basin (Tibet, China) (Wang et al. 2013) (Fig. 1). Li et al. (2003) reported the existence of another early *Nyctereutes* from the deposits of the Gaotege local fauna (Nei Mongol, Mongolia), roughly coeval with the record of *N. tingi* from China (early Gaozhuangian, Qiu et al. 2013). This taxon may represent a new undescribed species (Li et al. 2003). Younger deposits of the Yushe Basin yielded another species of fossil raccoon dog, *Nyctereutes sinensis* (Schlosser, 1903). Compared to the older *N. tingi*, this taxon possesses peculiar features (e.g. prominent subangular lobe and a larger angular process), more similar to the extant *N. procyonoides*. On the other side of Eurasia, the oldest form described in Western Europe is *Nyctereutes donnezani* (Depéret, 1890). It was first discovered in the late Pliocene of Perpignan (France; ca. 4.0 Ma) and then reported from older localities such as La Gloria-4 (Spain; Alcalá 1994) (Fig. 1). The latter site is referred to the Early Pliocene, MN14 (around 4.2 Ma) (Domingo et al. 2013), more or less coeval with the occurrence of *N. sinensis*. Other records of the species reported in the literature are Layna (Spain, MN15, Soria and Aguirre 1976) and Çalta-1 (Turkey, MN15, Ginsburg 1998), both 4 Myr-old localities, and Węże 1 (Poland, MN15, Ivanoff et al. 2014). *Nyctereutes donnezani* has been regarded as the Western European "equivalent" of earlier *N. tingi* for its consistent morphological affinity in

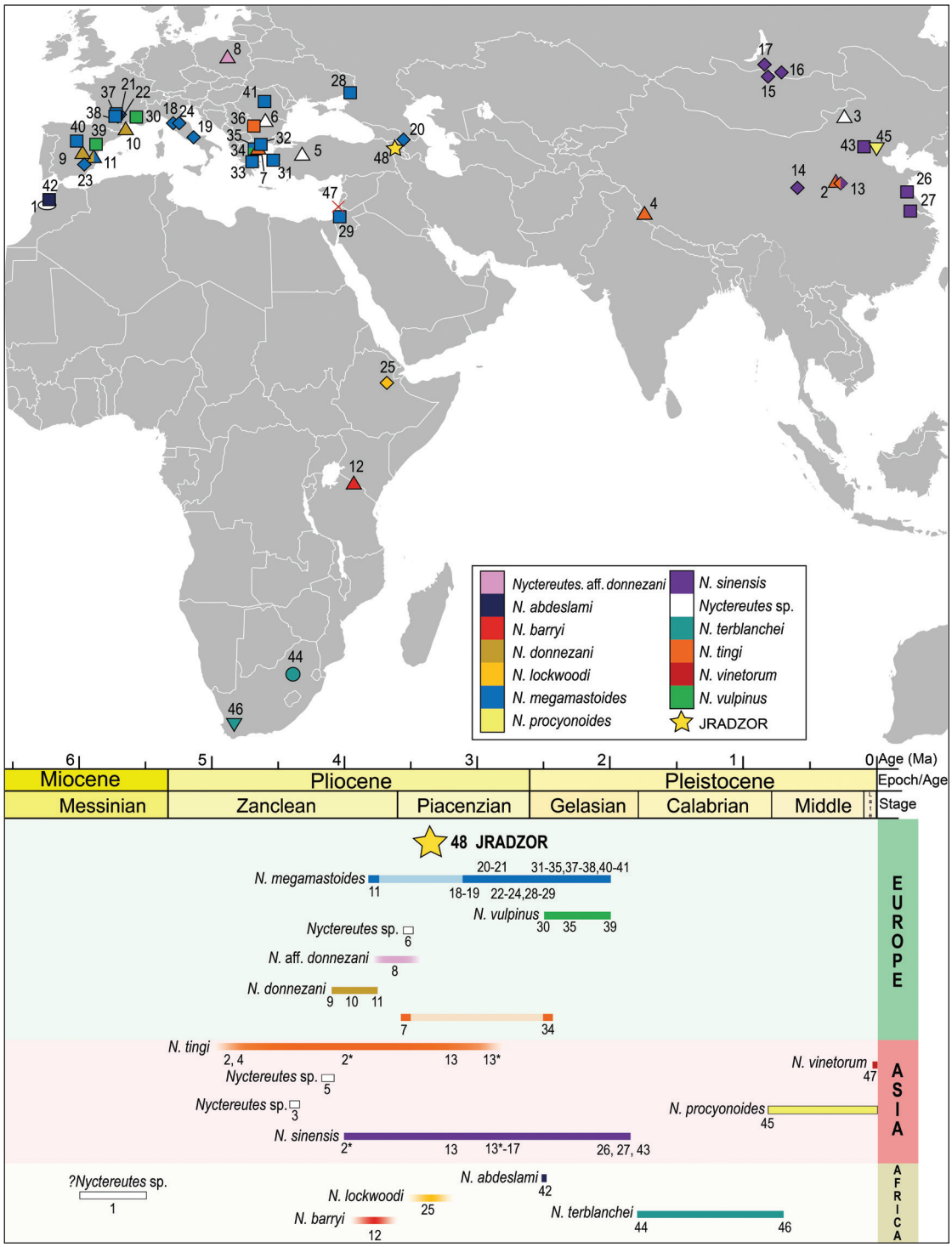

Figure 1. Map and stratigraphic occurrences of fossil *Nyctereutes* from Eurasia and Africa. Legends – Tortonian localities (+): 1, Lissasfa (Morocco); Zanclean localities (triangle): 2, Guaigou, Nanzhuanggou, Baihaicun (2*), Yushe Basin (China); 3, Gaotege, Nei Mogol (China); 4, Zanda Basin, Tibet (China); 5, Çalta-1 (Turkey); 6, Musselievo (Bulgaria); 7, Megalo Emvolon (Greece); 8, Węże 1 (Poland); 9, La Gloria 4 (Spain); 10, Perpignan (France); 11, Layna (Spain); 12, Laetoli, Upper beds (Tanzania); Piacenzian (diamond): 13, Zhangwagou and Liujiagou (13*), Yushe Basin (China); 14, Renjiapo (China); 15, Shamar (Mongolia); 16, Beregovaya, Transbaikalia (Russia); 17, Udunga, Transbaikalia (Russia); 18, S. Giusto (Italy); 19, Collepardo (Italy); 20, Kvabebi (Georgia); 21, Perrier-Les Etouaires (France); 22, Pardines (France); 23, El Rincón-1 (Spain); 24, Montopoli (Italy); 25, Dikika (Ethiopia); Gelasian localities (square): 26, Tuozidong (China); 27, Renzidong (China); 28, Volovaya Balka (Russia); 29, Bethlehem (Palestine); 30, St. Vallier (France); 31, Vatera (Greece); 32, Volax (Greece); 33, Sesklon (Greece); 34, Dafnero-1 (Greece); 35, Dafnero-3; 36, Varshets (Bulgaria); 37, Chihlac (France); 38, Senéze (France); 39, La Puebla de Valverde (Spain); 40, Villarroya (Spain); 41, Grăunceanu (Romania); 42, Ahl al Oughlam (Morocco); 43, Nihewan Basin (China); Calabrian localities (circle): 44, Kromdraai A (South Africa); Middle Pleistocene localities (inverted triangles): 44, Zhoukoudian Locality 1 (China); 46, Elandsfontein (South Africa); Late Pleistocene locality (x): 47, Tabun Cave, Level C (State of Palestine). Studied site (star): 48, Jrazor (Armenia).

comparison to *N. sinensis* or the extant *N. procyonoides* (Tedford and Qiu 1991). Spassov (2000) reported an unidentified and unstudied *Nyctereutes* sp. from the MN15 locality of Musselievo (Bulgaria). Fig. 1 shows that the fossil distribution of *Nyctereutes* was not limited to Eurasia, as *Nyctereutes* spp. were also recovered from several regions of Africa (see inter alios Geraads et al. 2010; Werdelin and Dehghani 2011). The earliest of these African findings is the dubious *?Nyctereutes barryi* Werdelin & Dehghani, 2011, from the Upper Laetoli Bed (Tanzania, 3.75 Ma, Harrison 2011). This taxon possesses several features resembling *N. tingi*, as noted by Werdelin and Dehghani (2011), deeming the taxon an intermediate form between *N. tingi* and *N. donnezani*. Several dentognathic features possessed by *N. procyonoides* are diagnostic for the genus, and at least part of them were acquired by the ancestors of extant raccoon dogs as a result of progressive adaptations towards a hypocarnivorous diet (less than 30% meat). Among these characteristics are the reduction of the slicing portions of the carnassials (P4/m1) and enlargement of the crushing surface of the molars, the developed subangular lobe of the mandible corpus, and the expansion of the angular process with the consequent development of the insertion areas of the *m. pterygoideus medialis* on the medial side of this process. Soria and Aguirre (1976) were among the first to study critically fossil raccoon dogs, considering their complete record, taking into account interspecific and intraspecific variability and the principal features of the fossil and extant species of the genus. They acknowledged the peculiarity of *N. procyonoides* and identified in certain mandibular and dental characters (i.e. depth of the mandible corpus, morphology of the angular region, inclination of the ascending ramus, premolar, and molar morphology) the key features for the evolutionary differentiation of the raccoon dog. Specifically, Soria and Aguirre (1976) outlined the first pattern of morphological affinity and relation among the species of *Nyctereutes*. This was achieved through the recognition of "primitive" taxa (with e.g. poorly developed subangular lobe and elongated and buccolingually narrow premolars) and "derived" taxa (in which e.g. there is marked development of the subangular lobe and stouter premolars) that resemble the extant *N. procyonoides* (Soria and Aguirre 1976). Since this pivotal work, in the scientific literature on *Nyctereutes*, this terminology has been used by several scholars to discuss the morphological features defining a fossil raccoon dog (Ficcarelli et al. 1984; Tedford and Qiu 1991; Argant 2004; Monguillon et al. 2004), with no explicit reference to phylogenetic relationship. Therefore, the terminology used while introducing the several taxa expresses only the degree of development of morphological features without implying evolutionary inference. In these terms, *N. tingi*, *N. donnezani* and *N. barryi* can be considered primitive taxa because of the absence or incipient development of these characters (as noted by Soria and Aguirre 1976; Tedford and Qiu 1991; Werdelin and Dehghani 2011), whereas *N. sinensis* is rather a derived form, resembling the morphologies of the living raccoon dogs (*N. procyonoides* and *N. viverrinus*).

The first pulse of diversity of raccoon dogs around ca. 4 Ma was characterised by the coexistence of primitive and derived species in eastern Asia (*N. tingi* and *N. sinensis*), the westward dispersal of primitive taxa as apparently testified to by the record of *N. tingi* in the Zanda Basin (Tibet, Wang et al. 2013) and Megalo Emvolon (Greece, Koufos 1997), of *N. donnezani* from Europe (Depéret 1890; Soria and Aguirre 1976; Ginsburg 1998), and of *N. barryi* from Tanzania (Fig. 1). If confirmed, the unusual MN17 occurrence of *N.* cf. *tingi* in Varshets (Bulgaria, Spassov 2000) might testify to the long persistence of primitive Asian forms in the European fossil record (Tamvakis et al. 2023). In the Late Pliocene (Mazegouan land mammal age of China), *N. sinensis* thrived in eastern Asia, persisting in the Yushe Basin with some of the latest undoubted occurrences of *N. tingi* (e.g. Liujiagou locality; Tedford and Qiu 1991) and spreading northward to Mongolia and Transbaikalia (Sotnikova 2004). The last records of *N. sinensis* are those of the Early Pleistocene (middle Nihewanian land mammal age of China) of Renzidong (Jin and Liu 2009), Tuozidong (Dong et al. 2013), the Nihewan Basin (Liu 2019; Liu et al. 2021), and Chutuoluan (Dong et al. 2017). A second burst of palaeodiversity can be considered between 3.5 and 2 Ma, when several forms appeared in both African and European fossil records. Several sites of western Eurasia recorded the presence of the derived species *Nyctereutes megamastoides* (Pomel, 1842), one of the most renowned fossil species of this genus. This late Pliocene–Early Pleistocene species had large distribution ranges spanning from Spain to Georgia. These localities include (Fig. 1): Chilhac, Perrier-Les Etouaires, Pardines and Senèze (France; Argant 2004, 2024; Monguillon et al. 2004); Kvabebi (Georgia; Vekua 1972; Rook et al. 2017); Dafnero-1, Sesklon, Volaks and Vatera-F (Greece; Koufos 2014); Montopoli and Collepardo (Italy; Del Campana 1917; Gliozzi et al. 1997; Bartolini-Lucenti 2017); Bethlehem (Palestine; Horowitz 1979); Volovaya Balka (Russia; Sotnikova et al. 2002); El Rincón-1 and Villarroya (Spain; De Villalta-Comella 1952; Alberdi et al. 1997). Many authors supported the idea that this taxon originated from *N. donnezani* (Soria and Aguirre 1976; Argant 2004; Monguillon et al. 2004). Nevertheless, the retention of strongly derived dental and cranio-mandibular features in *N. megamastoides* led some scholars to suggest a close relationship between *N. megamastoides* and *N. sinensis* (among the first, Soria and Aguirre 1976), although some morphological differences remain. The sample from St. Vallier (France), historically attributed to *N. megamastoides* (Viret 1954; Martin 1971) was classified as a separate taxon. The sample from St. Vallier (France), historically attributed to *N. megamastoides* (Viret 1954; Martin 1971) was later classified as a separate taxon (Monguillon et al. 2004). The first to acknowledge the difference between the Saint-Vallier *Nyctereutes* and the "*N. megamastoides*–forme typique" were Soria and

Aguirre (1976), who identified the presence of features resembling the genus *Vulpes* (e.g. elongation of the premolars and of both carnassials, mesiodistal shortening of the M2). The authors proposed the attribution to the subspecies *Nyctereutes megamastoides vulpinus* Soria & Aguirre, 1976. Monguillon et al. (2004) eventually upranked the taxon as a separate species. In this work, this interpretation is followed. Apart from St. Vallier, this taxon occurs in La Puebla de Valverde (Spain, Kurtén and Crusafont-Pairó 1977). Recently, Tamvakis et al. (2023) reported the presence of *N. tingi* in Dafnero-3 (Greece). The morphologies of the cranial and dentognathic specimens are more similar to those of the coeval *N. vulpinus* (e.g. reduced rostrocaudal elongation of the cranium, the evident and developed subangular lobe, smaller size, and reduced lingual cuspulids and talonids) than to the Chinese taxon. These doubts were solved by Savvidou and Kostopoulos (2025), who reassigned the specimens attributed to *N. tingi* from Dafnero-3 in Tamvakis et al. (2023) to *N. vulpinus*. The Varshets material apparently remains ascribed to *N. tingi* (see Savvidou and Kostopoulos 2025).

Apart from the controversial taxon *?N. barryi*, the African record of *Nyctereutes* is relatively scanty but diverse. Younger, although still early Pliocene in age (3.35 Ma, Geraads et al. 2010), the primitive *Nyctereutes lockwoodi* Geraads et al., 2010 from Dikika (Ethiopia) shows several peculiar and unusual morphologies that justify its separation as a distinct species (Fig. 1). Other findings in Africa are the Early Pleistocene species *Nyctereutes abdeslami* Geraads, 1997, from Morocco and the South African *Nyctereutes terblanchei* (Broom in Broom and Schepers 1946) (Fig. 1). The former, described from the site of Ahl al Oughlam in Morocco (2.5 Ma), possesses several derived dentognathic features that resemble those of *N. sinensis*, *N. vulpinus* and particularly *N. megamastoides*. Argant (2004) acknowledged these similarities and suggested a possible affinity between Eurasian species and the North African taxon. *Nyctereutes terblanchei* from Kromdraai A and Elandfontein in South Africa was reviewed by Ficcarelli et al. (1984), who recognised mandibular and dental features in this species similar to those of *N. megamastoides* and *N. sinensis*. Geraads et al. (2010) suggested the possibility of a close relationship (possibly ancestor–descendant) between *N. lockwoodi* and *N. terblanchei*. Reynolds (2012) questioned the generic attribution of this species, though the peculiar features of the type specimen (KA 1290, see Werdelin and Peigné 2010) cannot be mistaken for those of modern jackals (e.g. the subangular lobe, the deep angular process, and the vertical ramus of the mandible).

After 2 Ma and during the last part of the Early Pleistocene, the findings of *Nyctereutes* across the Old World became increasingly scarce, and the diversity of the genus declined. The first record of the extant *N. procyonoides* was considered that of the Middle Pleistocene of Zhoukoudian Locality 1 (Pei 1934; Tedford and Qiu 1991). Nevertheless, the Middle Pleistocene occurrences of *Nyctereutes* in China were recently reassigned to a new taxon, *Nyctereutes peii* Jiang et al., 2024 (Fig. 1). In their work, Jiang et al. (2024) suggested the erection of this new taxon on the basis of morphological, dimensional and ecological features. They also proposed it could be the basal taxon in common between extant *N. procyonoides* and *N. viverrinus*. According to the authors, the reliable records of *N. procyonoides* are only those of the Late Pleistocene and Holocene of the Asian mainland (Jiang et al. 2024). Regarding the Japanese taxon, some occurrences date back to the Middle Pleistocene (Matsumoto 1930; Shikama 1949), and according to Jiang et al. (2024), they share features comparable to *N. peii*. Finally, the latest additional fossil species proposed to date is the terminal Pleistocene Palestinian *Nyctereutes vinetorum* (Bates, 1937) (Fig. 1). Nevertheless, this taxon could be a larger form of the extant species (Kurtén 1965).

Canid neurology and palaeoneurology: state of the art

The domestic dog has been used as a model organism in neurological experiments for several decades; one of the earliest localisations of the visual cortex was in the dog, identified using focal lesions. Nowadays, the study of canid neuroanatomy receives more attention (Datta et al. 2012). Previous studies on carnivorans (e.g. Holekamp and Benson-Amram 2017; Michaud et al. 2022) have shown that increases in relative brain sizes are predominantly associated with environmental factors, especially in the context of a cognitive buffer of the brain against environmental instability during foraging. However, a full understanding of the variability (and its causes and effects) of the brain requires a focus not only on the size but also on the organisation of the brain itself (Boch et al. 2024). In different dog breeds, it was noted that regional differences in brain size correlate with their behavioural specialisations (Hecht et al. 2019), while the comparison between domesticated dogs and wild canids shows a difference in gyrification, which is defined as the complexification of the brain surface linked to the development of the brain *gyri* (Grewal et al. 2020). In particular, Grewal et al. (2020) noted a different pattern in the gyrification index (GI) of canids, highlighting a fox-like and a wolf-like pattern: *Vulpes vulpes* (Linnaeus, 1758) showed a low local GI for the frontal, rostral temporoparietal and caudal temporoparietal regions, while the "wolf-like" canids present a similar GI that is higher than one of the fox species. A divergent pattern in the sulcal anatomy of the brain was also highlighted in other studies (Lyras and Van Der Geer 2003; Lyras 2009). In particular, in the *sulci ansatus* and *coronalis* bounding the *sulcus cruciatus*, these differences in the complexity of folding within "fox-like" and "wolf-like" canids parallel differences in social cognition between these broad canid groups (Grewal et al. 2020). The differences in cerebral morphologies can also highlight different phylogenetic

histories and identify taxonomic-specific differences, at least to some extent (Dozo et al. 2023). Specifically, the Caninae are characterised by two different peculiar morphologies of the brain associated with two extant tribes (i.e. Canini and Vulpini): the sulcal pattern of the cortex between the *sulci coronalis* and the shape and relative size of the *gyrus proreus* of the frontal lobe (Lyras and Van Der Geer 2003). The neocortex of the brain can be either smooth (lissencephalic brain) or folded into numerous convolutions called *gyri* (gyrencephalic brain), and in this second case, the different *gyri* are separated by spaces called *sulci* (Kelava et al. 2013). The folding of the neocortex is caused by the anatomical constraint in tridimensional expansion and the need for surface expansion (Allman 1990). Given this physiological constraint and the fact that the head of larger mammals cannot scale isometrically with the body mass of the individual due to biomechanical stresses on the vertebrae or other body regions, the neocortex of larger-sized species tends to fold, creating these *gyri* and *sulci* (Kelava et al. 2013). In particular, out of many Carnivora species studied, the brains of Canidae possess the largest number of unique major *sulci* (Boch et al. 2024). Furthermore, the basic sulcal pattern of the cerebrum of members of the subfamily Caninae does not appear to be affected by brain size, since it is the same from the smaller (e.g. *Vulpes zerda* Zimmermann, 1780) to the larger (e.g. *Canis lupus* Linnaeus, 1758) species. The only difference of an allometric nature between these size groups involves a *sulci* on the cerebral cortex of the larger-brained Caninae that tends to be more wavy and marked by secondary *sulci* (Radinsky 1973). Many studies have characterised the different *gyri* and *sulci* of the canid brain (Lyras and Van Der Geer 2003; Boch et al. 2024). In the latter, the neocortex presents a *sulcus pseudosylvianus* on the surface of *gyrus sylvianus* that is surrounded by two other concentric *sulci* (the *ectosylvianus* and *suprasylvianus*) that identify the *gyrus ectosylvianus* (Boch et al. 2024).

Another typical feature of the canid neocortex folding is the *sulcus ectomarginalis* (or *ectolateralis*), which runs between the *sulci marginalis* and *suprasylvianus* and once again shows a curved pattern (Boch et al. 2024). The *sulci ansatus* and *coronalis*, in the frontoparietal region of the brain, define the *gyrus sigmoideus*, which in canids, according to Lyras and Van Der Geer (2003), can retain four different dorsal outlines: pentagonal (the *sulci coronalis* diverge caudally more than rostrally, giving the impression of a pentagonal outline); parenthesis-like outline (the *sulci coronalis* bow out laterally, giving the appearance of an oval outline); heart-shaped outline (the *sulci coronalis* bow out laterally but diverge rostrally more than in the parenthesis-like outline, and narrow considerably caudally); orthogonal outline (the *gyrus sigmoideus* expands more abruptly than in the previous groups, so that the *sulci ansatus* and *coronalis* form a square-to-bracket-shaped pattern, giving the impression of an oblong or square dorsal outline) (Lyras and Van Der Geer 2003; Dermitzakis et al. 2004; Lyras 2009). Rostrally to the *gyrus sigmoideus*, the wolf-like canids also present a peculiar *sulcus* (*sulcus proreus*) that is not evident in the fox-like canids. This character is probably linked to the expansion of the *gyrus proreus* (Boch et al. 2024). The *gyrus proreus* is one of the main differences between the fox and wolf lineages in canids, where the first group has a smaller *gyrus proreus* than the second (Lyras and Van Der Geer 2003). The presence of the *sulcus ectomarginalis* instead defines the existence of a characteristic *gyrus ectomarginalis* observable in all canids (Boch et al. 2024).

In palaeoneurological terms, after the pivotal studies of Radinsky (1973), the most relevant studies on fossil canids are those of Lyras and colleagues (e.g. Lyras and Van Der Geer 2003; Dermitzakis et al. 2004; Lyras 2009). In their works, they recognised the importance of the morphology of the *gyri* and *sulci* for taxonomic purposes, using particularly the pattern of the *sulci ansatus* and *coronalis*. Lyras and Van Der Geer (2003) studied all Caninae and, particularly relevant for the present study, described the morphology of the endocast in *N. procyonoides*, showing a peculiar heart-shaped outline of the *gyrus sigmoideus*, the absence of a developed *sulcus ansatus* and a reduced *gyrus proreus* (Lyras and Van Der Geer 2003). The heart-shaped morphology was also recognised in *Cerdocyon thous* (Lyras and Van Der Geer 2003). It fuelled the interpretation of a possible close relationship between *N. procyonoides* and *Ce. thous* (Lyras and Van Der Geer 2003; Dermitzakis et al. 2004), which is now disregarded on the basis of molecular evidence (as mentioned above). Lyras and Van Der Geer (2003) were the first to describe the endocast morphology of several fossil taxa, among them the fossil raccoon dogs *N. tingi* and *N. sinensis*. They acknowledged the greater gyrification of the fossil raccoon dogs compared to the extant *N. procyonoides*, probably related to size (Lyras and Van Der Geer 2003), the presence of a heart-shaped outline of the *coronal sulcus*, the presence of the *sulcus ansatus*, a long, bilaterally constricted *gyrus proreus* and a developed *gyrus orbitalis*. According to Lyras and Van Der Geer (2003), these morphologies further support the close relationship between *Nyctereutes* and *Cerdocyon* (see also Dermitzakis et al. 2004). Ivanoff et al. (2014) reported the morphologies of two natural endocasts from Węże 1 (Pliocene, Poland), MZ VIII-V-360/1 and MZ VIII-V-355/2, ascribing them to *N. donnezani*. The specimens from this locality have been variably interpreted in the literature, and the most recent interpretations favour the attribution as *N.* aff. *donnezani* (Marciszak et al. 2023), which is followed here. According to Ivanoff et al. (2014), the attribution of the endocasts from Węże 1 to *Nyctereutes* is based on the straight morphology of the *cerebellar vermis* in occipital view, apparently shared by *N. procyonoides* and *N. megamastoides* from Kvabebi (Georgia, described by Gabunia and Mchedlidze 1986), whereas the morphological features of the specimens were deemed consistent with other fossil *Nyctereutes* known in the literature.

The present study aims to (1) describe in detail the cranial, dental, and postcranial morphology of a new raccoon dog from the Late Pliocene site of Jradzor (Armenia); (2) reconstruct its endocranial anatomy through virtual endocast analysis, providing the first palaeoneurological data for a fossil *Nyctereutes* from the Caucasus; and (3) assess its phylogenetic position and ecological implications by integrating morphometric and geometric morphometric approaches. These results are discussed in the broader context of Pliocene canid diversification and the role of the Caucasus as a biogeographic corridor between Asia and Europe.

Materials and methods

In total, the Jradzor section is characterised by nineteen fossiliferous horizons with forty-eight identified vertebrate taxa. The paleoenvironmental reconstructions suggest that the succession was deposited within a short-lived dammed lake (between 4.3 and 3.03 Ma) that was subject to pyroclastic density flows and later evolved into a soil catena (Lazarev et al. 2023).

The studied material of *Nyctereutes* was exclusively found in the fossiliferous layer JZ-7 at 45.3–46.1 m (Lazarev et al. 2023) (Fig. 2). Integration of 40Ar/39Ar dating of the ash layer at the base of the fossiliferous lens provided an age of 3.45 ± 0.18 Ma. Magnetostratigraphic integration allowed a more precise estimate of the age of the fossiliferous horizon at 3.3 ± 0.03 Ma (Lazarev et al. 2023; Table 2). Together with raccoon dog fossils, remains of other carnivorans, hippopotamuses, artiodactyls, hyracoids and additional taxa have been found at the site. The sedimentological analysis of the bed that yielded the JZ-7 fauna suggests a lahar deposition – a rapidly flowing mixture of rock debris and water from a volcano (Smith 1986; Lazarev et al. 2023). Essentially, a catastrophic volcanic mudflow trapped and transported the large-sized mammals.

The *Nyctereutes* remains were found close to each other but not in articulation. The remains JRD–20/03 (skull) and JRD–19/03 (right hemimandible) probably belong to one individual since the occlusal surfaces of the upper and lower tooth rows match perfectly. Two other remains, JRD–21/01 (right portion of the palate with c, p3–m2) and JRD–22/18 (fragment of right hemimandible with p1–p3), being represented by right sides, might belong to one individual as well. However, no match of the preserved occlusal surfaces can be found, and therefore their assignment to one individual cannot be confirmed.

Our study considered the neuroanatomy of the tribe Vulpini, with particular attention to the fossil skull ascribed to the genus *Nyctereutes* from the Jradzor locality in Armenia, which is regarded as an important route for the dispersal of fossil specimens from Asia to Europe (Lazarev et al. 2023). The nomenclature of *sulci* and *gyri* follows that of Boch et al. (2024).

Studied material and data acquisition

The analyses performed in this study were based on a sample consisting of thirty-five specimens of extant canids and the fossil specimens of the genus *Nyctereutes* from the Jradzor locality. The fossils are stored in the collections of the Institute of Geological Sciences (IGS), National Academy of Sciences of the Republic of Armenia, Yerevan, Armenia. As comparative fossil material, we examined the collections of the Geology and Palaeontology section of the Museum of Natural History of Florence, the Georgian National Museum in Tbilisi, the Hungarian Museum of Natural History in Budapest, the Musée des Confluences in Lyon, the Université Claude Bernard 1 de Lyon, the American Museum of Natural History in New York, the Museo Nacional de Ciencias Naturales-CSIC in Madrid and the Musée National d'Histoire Naturelle in Paris. We also reviewed the relevant literature on Plio-Pleistocene raccoon dogs (Czyżewska 1969, 1981; Martin 1971; Soria and Aguirre 1976; Torre 1979; Tedford and Qiu 1991; Monguillon et al. 2004; Ivanoff et al. 2014; Bartolini-Lucenti 2017; Rook et al. 2017; Bartolini-Lucenti et al. 2018; Tamvakis et al. 2023; Jiang et al. 2024; Savvidou and Kostopoulos 2025). The fossil comparative sample includes specimens of *N. donnezani* from Layna, La Gloria 4 and Perpignan; *Nyctereutes* sp. from Çalta-1; *N. megamastoides* from the Lower Valdarno Basin, Kvabebi, Villarroya, Dafnero and Perrier-Les Etouaires; *N. vulpinus* from St. Vallier; *N. sinensis* from the Yushe and Nihewan basins; and *N. tingi* from the Yushe Basin.

To reconstruct the cerebral morphology and the bony labyrinth of the studied specimens, we relied on computed tomography (CT) and microcomputed tomography (μCT) scans of the crania. The number of species and specimens per species (with catalogue numbers) is reported in Suppl. material 1: table S1.

Most extant specimens are stored at the 'La Specola' Zoological Museum of Florence (MZUF), the Giacomo Doria Museum of Genoa (CE), the Borzatti-Lowenstein Collection of the Anthropology and Ethnology Museum of Florence (CBL) and the Natural History Museum Basel (NMB). Other virtual specimens of extant species were downloaded from the online repository MorphoSource and from the paper of Czeibert et al. (2024). The CT and μCT scans used to reconstruct the endocast morphology were obtained from different sources: specimens housed in the MZUF, CE and CBL collections were scanned at the Medical Radiology Centre ("SOS Radiologia") of the San Giovanni di Dio Hospital (Florence, Italy) using a Siemens Somatom Definition AS scanner. *Nyctereutes* sp. nov. JRD–20/03 was scanned at the Biomaterials Science Center of the University of Basel (Basel, Switzerland) using a Phoenix Nanotom (GE). The specimens of *Vulpes chama* (Smith 1833) and two specimens of *Lupulella mesomelas* (Schreber 1775), stored at the Department of Palaeontology at the Ditsong Museum in Pretoria, were kindly provided by Prof. Adams and scanned at the Donald Gordon Medical Centre of the University of Witwatersrand Medical School

(Johannesburg, South Africa) using a Philips Brilliance 180 PZ scanner (Adams et al. 2015). For the samples downloaded from MorphoSource, we report the information included in the metadata and accompanying files of the raw data in Suppl. material 1: table S2. Information for the specimens from Czeibert et al. (2024) can be found therein. The slice stacks obtained from the CT and µCT scans were imported into the software 3D Slicer (ver. 5.6.2, https://www.slicer.org; Fedorov et al. 2012) to perform automatic segmentation and digitally extract the 3D model of the endocasts.

The raw 3D model of each endocast was amended using Autodesk Meshmixer (ver. 3.5.474, Autodesk, https://www.autodesk.com) to improve and regularise the structure of the meshes. This software was also used to measure the morphometric variables of each specimen included in the dataset.

Since it was not possible to reconstruct the olfactory bulbs of the fossil specimen, as they are not preserved, we chose not to consider this region of the brain in the extant species as well. The following variables were measured:

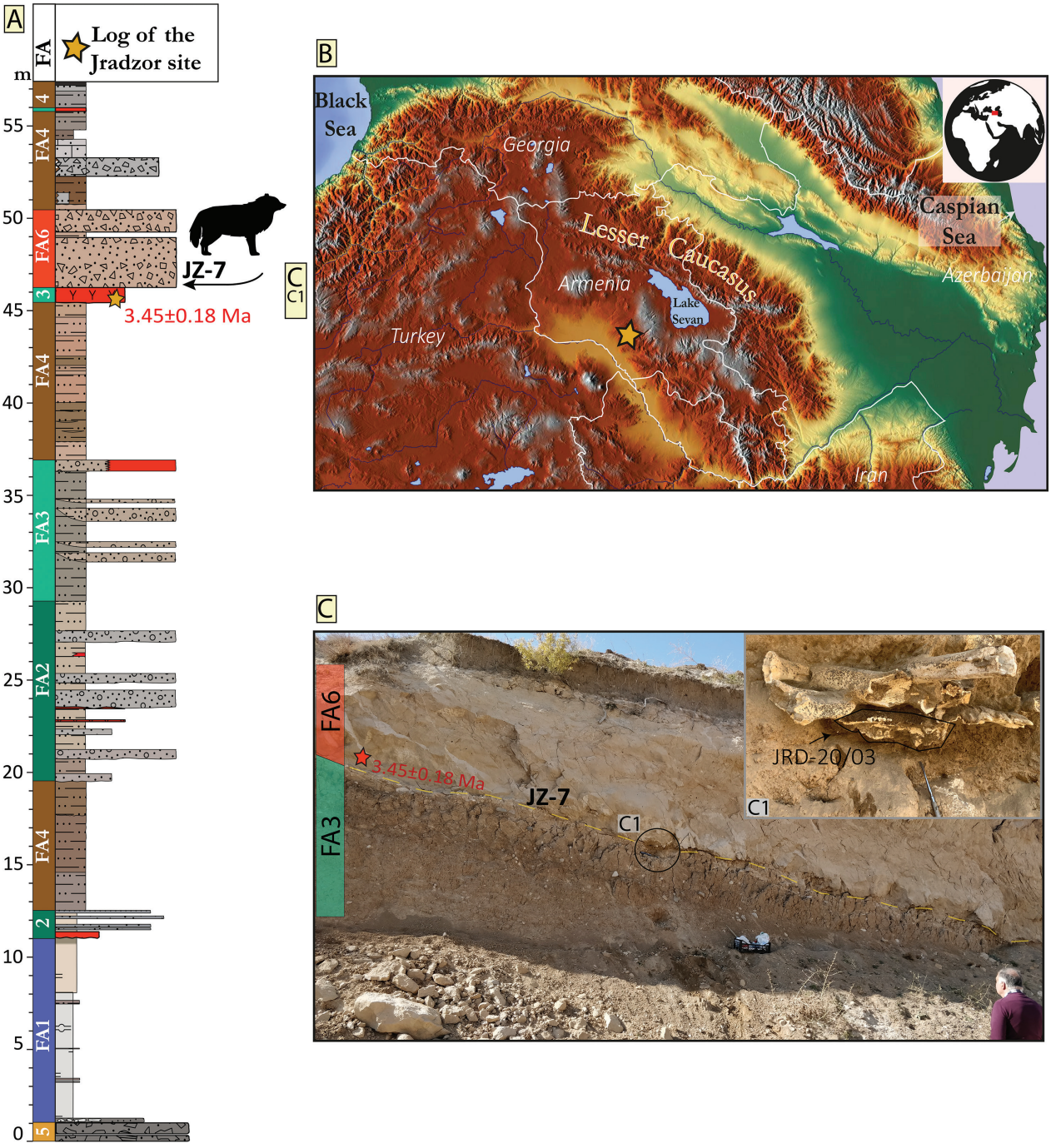

Figure 2. Log of the Jradzor section, with stratigraphic locations of the JZ-7 fossiliferous horizon with *Nyctereutes* finds and ages of the dated ashes (**A**). Geographical position of Jradzor locality (Late Pliocene, Armenia) in topographic map of the South Caucasus (**B**). (**C**) Photograph of the outcrops of JZ-7 fossiliferous horizons and corresponding collection numbers of the selected fossil remains. Figure redrawn from Lazarev et al. (2023), the codes for the facies associations see therein as well.

total length of the cerebrum (BTL, in mm), length of the neocortex (NeoCL, in mm), cerebellum width (CW, in mm), cerebellum maximum width (MaxW, in mm), total volume (TV, in mm³), total surface (TS, in mm²) and occipital condyles width (OCW, in mm). This last measurement was also used to estimate the body mass (BM, in kg) of each specimen according to the formula provided in Engelman (2022). Fig. 3 shows the positions of the obtained linear measurements on each cerebrum. We also measured the ratio between MaxW and NeoCL to evaluate the degree of rostrocaudal elongation of the neocortex. To clarify the relationship between the development of the neocortex and the degree of sociality of the species, following the results of Sakai and Arasznov (2017), we measured the volume of the anterior region of the cerebrum (AC – defined as the portion of the cerebrum between the olfactory bulbs and the rostral-most point of the cruciate *sulcus*). This region was separated from the rest of the neocortex using the software Slic3r (https://slic3r.org/, RRID:SCR-002315). The obtained AC volume was divided by TV to obtain the relative development of the region in comparison with the overall development of the endocast. To highlight the differences among social structures, the extant species of Canini were subdivided into two groups based on their sociality. In particular, we considered the wolf as representative of the social-hunters group and the jackal-like Canini (including *C. aureus*, *C. simensis*, and *L. mesomelas*). The relative development of the AC was then evaluated using a barplot that also reports the 95% confidence interval.

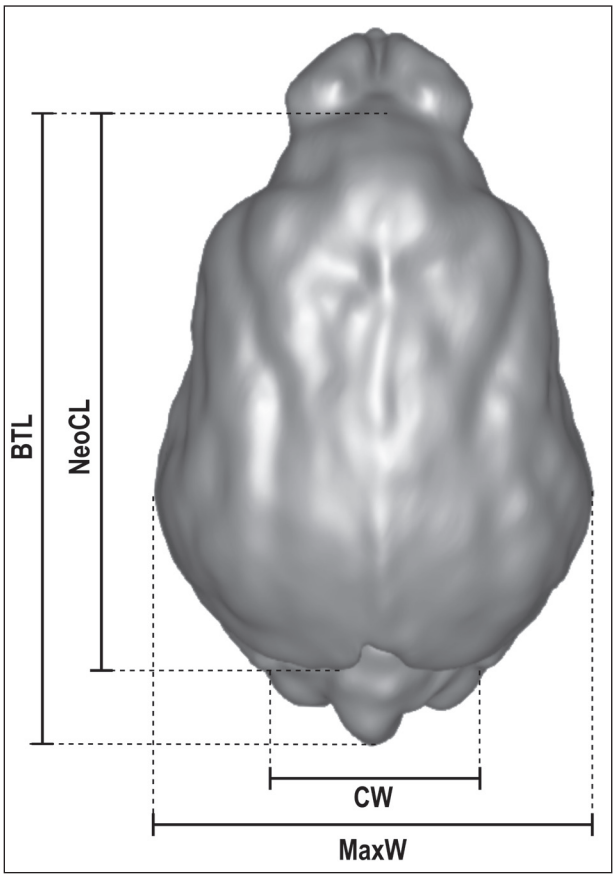

Figure 3. Linear measurements performed on the cerebrum. Abbreviations: BTL, total length of the cerebrum; NeoCL, neocortex length; Cerebrum MaxW, maximum width; CW, cerebellum width.

Statistical analyses and geometric morphometrics

To characterise the specimens from Jradzor, we performed three Principal Component Analyses (PCAs) on cranial, upper teeth and lower teeth variables, respectively. The variables used for the cranial specimens are the total rostrocaudal length of the cranium, the width of the zygomatic processes of the frontals, the width of the postorbital constriction, the length of the neurocranium, the width of the braincase and the skull height. For the dental specimens, we considered the length and width of the P3–M2 (for the upper teeth) and p4–m2 (for the lower teeth). To perform the analyses and plot the resulting graphs, we used the software RStudio (v. 2024.04.0+735 "Chocolate Cosmos" Release (a00d0e775dbc93e0d79a1bf474e3e8e8de677383 2024-04-24; RStudio Team 2024)) in the R environment v. 4.3.3 (R Core Team 2024). PCAs on upper and lower tooth measurements were carried out using the function prcomp() ("*stats*" package v. 4.3.2; R Core Team 2024). The plots of the PCA and the simple biplot were obtained with ggplot() ("*ggplot2*" package v. 3.4.0; Wickham et al. 2016).

To investigate the possibility of a grade shift in the dataset, we performed a covariance (ANCOVA) analysis on all variables, distinguishing two groups based on canid phylogeny (subtribe Canina vs. non-Canina).

To further investigate the shape change of the brain morphology within the included extant canids and the fossil specimen, we applied geometric morphometrics. A series of 14 homologous landmarks were placed on the left hemisphere of the endocast – the best-preserved hemisphere in the analysed fossil from Jradzor – using the software 3D Slicer (Fig. 4). The description of each landmark is reported in Table 1. The decision to use only a single hemisphere also arises from the need to avoid problems linked to natural asymmetries between the left and right hemispheres and to taphonomic or preservation biases. To perform a General Procrustes Superimposition (GPA), we used the function gpagen() ("*Geomorph*" package v. 4.0.8; Adams et al. 2016). Once the Procrustes coordinates were obtained, a PCA was performed using the function gm.prcomp() ("*Geomorph*" package). In this way, we were able to investigate the shape space of the dataset, highlighting the different patterns in shape changes in extant and fossil canids. To create the extreme conformations associated with the PCs analysed, we used the function plotRefToTarget() of the same R package.

Anatomical abbreviations

List of all anatomical abbreviations used throughout the text, in alphabetical order: **BL** = basal length of the cranium; **BM** = body mass; **BTL** = total length of the cerebrum; **c1-m3 L** =

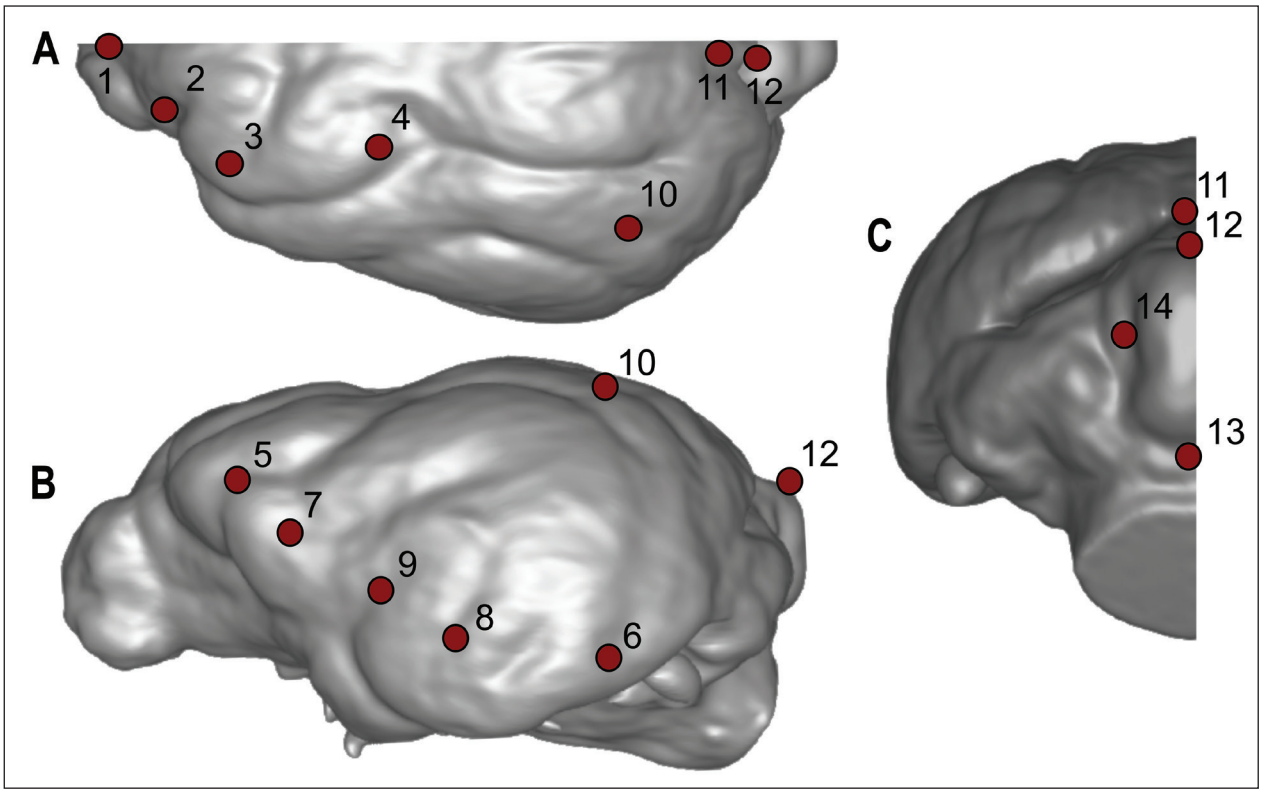

Figure 4. Dorsal (**A**), lateral (**B**) and caudal (**C**) views of the left hemisphere of *Otocyon megalotis* MZUF-1951 with the placed set of 14 landmarks used for the geometric morphometrics analysis. See the list in Table 1 for the explanation of the placement of the landmarks.

Table 1. Description of the set of 14 landmarks used in the geometric morphometrics analysis.

Landmark number	Description
1	Rostral-most point of the neocortex
2	Internal-most point of the presilvian sulcus
3	Rostral-most point of the cruciate sulcus
4	Caudal-most point of the posterior part of the sigmoid gyrus
5	Rostal-most point of the suprasylvian sulcus
6	Caudal-most point of the suprasylvian sulcus
7	Rostal-most point of the ectosylvian sulcus
8	Caudal-most point of the ectosylvian sulcus
9	Internal-most point of the pseudosylvian sulcus
10	Rostal-most point of the ectomarginal sulcus
11	Caudal-most point of the neocortex
12	Highest point of cerebellum vermis
13	Lowest point of the cerebellum vermis
14	Sulcus between the cerebellum vermis and the left hemisphere of the cerebellum

maximum length between the distal border of the alveolus of the canine and the distal border of the m3; **CBL** = condylobasal length of the cranium; **CW** = cerebellum width; **Ect** = frontal breadth across the zygomatic processes of the frontals; **Ent** = minimum width between the orbits; **Eu** = maximum neurocranium width; **FL** = length of the cranium from prostion to midpoint of the frontal at the level of the zygomatic process of the frontals; **FMB** = maximum width of the foramen magnum; **FMH** = height of the foramen magnum; **GBPP** = greatest breadth of the bases of the paraoccipital processes; **GMB** = maximum mastoid breadth; **L** = mesiodistal length in teeth measurements; **LMR** = length of the molar row (m1 - m3 or M1 - M2); **MaxW** = maximum width of the endocast; **Mm1B** = corpus breadth below m1; **Mm1H** = corpus height behind m1; **Mp2p3H** = corpus height between p2 and p3; **NCL** = neurocranium length from akrokranion to midpoint of the frontal at the level of the zygomatic process of the frontals; **NeoCL** = length of the neocortex; **OCW** = occipital condyles width; **OTH** = height of the occipital triangle; **P1-M2 L** = length of cheektooth row starting from P1; **p1-m3 L** = length of cheektooth row starting from p1; **p1-p4 L** = length of the premolar row starting from p1; **p2-m3 L** = length of cheektooth row starting from p2; **p2-p4 L** = length of the premolar row starting from p2; **PoCW** = minimum breadth of skull; **SL** = splanchnocranial length, from prostion to midpoint of the frontal at the level of the zygomatic process of the frontals; **SH** = cranium height (with sagittal crest); tdm1, m1 talonid; **TL** = total length of the cranium; trm1, m1 trigonid; **TS** = total surface of the endocast; **TV** = total volume of the endocast; **W** = buccolingual width in teeth measurements; **WBu** = maximum diameter of the auditory bulla.

Institutional abbreviations

List of institutional abbreviations used to describe the storing institutions of the specimens analysed: **AMNH** = American Museum Natural History, New York (U.S.A.); **CBL** = Borzatti-Lowenstein Collection of the Ethnology

and Anthropology Museum of Florence (Italy); **CE** = Giacomo Doria Natural History Museum, Genoa (Italy); **F:AM** = Frick Collection, Department of Vertebrate Palaeontology, American Museum of Natural History (U.S.A.); **GNM** = Georgian National Museum, Tbilisi (Georgia); **HMNH** = Hungarian Museum of Natural History, Budapest (Hungary); **IGF** = Palaeontological collection acronym in the Geology and Palaeontology Museum of Florence (Italy); **IGS** = Institute of Geological Sciences of the National Academy of Sciences of the Republic of Armenia (Armenia); **MNCN** = Museo Nacional de Ciencias Naturales-CSIC, Madrid (Spain); **MNHN** = Musée National d'Histoire Naturelle, Paris (France); **MZUF** = "La Specola" Zoology Museum of Florence (Italy); **NMB** = Natural History Museum, Basel (Switzerland); **THP** = Tianjin Museum (China); **TM** = Department of Palaeontology at the Ditsong Museum in Pretoria (South Africa); **UCBL FSL** = Université Claude Bernard Lyon 1, Lyon (France); **UCLA** = Robert R. Dickey Birds and Mammals Collection of the University of California Los Angeles, California (U.S.A.); **USNM** = Smithsonian National Museum of Natural History, Washington DC (U.S.A.).

Systematic Palaeontology

Order Carnivora Bowdich, 1821
Suborder Caniformia Kretzoi, 1945
Family Canidae Batsch, 1788
Subfamily Caninae Batsch, 1788
Tribe Vulpini Hemprich & Ehrenberg, 1833

Genus *Nyctereutes* Temminck, 1838

Included species and distribution. *Nyctereutes abdeslami* Geraads, 1997, Africa; *Nyctereutes barryi* Werdelin & Dehghani, 2011, Africa; *Nyctereutes donnezani* (Depéret, 1890), Europe; *Nyctereutes lockwoodi* Geraads et al., 2010, Africa; *Nyctereutes megamastoides* (Pomel, 1842), Europe, West Asia; *Nyctereutes procyonoides* (Gray, 1833), East Asia; *Nyctereutes sinensis* (Schlosser, 1903), Asia; *Nyctereutes terblanchei* (Broom in Broom, 1948), Africa; *Nyctereutes tingi* Tedford & Qiu, 1991, Europe, Asia; *Nyctereutes vinetorum* (Bate, 1937), West Asia; *Nyctereutes viverrinus* (Temminck, 1838), East Asia; *Nyctereutes vulpinus* Soria & Aguirre, 1976, Europe.

Nyctereutes urartuensis sp. nov.

https://zoobank.org/C27150AD-93A7-45D3-B911-BBE1DFFB678E
Figs 5, 6; Table 2

Derivatio nominis. from the Iron Age kingdom of Urartu, which spanned Asia Minor, the Caucasus and Mesopotamia.

Diagnosis. Elongated cranium with marked postorbital constriction; high sagittal crest and marked parasagittal crests; depressed vulpine crease on the dorsal surface of the zygomatic processes; rugose parietals and wide interparietals with a fan-shaped nuchal crest; knob-like mastoid process; inflated but rostrocaudally shortened bullae; equal-sized M1 paracone and metacone, shelf-like buccal cingulum, enlarged protocone with protoconule and metaconule, and a marked hypocone; wide M2, with larger paracone, prominent protocone, and individualised metaconule with no postprotocrista; reduced development of the mandibular subangular lobe; no diastemata in the lower premolars; elongated m1 trigonid, large metaconid, wide talonid with a shallow cristid between hypoconid and entoconid, and entoconulid lingually; m2 has two small cuspulids on the distolingual cingulid; *sulcus proreus* does not reach *sulcus praesylvius*; *gyrus proreus* small and mediolaterally enlarged; peculiar rostrally curved outline of the *sulcus praesylvius*, defining a rostrally protruded *sulcus compositus*; flat *sulcus cruciatus* unlike *N. tingi* and *N. sinensis*; parenthesis-like outline of the *gyrus sigmoideus* with a larger *pars posterior* compared to the *pars anterior*; most developed *sulcus pseudosylvius* among fossil *Nyctereutes*, reaching half the height of *gyrus sylvius*; laterally twisted cerebellum vermis; Straight caudal portion of the *sulcus suprasylvius*, similar to *N. procyonoides*; its rostral portion more protruded, resembling Canini species.

Differential diagnosis. The cranium is elongated, unlike *N. megamastoides*, *N. sinensis*, *N. vulpinus*. The P3 in the Jradzor specimen has a high-crowned and sharp protocone with an evident accessory cuspule, unlike *N. tingi* and *N. donnezani*, more similar to *N. sinensis* and *N. vulpinus*. The P4 protocone of Jradzor differs from the developed one of *N. donnezani* and for the P4 shelf-like lingual cingulum on the distolingual side in the latter species. The M1 of the Jradzor specimens has a large buccal side, but the paracone and metacone are more or less of the same size, and the lingual portions of the trigon and talon are enlarged. These features sharply contrast with the shape of *N. tingi*. Instead, they resemble more advanced forms such as *N. megamastoides*, but also *N. donnezani*. The mesiolingual notch between M1 protocone and hypocone contrasts with *N. tingi* and *N. donnezani*. M2 lacks postprotocrista connecting protocone and metaconule such as *N. sinensis* and *N. vulpinus*. The Jradzor specimen possesses a poorly developed subangular lobe in terms of both dorsoventral sense and curvature in contrast to *N. donnezani* and sharp contrast with *N. megamastoides*, *N. sinensis* and *N. vulpinus*. The m1 talonid of the Jradzor specimen is simple, with few cuspulids, unlike *N. megamastoides*. Moreover, it is more elongated compared to *N. donnezani*. No transverse cristid between hypoconid and entoconid can be seen, in contrast with *N. megamastoides* and *N. sinensis*. The m2 of the Jradzor specimen differs from *N. donnezani* because m2 protoconid and metaconid are different in size from one another. Furthermore, the distal elongation of the talonid in the Jradzor m2 contrasts with the shorter morphology found in *N. donnezani*.

Table 2. Cranial and dentognathic measurements of *Nyctereutes urartuensis* sp. nov. from Jradzor (in mm). Abbreviations: BL, basal length of the cranium; c1–m3 L, maximum length between the distal border of the alveolus of the canine and the distal border of the m3; CBL, condylobasal length of the cranium; Ect, frontal breadth across the zygomatic processes of the frontals; Ent, minimum width between the orbits; Eu, maximum neurocranium width; FL, length of the cranium from prostion to midpoint of the frontal at the level of the zygomatic process of the frontals; FMB, maximum width of the foramen magnum; FMH, height of the foramen magnum; GBPP, greatest breadth of the bases of the paraoccipital processes; GMB, maximum mastoid breadth; L, mesiodistal length in teeth measurements; LMR, length of the molar row (m1–m3 or M1–M2); MaxW, maximum width of the endocast; Mm1B, corpus breadth below m1; Mm1H, corpus height behind m1; Mp2p3H, corpus height between p2 and p3; NCL, neurocranium length from akrokranion to midpoint of the frontal at the level of the zygomatic process of the frontals; OTH, height of the occipital triangle; P1–M2 L, length of cheektooth row starting from P1; p1–m3 L, length of cheektooth row starting from p1; p1–p4 L, length of the premolar row starting from p1; p2–m3 L, length of cheektooth row starting from p2; p2–p4 L, length of the premolar row starting from p2; PoCW, minimum breadth of skull; SL, splanchnocranial length, from prostion to midpoint of the frontal at the level of the zygomatic process of the frontals; SH, cranium height (with sagittal crest); tdm1, m1 talonid; TL, total length of the cranium; trm1, m1 trigonid; TS, total surface of the endocast; TV, total volume of the endocast; W, buccolingual width in teeth measurements; WBu, maximum diameter of the auditory bulla.

	TL	CBL	BL	NcL	FL	SL	P1 - M2 L	LMR	P1 - P4 L	Wbu	GMB	GBPP	FMB	FMH	Eu	PoCW	Ect	Ent	SH	OTH	
JRD - 20/03	179	171	162	82.3	102	76	59.5	18.8	40.7	25.4	53	54	15	12.8	53.1	32.9	50.4	30*	46.4	36.6	
	CL	**CW**	**P1L**	**P1W**	**P2L**	**P2W**	**P3L**	**P3W**	**P4L**	**P4W**	**M1L**	**M1W**	**M2L**	**M2W**							
JRD - 20/03	7.8	4.8	4.7	2.9	8.48.38	3.2	9.6	3.5	15.4	7.2	12.6	13.4	8.3	11.4							
JRD - 21/01							9.6	3.7	14.5	6.7	12.6	14.1	7.3	9							
	cL	**cW**	**p3L**	**p3W**	**p4L**	**p4W**	**m1L**	**m1W**	**trm1L**	**tdm1W**	**m2L**	**m2W**	**c1 post - m3 L**	**p1 - m3 L**	**p2 - m3 L**	**LMR**	**p1 - p4 L**	**p2 - p4 L**	**Mm1B**	**Mm1H**	**Mp2-p3H**
JRD - 19/03	6.4	5.3	8.2	3.2	10.5	4.3	17.8	7.1	11.2	7.2	10.6	7.4	74.4	68.5	63	32.9	35.4	29.9	7.3	20.2	15.1

Holotype. JRD–20/03, skull made of a fairly complete cranium with left I1-M2 and right I1-C and P3-M2; JRD–19/03, right hemimandible with c, p3 - m2.

Hypodigm. JRD - 21/01, right portion of the palate with right P3, right P4, right M1; JRD–22/18, fragment of right hemimandible with p1 - p3; JRD–19/93, right i1; JRD–20/24, right i2; JRD–19/94.

Fossil horizons. JZ-7, 3.3 ± 0.03 Ma (Lazarev et al. 2023).

Distribution. Late Pliocene from Caucasus (MN15-early MN16)

Cranial and dentognathic description. The cranial specimen JRD–20/03 is well preserved, with only the zygomatic arches, the occipital condyles and the right bulla missing. Rostrally, the muzzle shows right lateral compression and breakage due to taphonomic agents. The cranium is considerably elongated rostrocaudally and large. In lateral view, the caudal margin of the infraorbital foramina is at the level of the mesial root of the P4. The cranium is characterised by marked postorbital constriction and evident parasagittal and sagittal crests in dorsal view, and the sagittal crest is also high in lateral view. On the dorsal surface of the zygomatic processes of the frontals, a marked and depressed vulpine crease is present. In dorsolateral view, the parietals are rugose. Caudally, the interparietals are wide with a sharp and prominent nuchal crest, which is fan-shaped in occipital view and ends ventrally in a knob-like mastoid process. In ventral view, the bullae are fairly inflated dorsoventrally but shortened rostrocaudally. The palate is deformed due to taphonomic compression and extends caudally to the distal portion of the M2. The first two upper incisors are characterised by a large main cusp and two side cuspules of comparable size, and the I3 is canine-form. The canine has a flattened conical crown, not very high dorsoventrally and moderately arched distally. The P1 is oval in occlusal shape, with a principal cusp marked by a sharp crest that bounds the mesiolingual margin to the distal one. The P2 and P3 are similar in shape, mesiodistally elongated with a pointy cusp but lacking a distal accessory cusp. Distally, the P3 has a prominent cuspule-like cingulum, and JRD–21/01 also possesses an additional cuspule mesial to the distobasal cingulum. Small diastemata can be seen between the first three premolars. The P4 is characterised by an enlarged protocone in occlusal view and by a metastylar blade that is shorter than the paracone in both occlusal and buccal views. The P4 protocone is advanced mesially relative to the mesial margin of the paracone, where no parastyle is visible. In JRD–20/03, it is slightly separated from the paracone, whereas in JRD–21/01, it is even more attached. The lingual side of the P4 is bounded by a cingulum, marked especially in the distal portion of the blade but also close to the P4 protocone. The M1 is characterised by two large and equal-sized paracone and metacone, bounded by a prominent, shelf-like buccal cingulum. Lingually, there is an enlarged protocone with a protoconule on its mesiobuccal side, connected to an evident metaconule by a high and sharp postprotocrista. Further lingually, the hypocone is marked and wide and forms part of a prominent cingulum. JRD–21/01 has a notch between the M1 protocone and the mesial cingulum, giving the

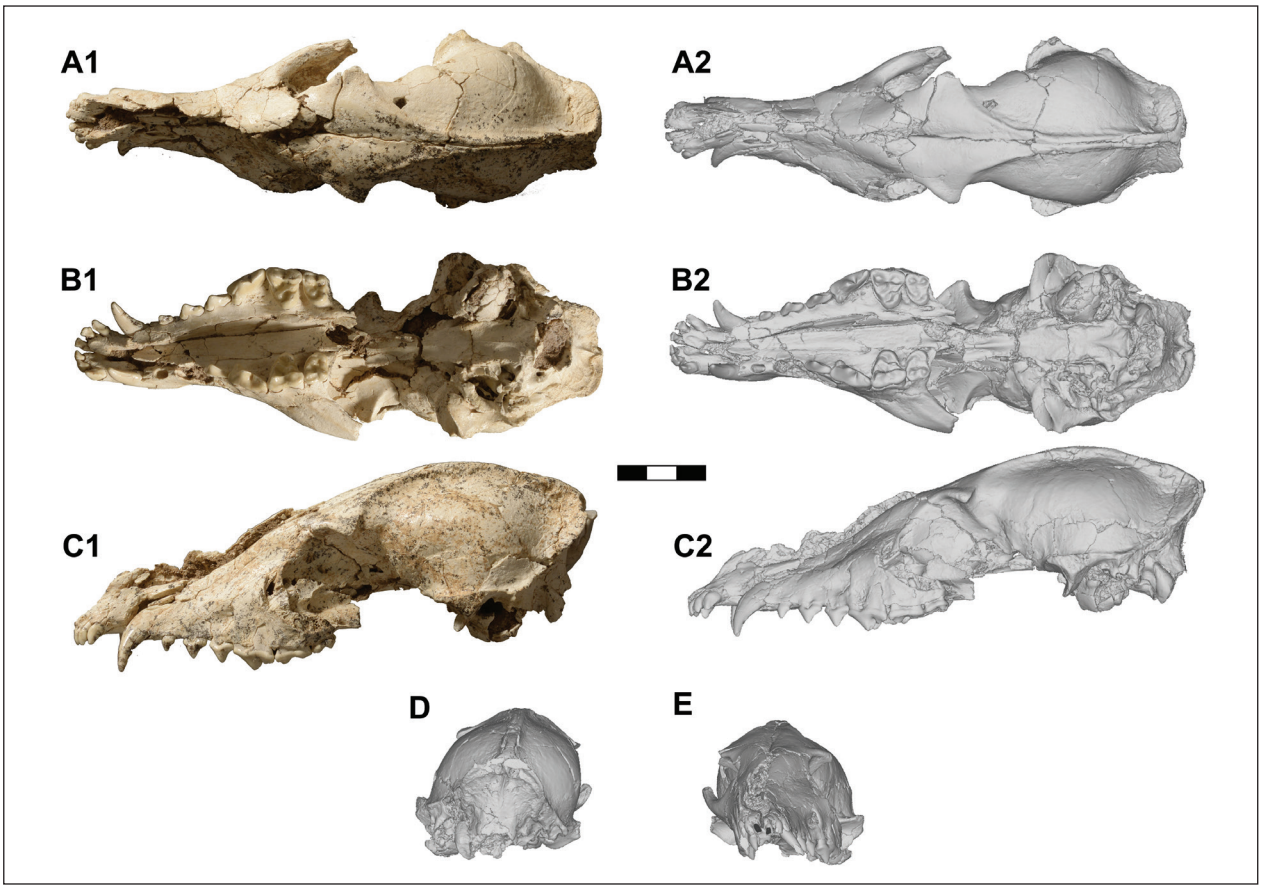

Figure 5. *Nyctereutes urartuensis* sp. nov. from Jradzor. JRD–20/03, cranium with left I1–M2 and right I1–C and P3–M2 in dorsal (**A**), ventral (**B**), left lateral (**C**), occipital (**D**) and rostral (**E**) views. **A2**, **B2**, **C2**, **D–E** are digital scans obtained from the CT-scan of the specimen. Scale bars: 3 cm.

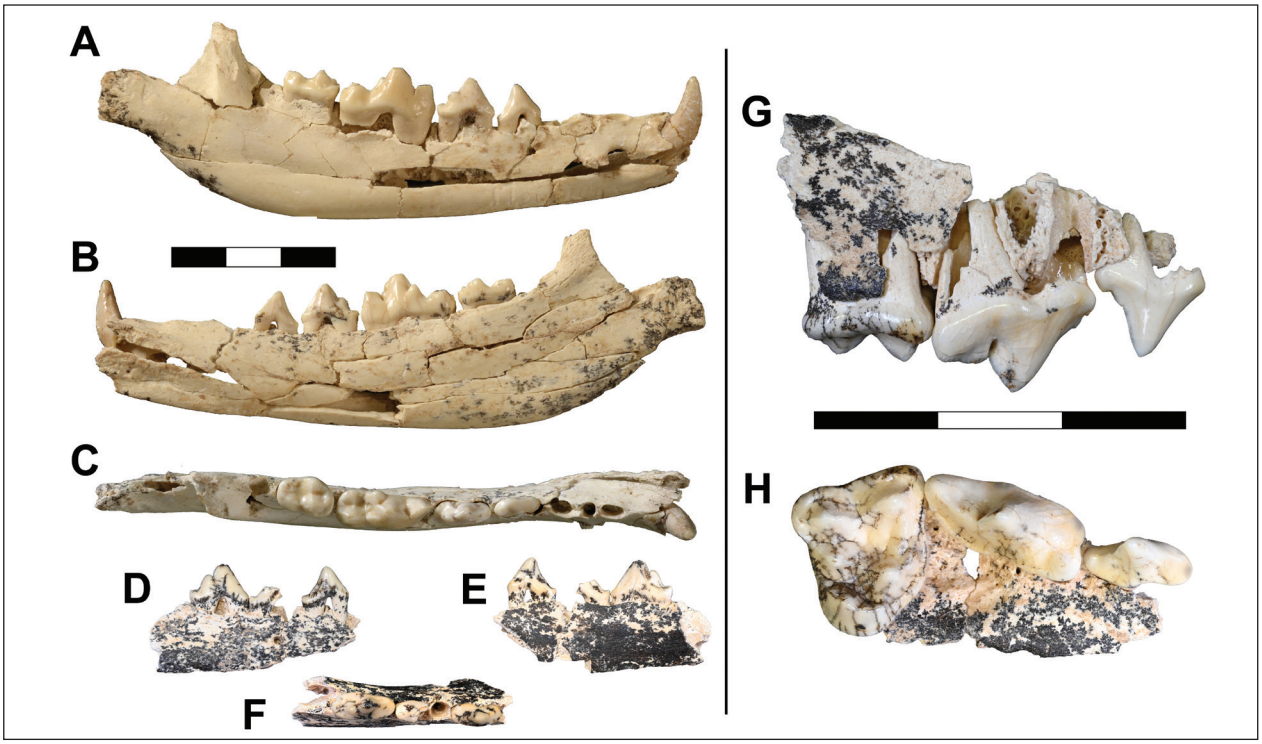

Figure 6. *Nyctereutes urartuensis* sp. nov. from Jradzor. **A–C.** JRD–19/03, right hemimandible with c, p3–m2 in buccal (**A**), lingual (**B**) and occlusal (**C**) views. **D, E.** JRD-22/18 right hemimandible fragment with p2, broken p3 and p4 in buccal (**D**), lingual (**E**) and occlusal (**F**) views. **G, H.** JRD–21/01 right maxillary fragment with P3-M1 (**D, E**), right P4 (**F–H**), right M1 (**I**) in buccal (**G**), lingual (**E**), buccal (**F**), lingual (**G**), occlusal (**H**) and occlusal (**H**) views. Scale bars: 3 cm.

occlusal outline an even more lingual projection; a faint notch is also present in JRD–20/03. The mesial cingulum is well developed, particularly expanded in JRD–21/01. The M2 is wide mesiodistally, with a larger paracone compared to the metacone. A prominent protocone is visible in occlusal view, and lingually, a distal cingulum joins buccally with an individualised metaconule. No postprotocrista is evident between the protocone and the metaconule, creating a wide basin between these cusps. The mandible JRD–19/03 is partially preserved, missing its vertical ramus, and possesses two mental foramina: the larger and more rostral one lying under the p1, and the smaller caudal one lying under the p3. The ventral margin is fairly straight, and the subangular lobe is evident but not high. The tooth row is fairly straight, with no diastemata between the lower teeth. The lower canine is short-crowned and distally arched. The p3 is simple, with no accessory cuspulid and a sharp protoconid that is not particularly high-crowned. The p4 is larger than the p3 and is characterised by a protoconid, a larger distal accessory cuspulid and a basal distal cuspulid-like cingulid. The m1 possesses a fairly elongated trigonid, a large metaconid and a buccolingually wider talonid with a hypoconid slightly larger than the entoconid. The paraconid is short mesiodistally and dorsoventrally and is considerably shorter in height than the p4 protoconid. A shallow cristid is present between the hypoconid and entoconid. The talonid basin is fairly deep and bounded lingually by a small entoconulid. The m2 is mesiodistally elongated, with a protoconid slightly larger than the metaconid. Mesial to the protoconid, a curved cristid extends mesially, curving towards the m2 metaconid, and an expanded cingulid bounds the mesiobasal side of the protoconid. Distally, the talonid is mesiodistally elongated with a developed hypoconid, and distolingually, an evident entoconid with two small additional cuspulids on the distolingual cingulid is present.

Endocast description. The fossil specimen JRD–20/03 from the Jradzor locality shows a well-preserved endocast, with the exception of the missing olfactory bulbs. Regarding the neocortex region, the left hemisphere was better preserved and well developed with all *sulci* present. It shows a well-developed convolution of the neocortex with evident *sulci* on its surface (Fig. 7).

The specimen shows a rostrocaudally elongated brain, rather than mediolaterally inflated. The rostral region shows a clear *sulcus proreus* that defines a small *gyrus proreus*. The latter is rather mediolaterally enlarged than rostrocaudally developed. The *sulcus proreus* runs dorsoventrally alongside the *gyrus orbitalis*, which is placed close to the *sulcus praesylvius*. This latter *sulcus* is characterised by a rostrally curved outline that defines a rostrally protruded *sulcus compositus*. In dorsal view, the *sulcus cruciatus* is flat, and the *pars anterior sigmoidei gyri* is slightly less developed than the *pars posterior sigmoidei gyri*. In the same view, the *gyrus sigmoideus* possesses a parenthesis-like shape, and the *sulcus ansatus* is well developed only on the right hemisphere. However, this hemisphere is more taphonomically altered, so we cannot exclude a possible taphonomic alteration. This raises the question of whether the asymmetry is biological or preservation-related. The dorsocaudal region also shows two medial *sulci* that run parallel to the sagittal plane. However, given their position, they could rather represent tracts for blood vessels. More laterally compared to these, the *sulcus marginalis* does not show any bifurcation, and the *sulcus ectomarginalis* is well developed, reaching half the length of the endocast but not reaching the *sulcus suprasylvius* (Fig. 7). In lateral view, a well-developed *sulcus pseudosylvius* is visible that reaches half of the height of the *gyrus sylvius*. The *gyrus ectosylvius* is rostrally protruded, creating the *pars anterior compositi gyri*, which is rostrally protruded under the rostralmost point of the *pars anterior sigmoidei gyri*, whereas the *gyrus sylvius* is not so developed (Fig. 7). However, this hemisphere is more taphonomically altered, so the asymmetry may be due to preservation bias.

Results

Morphological and morphometric comparisons

The Jradzor canid is attributed to *Nyctereutes* based on the presence of a vulpine crease on the zygomatic processes of the frontals, the short-crowned upper and lower canines and the presence of a rounded and evident subangular lobe (although not dorsoventrally expanded). This is in contrast with *Vulpes* for the morphology of the canines and the presence of a subangular lobe. It lacks the derived features of *Otocyon megalotis*, e.g. the duplication of the molars or the round-shaped expansion of the subangular lobe. Compared to *Eucyon*, it possesses a vulpine crease obliterating sinus expansion within the zygomatic process of the frontal, although a certain degree of the frontal sinus is present medially, as also possessed by other extant and fossil *Nyctereutes*.

The rostrocaudally elongated cranium resembles the morphologies of *N. tingi* from China or Greece (Tedford and Qiu 1991; Koufos 1997), *N. donnezani* from France and Spain and *Nyctereutes* sp. from Çalta-1 (Ginsburg 1998). Unlike *N. megamastoides* from Europe (see Rook et al. 2017), *N. sinensis* from China (see, among others, Tedford and Qiu 1991; Dong et al. 2013), and *N. vulpinus* from St. Vallier (Viret 1954; Soria and Aguirre 1976), both the muzzle and the braincase are more elongated. This elongation and morphological similarity are also confirmed by the morphometric analysis based on cranial variables (see below). The zygomatic processes of the frontals in JRD–20/03 are fairly short, not expanded laterally, and sharp, such as in *N. megamastoides*, *N. vulpinus*, and *N. sinensis* (Viret 1954; Kurtén and Crusafont-Pairó 1977; Rook et al. 2017; Tamvakis et al. 2023; Argant 2024). The morphology of the zygomatic processes of JRD–20/03 is closer to the shape of those of *N. tingi* (Tedford and Qiu 1991; Koufos 1997) and *N. donnezani* (Kurtén and

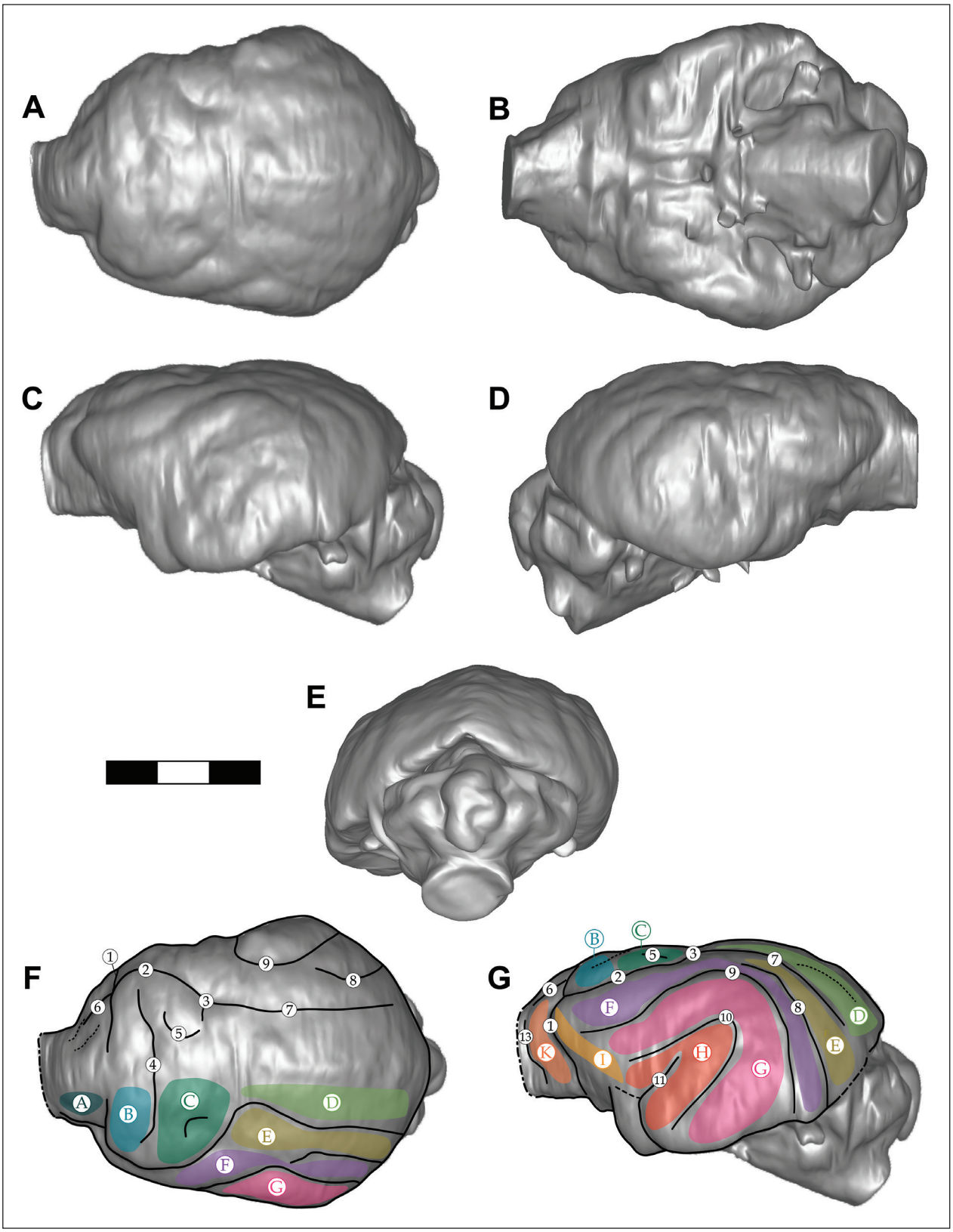

Figure 7. Digital endocast of *Nyctereutes urartuensis* sp. nov. from Jradzor JRD–20/03 in dorsal (**A**), ventral (**B**), left lateral (**C**), right lateral (**D**) and occipital (**E**) views. Scale bar equals 3 cm. Dorsal (**F**) and lateral (**G**) views showing the *sulci* and *gyri* visible on the endocast. Number and coloured letter code: 1, *sulcus praesylvius*; 2, *sulcus coronalis*; 3, *sulcus ansatus*; 4, *sulcus cruciatus*; 5, *sulcus postcruciatus*; 6, *sulcus proreus*; 7, *sulcus marginalis*; 8, *sulcus ectomarginalis*; 9, *sulcus suprasylvius*; 10, *sulcus ectosylvius*; 11, *fissura pseudosylviana*; 12, *sulcus endomarginalis*; 13, *sulcus rhinalis*. A, *gyrus proreus*; B, C, *gyrus sigmoideus*; B, *pars anterior gyri sigmoidei* (or *gyrus precruciatus*); C, *pars posterior gyri sigmoidei* (or *gyrus postcruciatus*); D, *gyrus marginalis*; E, *gyrus ectomarginalis*; F, *gyrus suprasylvius*; G, *gyrus ectosylvius*; H, *gyrus sylvius*; I, J, *gyrus compositus*; I, *pars rostralis*; J, *pars caudalis*; K, *gyrus orbitalis*.

Crusafont-Pairó 1977) and, to some extent, to *Nyctereutes* sp. from Çalta-1 (Ginsburg 1998). In these taxa, the processes are reduced, with a reduced degree of variability. From the upper teeth, the carnassial and the molars are more diagnostic. The morphology of the high-crowned and sharp P3 protocone with an evident accessory cuspule before the basal cingulum is a feature absent in the primitive-like taxa (i.e. *N. tingi* and *N. donnezani*) and more frequent in derived taxa such as some *N. sinensis* from the Yushe Basin (Tedford and Qiu 1991). The P4 is characterised by a reduced protocone unlike the typical isolated and mesially displaced morphology of *N. donnezani* (Depéret 1890; Soria and Aguirre 1976; Bartolini-Lucenti et al. 2018) and *N. vulpinus* (Monguillon et al. 2004). The reduction is more similar to some specimens of *N. tingi* (Tedford and Qiu 1991), *Nyctereutes* sp. from Çalta-1 (especially MNHN.F.ACA291) and *N. megamastoides* (Morales 2016; Rook et al. 2017). The similarity with *N. megamastoides* is considerable, especially for JRD–21/01, in which the P4 protocone is reduced and advanced as in several samples of *N. megamastoides*, e.g. from Dafnero-1, Dafnero-3 and Villarroya (Koufos 1993; Morales 2016; Tamvakis et al. 2023; Savvidou and Kostopoulos 2025), and *N.* aff. *donnezani* from Węże 1 (Czyżewska 1969) as well. In comparison to *N. donnezani* from the Roussillon Basin or Layna (Depéret 1890; Bartolini-Lucenti et al. 2018), the specimens from Jradzor lack the shelf-like lingual cingulum on the distolingual side of the P4. In its morphology, the cingulum of *Nyctereutes* from Jradzor is comparable to *N. tingi* from China or Greece (Tedford and Qiu 1991; Koufos 1997), *Nyctereutes* sp. from Çalta-1 and *N.* aff. *donnezani* from Węże 1 (Czyżewska 1969). The M1 of the specimens from Jradzor has a large buccal side, but with paracone and metacone of more or less the same size. Moreover, the lingual portions of the trigon and talon are enlarged. These features sharply contrast with the shape of *N. tingi* from China or Greece (Tedford and Qiu 1991; Koufos 1997), resembling more advanced forms, even *N. donnezani* from Layna and Roussillon (Depéret 1890; Soria and Aguirre 1976; Bartolini-Lucenti et al. 2018), *Nyctereutes* sp. from Çalta-1 (Ginsburg 1998), and *N. megamastoides*, *N. sinensis* and *N. vulpinus*. The crushing portion of the M1 is developed, as are its cusps/cuspules in occlusal view. The specimens from Jradzor lack the squared occlusal morphology typical of *N. megamastoides*, e.g. from Dafnero-1, Dafnero-3, Kvabebi, and Villarroya (see Koufos 1993; Morales 2016; Rook et al. 2017; Tamvakis et al. 2023; Savvidou and Kostopoulos 2025), and retain a buccolingually longer and mesiodistally narrower M1 similar to *N. donnezani* from Layna and Serrat-d'en-Vaquer, *Nyctereutes* sp. from Çalta-1 (Ginsburg 1998), and *N. sinensis* or *N. vulpinus* (Viret 1954; Tedford and Qiu 1991; Monguillon et al. 2004). The mesiolingual notch between the M1 protocone and hypocone visible in the specimens from Jradzor, especially JRD–20/03, resembles closely that of *Nyctereutes* sp. from Çalta-1, where three specimens out of four complete M1 show it (i.e. MNHN.F.ACA291; MNHN.F.ACA296; MNHN.F.ACA297; Daguenet and Sen 2019). The notch is also present in some specimens of *N. vulpinus* (a single one in the sample from St. Vallier, i.e. MdC 20.161612) and *N. sinensis* from the Yushe Basin (at least three: FAM 96770, FAM 97016, and FAM 97018; Tedford and Qiu 1991). The M2 is developed with a paracone mesiodistally larger than the metacone, such as in the case of *N. tingi* from China and Greece (Tedford and Qiu 1991; Koufos 1997), *N. donnezani* from Roussillon and Layna (Depéret 1890; Soria and Aguirre 1976; Bartolini-Lucenti et al. 2018) and *Nyctereutes* sp. from Çalta-1 (Ginsburg 1998). It is proportionally more elongated buccolingually than more derived species such as *N. megamastoides* (Morales 2016; Rook et al. 2017; Bartolini-Lucenti et al. 2018), *N. sinensis* from China (Teilhard de Chardin and Piveteau 1930; Tedford and Qiu 1991; Dong et al. 2013), and *N. vulpinus* from St. Vallier (Monguillon et al. 2004). Furthermore, the M2 of JRD–20/03 lacks the postprotocrista connecting the protocone and metaconule, such as in some *N. sinensis* from the Yushe Basin (Tedford and Qiu 1991) and *N. vulpinus* from St. Vallier (Monguillon et al. 2004). On the mandible, the most prominent feature is the presence of a poorly developed subangular lobe, both in the dorsoventral sense and in terms of curvature. The morphology contrasts sharply with the derived species such as *N. megamastoides* (Bartolini-Lucenti et al. 2018; Tamvakis et al. 2023), the general shape of *N. sinensis* from the Yushe Basin (Tedford and Qiu 1991) and *N. vulpinus* from St. Vallier (Monguillon et al. 2004). The development of the subangular lobe is comparable to that of the general lateral outline of the mandible of *N. tingi* from China (Tedford and Qiu 1991), *Nyctereutes* sp. from Çalta-1 (Ginsburg 1998), and *N.* aff. *donnezani* from Węże 1 (Czyżewska 1969). Interestingly, the specimens of *N. donnezani* from Roussillon and Layna show a higher and more developed subangular lobe (Depéret 1890; Bartolini-Lucenti et al. 2018), with a more sinuous-like outline of the mandible in lateral view compared to other primitive-like forms (namely, *N. tingi* and *Nyctereutes* sp. from Çalta-1). The lower carnassial in JRD–19/03 is slender in occlusal view, unlike *N. megamastoides* from Kvabebi, Dafnero-1, and Dafnero-3 (Rook et al. 2017; Tamvakis et al. 2023), whose m1 is shortened mesiodistally and wide buccolingually. Moreover, *N. megamastoides* is characterised by multiple cuspulids that characterise the m1 talonid of this taxon. In contrast, *Nyctereutes* from Jradzor possesses only the entoconulid on the lingual portion of the talonid, a condition similar to *N. tingi* from China, *N. donnezani* from Roussillon and Layna (Depéret 1890; Soria and Aguirre 1976; Bartolini-Lucenti et al. 2018), *Nyctereutes* sp. from Çalta-1 (Ginsburg 1998), and *N. vulpinus* from St. Vallier (Monguillon et al. 2004). In contrast to other more derived taxa of the genus, e.g. *N. megamastoides* and *N. vulpinus*, the m1 talonid of JRD–19/03 is not greatly enlarged buccolingually compared to the width of the m1. Its buccolingual width fits in the variability of primitive taxa such as *N. tingi*, *N. donnezani*, and *Nyctereutes* sp. from Çalta-1 (Ginsburg 1998), but it appears more elongated compared to *N. donnezani* (Depéret 1890; Soria and Aguirre 1976; Bartolini-Lucenti et al. 2018), whereas in terms of length, the talonid is proportionally similar to *N. tingi* and *Nyctereutes* sp. from Çalta-1 (Ginsburg

1998). It should be noted that there are also some specimens ascribed to *N. sinensis* with similar carnassial morphology. The occlusal morphology of the metaconid and entoconid are fairly developed and slightly reduced, respectively. This morphology resembles the condition of primitive taxa (*N. tingi*, *N. donnezani*, and *Nyctereutes* sp. from Çalta-1). The m2 of the specimen from Jradzor is similar to *N. tingi* and *Nyctereutes* sp. from Çalta-1, contrasting with *N. donnezani* for the difference in size between the m2 protoconid and metaconid. In the sample from the Roussillon Basin and Layna (Depéret 1890; Soria and Aguirre 1976; Bartolini-Lucenti et al. 2018), two cuspulids are large and similar-sized (Bartolini-Lucenti et al. 2018). Moreover, the distal elongation of the talonid contrasts with the shorter morphology of *N. donnezani* from the Roussillon and Layna (Depéret 1890; Soria and Aguirre 1976; Bartolini-Lucenti et al. 2018).

Cranial and dental morphometric comparisons

Fig. 8A shows the results of a PCA on the total rostrocaudal length of the cranium, the width of the zygomatic processes of the frontals, the width of the postorbital constriction, the length of the neurocranium, the width of the braincase, and the skull height (see also Suppl. material 1: table S3). The PC1 accounts for 79.96% of the variability, whereas the PC2 accounts for 11.84% of the total variance. The PC1 is prevalently influenced by size and particularly by the total length of the cranium and the width of the postorbitals. In contrast, the PC2 is positively influenced by the postorbital constriction and the width of the brain case and negatively by the height of the skull and the length of the neurocranium. In this graph, the extant species are well separated from the fossil ones, occupying negative values of the PC1–PC2. The fossil taxa seem to be fairly separated from each other, particularly *N. megamastoides* from the rest. *Nyctereutes sinensis* and *N. vulpinus* partially overlap in their convex hulls. Primitive-like forms are known from scantier material and are less represented in literature. The specimens referred to this group are all localised in the right, bottom corner of the morphospace. The specimen from Jradzor falls close to this group of specimens, not far from *N.* cf. *tingi* of Megalo Emvolon (Greece) and Tsaochuang (China). The specimens from Çalta-1 can be attributed to the same group. Within this group, it is possible to see how specimens from the same locality are separated from one another in the graph.

Fig. 8B shows the PCA result on the length and width of the upper teeth, between the P3–M2 (Suppl. material 1: table S4). The PC1 explains 78.09% of the variance, whereas PC2 accounts for 10.12% of the total variance. On the PC1, all used variables positively load the axis. On the contrary, on the PC2, the width of the P3 and P4 positively influences the axis, whereas the length and width of the M2 have a negative influence on the PC2. The extant *Nyctereutes* are well separated from the fossil ones, particularly with the reduced size of *N. procyonoides* and *N. viverrinus*. The fossil taxa are poorly separated from each other, especially due to the wide variability of *N. sinensis*. Its range is partially overlapping that of *N. tingi* and completely encloses the range of *N. vulpinus*. The more derived *N. megamastoides* is fairly separated from the other fossil forms, occupying an area of prevalently negative values of the PC1 and PC2. Even more so can be said for *N. abdeslami*. *Nyctereutes donnezani* lies in the variability of *N. megamastoides* and *N. sinensis*. *Nyctereutes* from Çalta-1 and Jradzor are distant from the convex hulls of the other taxa, although one specimen of *Nyctereutes* from Jradzor is close to the variance of *N. tingi*, whereas *Nyctereutes* from Çalta-1 is close to *N. megamastoides*.

Fig. 8C shows the result of the PCA on the length and width of the p4 to m2 (see also Suppl. material 1: table S5). The PC1 explains 86.03% of the variance, whereas PC2 accounts for 4.72% of the total variance. On the PC1, all the variables used positively load the axis with a predominance of the length of the lower carnassial, the width of the talonid, and the m1. On the contrary, the PC2 is positively loaded by the dimensions of the p4 and negatively influenced by the size of the m2. As in the previous graphs, the extant *Nyctereutes* are well separated from the fossil taxa, again due to the reduced size of *N. procyonoides* and *N. viverrinus*. Among fossil forms of *Nyctereutes*, remarkably, the fossil *N. tingi* does not overlap with other taxa. The other primitive-like taxon, *N. donnezani*, overlaps, on the contrary, within its variability with both *N. sinensis* and *N. vulpinus*. Despite the similar size of all three derived-like taxa, it is interesting to notice the distinction along the PC2 with *N. vulpinus*, characterised by the positive values of this axis; *N. megamastoides* with negative values; and *N. sinensis* intermediate between them. *Nyctereutes abdeslami* from Morocco shows a wide variability, especially on the PC2, but it is comparable to that of *N. megamastoides*. The fossil taxa with uncertain taxonomy are located close together, in an area of the positive PC1 values and negative PC2 ones. *Nyctereutes* sp. from Jradzor lies close to MNHN.F.ACA549 from Çalta-1, whereas MNHN.F.ACA294 is close to the specimen from Węże 1.

Endocranial morphological comparison

Fossil species

The fossil species of the genus *Nyctereutes* show a certain variability in the sulcal and gyral morphologies. Fig. 9 shows the herein described morphologies. The type specimen of *N. tingi* (F:AM 96757, Fig. 9A) preserves a partial endocast, which lacked the caudal region of the brain but almost the entire left hemisphere (Lyras and Van Der Geer 2003). The *sulcus proreus* in this species is fairly shallow and defines a small and flat *gyrus proreus*. The *sulcus cruciatus* is not particularly wide. A well-developed *sulcus postcruciatus* is visible. The *gyrus*

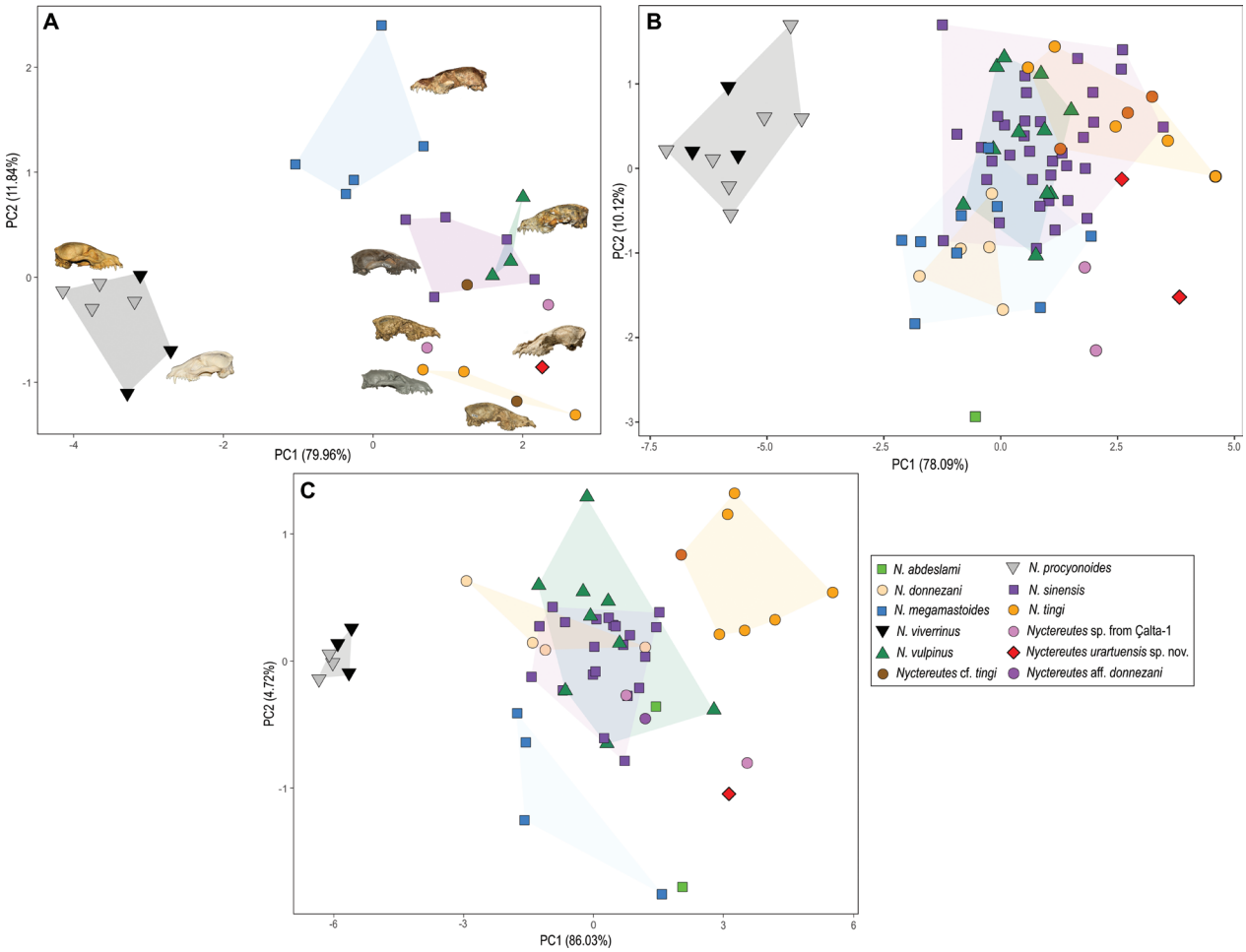

Figure 8. A. Principal component analysis on cranial variables on fossil and extant *Nyctereutes* spp. Symbols are explained in the legend. The following crania are depicted: *N. megamastoides*, DFN-20; *N. procyonoides*, AMNH 249767; *N. sinensis*, F:AM 96783; *N. tingi*, THP 22714 (AMNH cast); *N. viverrinus*, NMB 8759; *N. vulpinus*, MdC 20.161648; *Nyctereutes* cf. *tingi*, MEL-1; *Nyctereutes* sp. from Çalta-1, MNHN.F.ACA292; *Nyctereutes urartuensis* sp. nov. from Jradzor, JRD–20/03. **B.** Principal component analysis on upper teeth variables on fossil and extant *Nyctereutes* spp. **C.** Principal component analysis on lower teeth variables on fossil and extant *Nyctereutes* spp. Symbols are explained in the legend.

sigmoideus probably presents a heart-shaped outline. The less well-preserved side of the endocast shows a more parenthesis-like outline, but it might be caused by taphonomic processes (as doubted by Lyras and Van Der Geer 2003). Within the *gyrus sigmoideus*, the *pars anterior* is much less developed in comparison to the *pars posterior*, which is instead the part that makes up the largest portion of this *sulcus* (Fig. 9A). The *sulcus ansatus* is well-developed only on the right hemisphere, showing a protrusion that deepens inside the *pars posterior sigmoidei gyri*. The endocast shows also, in lateral view, a *sulcus praesylvius* that runs dorsoventrally along the entire brain, reaching the ventral region and well separating the *gyrus orbitalis* from the caudal portion of the neocortex. Lastly, the *sulcus pseudosylvius* reaches deep inside the *gyrus sylvius* and also shows a well-developed rostral portion of the *sulcus* (Fig. 9A), which is usually not clearly developed in other forms.

The MZ VIII-V-360/1 from Węże 1, described as *N.* aff. *donnezani* (Ivanoff et al. 2014), represents a natural endocast of the right hemisphere of the brain (Fig. 9B). The rostralmost region of the endocast is not perfectly preserved, but it shows an underdeveloped *sulcus proreus* that defines a small *gyrus proreus* not extended rostrally. This *gyrus* is more mediolaterally enlarged in comparison to the ones of *N. megamastoides*, *N. sinensis* and *N. tingi*. It rather resembles that of the *Nyctereutes* from Jradzor. In *N.* aff. *donnezani*, a *sulcus praesylvius*, which runs dorsoventrally on the *gyrus orbitalis*, can be observed. However, it is not possible to evaluate its true dorsoventral development since the specimen was not available for this study. The *sulcus cruciatus* is the *sulcus* forming the most acute angle with the sagittal plane, possibly suggesting a more V-shaped morphology of this *sulcus*. The *gyrus sigmoideus* shows a heart-shaped outline, and the *pars anterior* is more developed than the *pars posterior*. The *sulcus ansatus* is well-developed and deepens inside the *pars posterior*. Its development is comparable to that of *N. tingi* and *N. megamastoides*. No *sulcus endomarginalis* is visible, and the development of

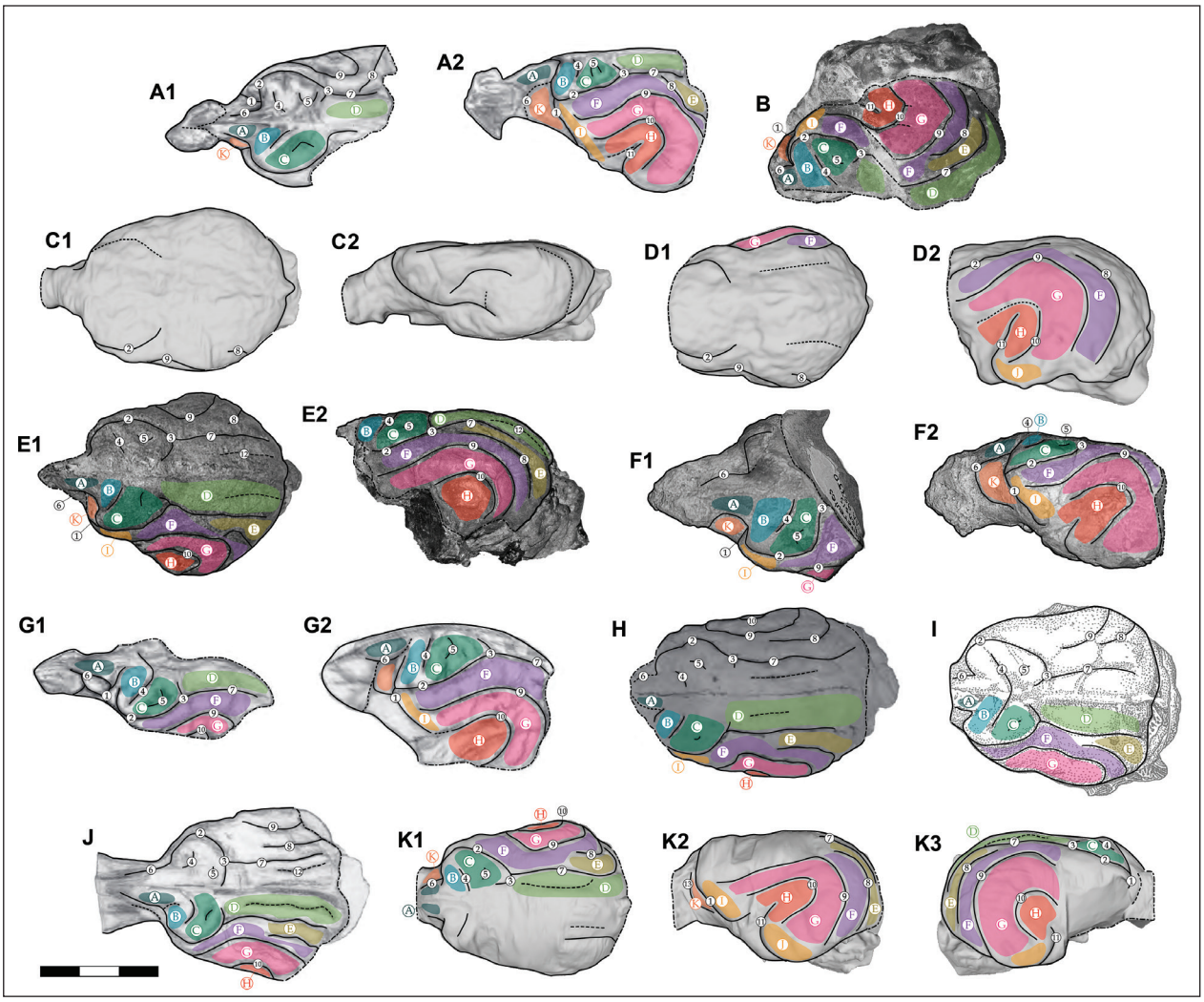

Figure 9. Comparative fossil endocast of extinct *Nyctereutes*. **A.** F:AM 96757, *N. tingi* from Yushe Basin in dorsal (**A1**) and left lateral (**A2**) views (modified from Lyras and Van der Geer 2003). **B.** MZ VIII-V-360/1, *Nyctereutes* aff. *donnezani* from Węże-1 in dorsal view (modified from Ivanoff et al. 2014). **C.** MNHN.F.ACA291, *Nyctereutes* sp. from Çalta-1 in dorsal (**C1**) and left lateral (**C2**) views. **D.** MNHN.F.ACA292, *Nyctereutes* sp. from Çalta-1 in dorsal (**D1**) and left lateral (**D2**) views. **E.** F:AM 22336, *N. sinensis* from the Yushe Basin in dorsal (**E1**) and right lateral reflected (**E2**) views. **F.** F:AM 96750, *N. sinensis* from the Yushe Basin in dorsal (**F1**) and left lateral (**F2**) views. **G.** F:AM 96792, *N. sinensis* from the Yushe Basin in dorsal (**G1**) and right lateral reflected (**G2**) views. **H.** GIN uncatalogued, *N. sinensis* from Beregovaya in dorsal view. **I.** uncatalogued specimen of *N. peii* in dorsal view (modified from Pei 1934). **J.** AMNH (Y)-Σ 384, *N. megamastoides* from Sesklon in dorsal view (modified from Lyras 2009). **K.** NMB. Se 313, *N. megamastoides* from Senèze in dorsal (**K1**), left lateral (**K2**) and righ lateral (**K3**) views. Scale bar equals 3 cm. Number and coloured letter code: 1, *sulcus praesylvius*; 2, *sulcus coronalis*; 3, *sulcus ansatus*; 4, *sulcus cruciatus*; 5, *sulcus postcruciatus*; 6, *sulcus proreus*; 7, *sulcus marginalis*; 8, *sulcus ectomarginalis*; 9, *sulcus suprasylvius*; 10, *sulcus ectosylvius*; 11, *fissura pseudosylviana*; 12, *sulcus endomarginalis*; 13, *sulcus rhinalis*. A, *gyrus proreus*; B, C, *gyrus sigmoideus*; B, *pars anterior gyri sigmoidei* (or *gyrus precruciatus*); C, *pars posterior gyri sigmoidei* (or *gyrus postcruciatus*); D, *gyrus marginalis*; E, *gyrus ectomarginalis*; F, *gyrus suprasylvius*; G, *gyrus ectosylvius*; H, *gyrus sylvius*; I, J, *gyrus compositus*; I, *pars rostralis*; J, *pars caudalis*; K, *gyrus orbitalis*.

the *sulcus pseudosylvius* is difficult to assess due to the poorly preserved *gyrus sylvius*. In this area, this *sulcus* has a development comparable to that of *N. tingi*. The *sulcus ectosylvius* also possesses on its dorsocaudal region two additional small *sulci* that are not present in any other herein analysed fossil species. The two specimens from Çalta-1 are strongly taphonomically altered: MNHN.F.ACA291 is dorsoventrally compressed and does not preserve almost any sulcal or gyral morphology (Fig. 9C), while the specimen MNHN.F.ACA292 does not present a preserved rostral region, and the dorsal surface shows a poorly preserved morphology of the sulcal and gyral patterns (Fig. 9D). Despite this alteration, we were still able to highlight some features in both endocasts. MNHN.F.ACA291 shows a well-developed proreal region (also visible is the beginning of the olfactory bulbs region), which seems to possess a small *gyrus proreus* similar to that of the Jradzor specimen, even if more slender (Figs 7, 9C). The dorsal pattern of *sulci* and *gyri* is not well preserved, but the plausible *gyrus sigmoideus*

appears to have a clear parenthesis-like outline. On lateral view, a possible dorsoventral incision that starts from the ventralmost point of the endocast seems to be visible, and it could represent the *sulcus pseudosylvius*. This *sulcus* does not look particularly well-developed, but the taphonomic alteration is too strong to confidently determine the relative development of this incision in comparison to the others (which are not even clearly visible). On the other specimen from Çalta-1 (MNHN.F.ACA292), the proreal region is not preserved at all, but the region of the *gyrus sigmoideus* is decently preserved and highlights an overall parenthesis-like morphology (Fig. 9D). In dorsal view no other *sulci* or *gyri* can be highlighted, whereas in lateral view the sulcal and gyral pattern is clear and well-preserved. The *sulcus pseudosylvius* is well-developed and deepens inside the *gyrus sylvius* in a similar way to the Jradzor specimen (Fig. 7). The *sulcus suprasylvius* also shows a similar morphology to the Jradzor specimen, especially in the rostralmost portion (in the caudal region it is instead more rostrally curved). Due to the fact that the portion of the endocast rostral to the *gyrus sigmoideus* is not preserved at all, it is not clear how much the *pars anterior gyri compositi* is rostrally protruded.

For comparison with *N. sinensis*, we used published illustrations of three different specimens: F:AM 96750 and F:AM 96792 from the Yushe Basin, figured in Lyras and Van Der Geer (2003), and GIN-uncatalogued specimens from Beregovaya, ascribed to *N. megamastoides* in Lyras (2009) (Fig. 9F–H). Furthermore, the natural endocast of F:AM 22336 from the Yushe Basin has been used for the comparison (Fig. 9E). The latter specimen does not preserve the morphology of the rostralmost portion of the brain nor the ventrolateral morphology of the *gyri*. It is, though, clear that the specimen shows an underdevelopment of the *gyrus proreus*. This feature is shared with other specimens of this species (F:AM 96750, F:AM 96792) in which this region of the endocast is preserved. *N. sinensis* (F:AM 96750) also shows a *sulcus proreus* that runs dorsoventrally on the *gyrus orbitalis*, reaching almost the ventralmost portion of this latter *gyrus* (Fig. 9F), while in F:AM 96792, it is caudally curved and reaches the rostralmost portion of the *sulcus praesylvius*, delimiting completely the *gyrus orbitalis* (Fig. 9G). The dorsoventral development of *sulcus proreus* cannot be evaluated in the other specimens due to the poor preservation of the *gyrus orbitalis*. The *sulcus cruciatus* is well-preserved, especially in the F:AM 22336 (Fig. 9E), which shows a particularly wide morphology. This *sulcus* in *N. sinensis* possesses a more elongate outline in comparison to the more U-shaped *sulcus cruciatus* of the aforementioned *N. tingi*. Apart from this, it is highly different from the flat *sulcus cruciatus* of the Jradzor specimen (JRD–20/03). Furthermore, the *pars anterior sigmoidei gyri* of the left hemisphere seems to be taphonomically altered, giving this side of the *gyrus sigmoideus* a heart-shaped outline. It is more plausible to suggest that the correct outline of the *gyrus sigmoideus* is the one shown on the right hemisphere of the specimen (i.e. a parenthesis-like outline), given also the fact that the other specimens at our disposal, ascribed to this species, show a parenthesis-like outline. The *sulcus ansatus* is preserved clearly only in F:AM 22336 and F:AM 96792. It shows a well-developed morphology (especially on the right hemisphere of F:AM 22336), which deepens inside the *pars posterior sigmoidei gyri*. The development of this *sulcus* is proportionally greater in *N. sinensis* than in *N. tingi*. It suggests that the *sulcus ansatus* is probably deeper in *N. sinensis* than in *N. tingi*. The comparison with the specimen from Jradzor (JRD–20/03) is difficult because the hemisphere with the well-developed *sulcus ansatus* is also the more taphonomically affected. Thus, we cannot exclude that the observable *sulcus* has been formed due to taphonomic processes. If not taphonomically related, the development of the *sulcus ansatus* in *N. sinensis* is also greater than in *Nyctereutes* from Jradzor (JRD–20/03). Four endocasts also show the higher development of the *pars posterior sigmoidei gyri* in comparison to the *pars anterior*, which is especially visible in F:AM 22336. The *sulcus praesylvius* is preserved clearly only in the F:AM 96750 and F:AM 96792. It appears to be less developed than the same *sulcus* in *N. tingi*, because in this species it does not reach the ventralmost portion of the endocast, and at its ventral end, it is curved towards the caudal region. In the F:AM 96792, most probably this *sulcus* is connected to *sulcus suprasylvius*. However, a taphonomic alteration, given the fact that in that same region there is another fracture on the lateral side of the hemisphere, cannot be excluded. The development of this *sulcus* in *N. sinensis* is more similar to that of the specimen from Jradzor (JRD–20/03), even if the latter does not present the curved ventral end that can be seen in *N. sinensis*. Also, the *sulcus pseudosylvius* is preserved only in the F:AM 96750 and F:AM 96792. It is not well-developed, suggesting that it stops at the beginning of the *gyrus sylvius*. The specimen F:AM 22336 also preserves the caudal region of the endocast, where a possible *sulcus endomarginalis* seems to be present. It is an unusual feature, since in literature it has been known to be present only in the Canini tribe (see Boch et al. 2024). An additional *sulcus* is also present in the GIN-uncatalogued specimen (Lyras 2009). In Pei (1934), *N. procyonoides peii* from Zhoukoudian Loc. 1 is illustrated and shows a low-quality definition and the lack of the olfactory bulbs, but we were able to identify some of the main characteristics of this endocast (Fig. 9I). We observe an underdeveloped *sulcus proreus* mainly comparable with that of *N.* aff. *donnezani* and *N. sinensis*. The *sulcus cruciatus* is also visible and forms a parabolic outline, comparable once again with that of *N. sinensis*. On the other hand, the overall outline of the *gyrus sigmoideus* is heart-shaped, particularly similar to that of *N.* aff. *donnezani* from Węże 1 and *N. megamastoides* from Senèze. The *pars anterior* and *pars posterior* of this same *gyrus* are comparable in development, and a *sulcus ansatus* is also clearly present, which deepens within the *pars posterior*, such as that of the *N. megamastoides* from Senèze and *N.* aff. *donnezani*. Neither a clear *sulcus endomarginalis* is visible, nor could we evaluate the development of the *sulcus pseudosylvius*.

Both the specimen of *N. megamastoides* from Sesklo (AMNH (Y)-Σ 384) and from Senèze (NMB.Se 313) do not preserve either the caudalmost portion of the endocast or the olfactory bulbs (Fig. 9J, K). The specimen NMB. Se 313 also shows taphonomic damage on the right rostrodorsal and on the left rostrolateral regions of the endocast. Despite that, the overall 3D model that we obtained from the CT scans of the specimen from Senèze preserved the overall morphology of the endocast of this species in great detail (Fig. 9K). The *sulcus proreus* appears to be with the same degree of development as in *N. sinensis*. In the AMNH (Y)-Σ 384 specimen, it is not clear if it also runs dorsoventrally on the *gyrus orbitalis* (Fig. 9J), but in the NMB. Se 313 specimen on the left side, a clear *sulcus rhinalis* that runs dorsoventrally on the *gyrus orbitalis* is visible (Fig. 9K). The *sulcus rhinalis* is particularly close to the *sulcus praesylvius*, thus defining a thin *gyrus orbitalis*. The region of the *gyrus sigmoideus* shows significant differences between the two specimens of *N. megamastoides* analysed. In particular, the *sulcus cruciatus* is more curved out in the Sesklo specimen in comparison to that from Senèze, which instead shows a curvature more comparable to that of other fossil specimens analysed (e.g. the specimens F:AM 22336 and F:AM 96750 of *N. sinensis* from the Yushe Basin, Fig. 9E, F). Furthermore, the *gyrus sigmoideus* has two completely different outlines, because in the specimen AMNH (Y)-Σ 384 it is parenthesis-like, while in the specimen NMB.Se 313 it is heart-shaped (Fig. 9J, K). The difference in the outline of this *gyrus* seems to be linked to a different development of the *pars anterior*, because the Sesklo specimen has a less developed *pars anterior sigmoidei gyri* in comparison to the Senèze specimen (in both cases the *pars anterior* is still less developed than the *pars posterior*). This difference might be linked to a taphonomic problem in the Sesklo specimen that did not correctly preserve the rostralmost region of the endocast; thus, it is plausible to think that the correct morphology is the one we can see in the specimen NMB.Se 313. The *pars anterior sigmoidei gyri* of the Sesklo specimen seems to possess also an additional *sulcus* absent in other species of this genus and also absent in the other specimen of the same species here analysed. Due to a plausible poor preservation of the rostral region of the endocast of this specimen, it is possible that this additional *sulcus* is just a taphonomic artefact. The *sulcus ansatus* is well-developed (more than in *N. tingi* or in the specimen from Jradzor) in both specimens and bounds caudally the *pars posterior sigmoidei gyri*, in a way similar to the specimens of *N. sinensis* from the Yushe Basin. The caudal portion also shows in both specimens a possible *sulcus endomarginalis*, which seems especially well-developed. In the specimen NMB.Se 313 the *sulcus endomarginalis* looks caudally attached to the *sulcus marginalis*, while in the rostral region it almost reaches the *sulcus ansatus*; in the AMNH (Y)-Σ 384 specimen it is not visible if it is caudally fused with the *sulcus marginalis*, but it is clear that it runs rostrocaudally on the dorsal surface of the endocast, almost reaching the *sulcus ansatus* (Fig. 9J, K). This marked development of the *sulcus endomarginalis* is not seen even in the species of the tribe Canini (Boch et al. 2024). Two more possible *sulci* that run parallel to the sagittal plane are visible on the caudal portion of the endocast of the specimen from Sesklo. Given their positions (i.e. more medial than the putative *sulcus endomarginalis*), they are possibly the result of blood vessels that ran alongside the sagittal plane of the brain rather than an actual *sulcus* of the cerebral matter. NMB.Se 313 shows the lateral morphology of the endocast of *N. megamastoides*, showing a shallow *sulcus pseudosylvius* (Fig. 9K). The *pars anterior gyri compositi* is well-developed but less rostrally protruded in comparison to the Jradzor specimen, from which it differs also in the morphology of the *sulcus suprasylvius*, which is flatter in the dorsal region of the *N. megamastoides* endocast and more rostrally curved in the posterior region (Fig. 9K). The overall morphology in lateral view seems more similar to other fossil species, in particular to that shown in *N. sinensis*.

The rostral region of the specimen from Jradzor shows a well-developed *sulcus proreus* that defines a small *gyrus proreus*. The latter is more mediolaterally enlarged rather than rostrocaudally developed. The *sulcus proreus* runs dorsoventrally alongside the *gyrus orbitalis*, but it is less developed than in *N. sinensis* and more closely placed to the *sulcus praesylvius*. This latter *sulcus* shows a peculiar morphology absent in the rest of the fossil specimens, characterised by a more rostrally curved outline, which defines a rostrally protruded *sulcus compositus*. The *sulcus cruciatus* is flat. The *pars anterior sigmoidei gyri* is slightly less developed than the *pars posterior*. The *gyrus sigmoideus* shows a parenthesis-like outline, and the *sulcus ansatus* seems developed. In lateral view, a well-developed *sulcus pseudosylvius* is visible that reaches half the height of the *gyrus sylvius*. It represents the most developed *sulcus pseudosylvius* among all analysed fossil specimens.

In Ivanoff et al. (2014), the morphology of the cerebellar vermis has been used for taxonomical attribution, in particular highlighting how this part of the cerebellum is straight in the genus *Nyctereutes* and curved in the genus *Canis*. In the analysed specimens, we have observed that some species of the genus *Nyctereutes* also show a laterally twisted vermis of the cerebellum, in particular the natural endocast of *N. sinensis* F:AM 22336 and the 3D reconstruction of the brain of the specimen from Jradzor and of the specimen MNHN.F.ACA292 (Figs 7, 9D). This feature cannot then be used as a taxonomically relevant trait to distinguish different genera of canid species. We suggest it is more likely linked to other factors, such as the ecology of the species or the dimensions of the brain.

Extant species

In the specimen from Jradzor, the *sulcus marginalis* does not show any bifurcation as in most species of the tribe Vulpini (Fig. 10). The width-to-length ratio of the neocortex is lower than that of *N. procyonoides*, meaning that this specimen shows a more rostrocaudally elongated brain than the extant *Nyctereutes* species (Table 3). On

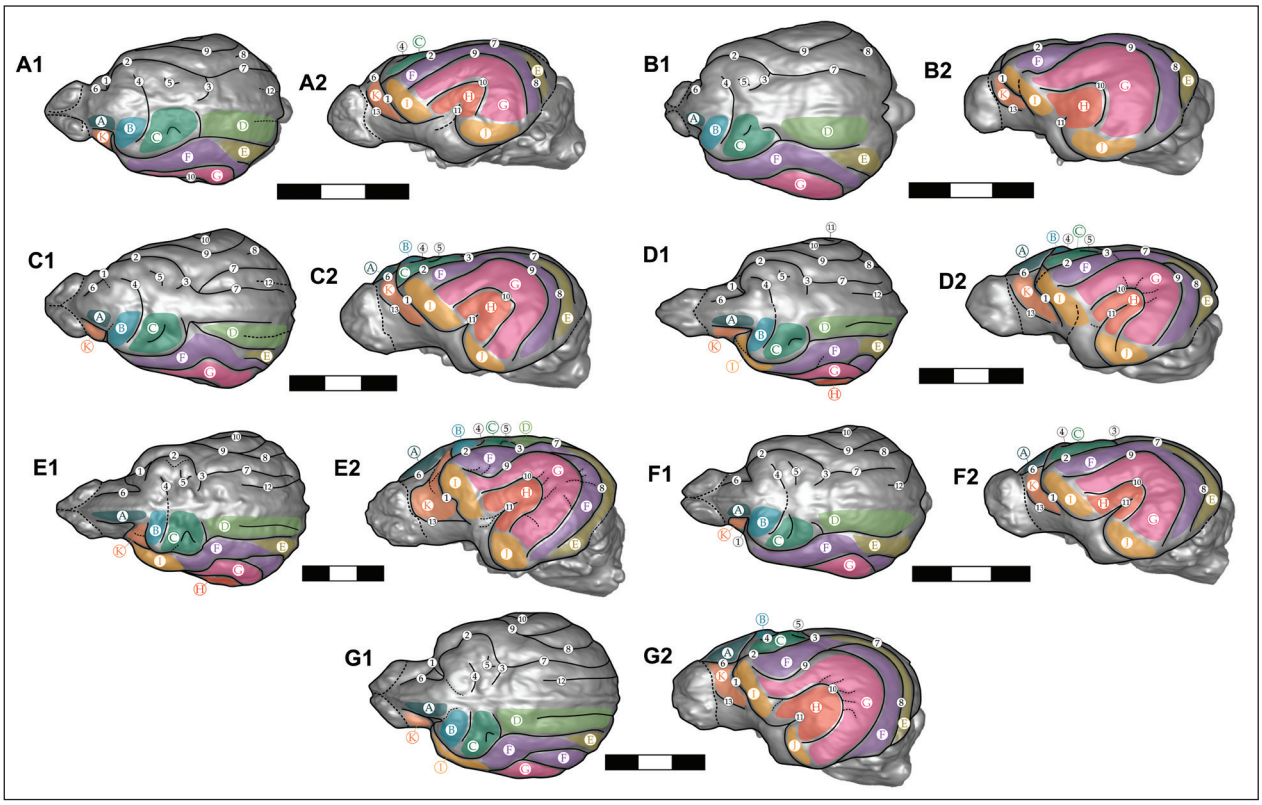

Figure 10. Comparative endocast of selected extant Canidae. **A.** *Nyctereutes procyonoides*, USNM 254641, in dorsal (**A1**) and left lateral (**A2**) views. **B.** *Otocyon megalotis*, MZUF-1951, in dorsal (**B1**) and left lateral (**B2**) views. **C.** *Vulpes vulpes*, MZUF-5882, in dorsal (**C1**) and left lateral (**C2**) views. **D.** *Canis aureus*, CBL298, in dorsal (**D1**) and left lateral (**D2**) views. **E.** *Canis lupus*, MZUF-11874, in dorsal (**E1**) and left lateral (**E2**) views. **F.** *Cerdocyon thous*, MZUF-4062, in dorsal (**F1**) and left lateral (**F2**) views. **G.** *Lupulella mesomelas*, TM3028, in dorsal (**G1**) and left lateral (**G2**) views. Scale bars equal 3 cm while all the endocast are at the same size, to visualise morphological and proportional differences. Number and colored letter code: 1, *sulcus praesylvius*; 2, *sulcus coronalis*; 3, *sulcus ansatus*; 4, *sulcus cruciatus*; 5, *sulcus postcruciatus*; 6, *sulcus proreus*; 7, *sulcus marginalis*; 8, *sulcus ectomarginalis*; 9, *sulcus suprasylvius*; 10, *sulcus ectosylvius*; 11, *fissura pseudosylviana*; 12, *sulcus endomarginalis*; 13, *sulcus rhinalis.* A, *gyrus proreus*; B, C, *gyrus sigmoideus*; B. *pars anterior gyri sigmoidei* (or *gyrus precruciatus*); C, *pars posterior gyri sigmoidei* (or *gyrus postcruciatus*); D, *gyrus marginalis*; E, *gyrus ectomarginalis*; F, *gyrus suprasylvius*; G, *gyrus ectosylvius*; H, *gyrus sylvius*; I, J. *gyrus compositus*; I, *pars rostralis*; J, *pars caudalis*; K, *gyrus orbitalis*.

the contrary, the morphology of the *sulcus suprasylvius* closely resembles the morphology of *N. procyonoides* (Fig. 10A), because in both species the caudal portion of this *sulcus* is straight. In the rest of the analysed species, it is curved towards the rostral portion of the brain, giving a more rounded morphology to the *pars posterior gyrus ectosylvi*. It is difficult to evaluate the morphology of this region in the rest of the fossil specimens at our disposal because none of them clearly showed a well-preserved *pars posterior suprasylvii sulci*. On the other hand, the *pars anterior suprasylvii sulci* is more rostrally protruded in the Jradzor specimen in comparison to the other extant Vulpini species. It resembles more closely the condition seen in Canini species such as *C. aureus* (Fig. 10D) and *L. mesomelas* (Fig. 10G), where the rostrodorsal portion of the *gyrus compositus* is rostrally developed more than the rostralmost portion of the *gyrus praecruciatus*. The development of the *sulcus pseudosylvius* is also highly different in *N. procyonoides* and the specimen from Jradzor, because the latter presents a much deeper *sulcus* in comparison to the extant Vulpini species (Fig. 10A–C). The development of the *sulcus proreus* is also different in these two species, due to the fact that *N. procyonoides* shows a *sulcus* that is tilted backwards and that reaches the *sulcus praesylvius*, completely delimiting the *gyrus orbitalis*. In the specimen from Jradzor, this character is not visible, and the *sulcus proreus* runs straight dorsoventrally without ever reaching the *sulcus praesylvius*. The *sulcus cruciatus* of *N. procyonoides*, with its more parabolic outline, is different from the specimen JRD–20/03, in which it is more similar to that of other fossil species (e.g. *N. procyonoides peii*; Fig. 9I). The extant species of *Nyctereutes* (Fig. 10A) also shows a possible *sulcus endomarginalis*, which is known to be present only in Canini species (Boch et al. 2024). However, in our sample *V. vulpes* (Fig. 10C) also appears to possess such a *sulcus*, so it is possibly a more variable character than previously considered. Thus, the presence of this *sulcus* cannot be used as a feature to ascribe a species to the tribe Canini. Also, in the Canini species,

Table 3. Results of the morphometric measurements and ratios performed on the endocasts and body mass estimations of all the canid species taken into account in the study.

Species	ID	BM (kg)	TV (mm^3)	TS (mm^2)	TL (mm)	NeoCL (mm)	MaxW (mm)	CW (mm)	TV/BM (mm^3/kg)	TS/TV (mm^{-1})	MaxW/ NeoCL
C. aureus	MZUF-11880	7.98	66584.17	9475.93	69.37	65.70	48.36	36.50	8343.88	0.14	0.74
	CBL296	9.78	59392.61	9330.95	69.29	64.45	44.40	32.64	6072.86	0.16	0.69
	CBL297	7.72	62645.28	9299.78	68.53	64.18	44.30	34.19	8114.67	0.15	0.69
	CBL298	8.92	57369.48	8645.93	67.84	63.90	45.92	37.10	6431.56	0.15	0.72
	CBL299	8.92	72172.68	9964.85	70.37	63.61	45.26	37.41	8091.11	0.14	0.71
C. lupus	CBL117	32.32	113532.44	14870.85	83.24	74.15	57.06	43.66	3512.76	0.13	0.77
	MZUF-2032	28.83	109359.65	15028.97	80.64	75.61	53.37	44.51	3793.26	0.14	0.71
	MZUF-11874	33.74	134475.83	16115.34	88.80	78.59	59.97	44.52	3985.65	0.12	0.76
	MZUF-16534	25.30	129712.37	15748.66	88.84	81.68	56.77	44.28	5126.97	0.12	0.70
C. simensis	CE818	29.71	96642.59	12113.61	77.32	70.21	53.04	39.22	3252.86	0.13	0.76
	AMNH m-81001	22.64	101908.05	12925.80	81.23	75.55	51.31	42.93	4501.24	0.13	0.68
Ce. thous	MZUF-4062	6.12	45744.20	7670.84	61.38	53.27	37.99	30.92	7474.54	0.17	0.71
L. mesomelas	TM3028	6.15	61331.81	9504.20	64.82	60.40	48.24	30.50	9972.65	0.15	0.80
	TM1571	5.90	52694.26	8364.69	63.84	56.61	45.66	33.02	8931.23	0.16	0.81
	MZUF-3293	4.38	50563.53	8295.54	61.64	56.57	47.17	33.10	11544.18	0.16	0.83
	MZUF-1128	8.22	54946.35	8942.29	65.69	59.83	43.63	33.72	6684.47	0.16	0.73
N. procyonoides	BLOC20723	3.70	29134.72	5578.76	50.63	40.52	36.72	25.63	7874.25	0.19	0.91
	BLOC210119	2.92	26509.22	5109.08	51.15	40.23	35.83	26.65	9078.50	0.19	0.89
	BLOC210121	2.32	27337.43	5508.19	51.00	41.00	37.23	25.79	11783.38	0.20	0.91
	MZUF-14375	3.93	29165.87	6020.72	51.59	42.65	36.29	21.82	7421.34	0.21	0.85
	USNM 255530	2.89	32319.77	5858.07	51.85	43.11	36.73	25.14	11183.31	0.18	0.85
	USNM 254641	3.78	28082.11	5692.47	51.23	43.20	36.33	31.70	7429.13	0.20	0.84
***Nyctereutes urartuensis* sp. nov.**	JRD - 20/03	9.51	55511.52	9348.77	69.02	60.39	46.36	33.34	5837.17	0.17	0.77
O. megalotis	158_C_BFOX	2.53	27630.93	5638.51	52.12	38.98	38.94	27.20	10921.32	0.20	1.00
	MZUF-1951	1.53	25566.75	5912.02	49.39	40.35	38.12	26.23	16710.29	0.23	0.94
U. cinereoargenteus	UCLA E2	4.62	32369.74	6232.43	56.74	52.13	39.10	26.61	7006.44	0.19	0.75
	UCLA Mammals 6928	4.47	35372.99	6576.30	57.58	51.02	38.36	29.98	7913.42	0.19	0.75
V. chama	TM1193	2.74	37065.38	6928.51	57.91	49.40	37.90	26.16	13527.51	0.19	0.77
	TM1493	2.13	32411.03	5794.18	53.16	45.36	39.26	25.93	15216.45	0.18	0.87
	TM1503	4.39	40696.96	7017.48	57.90	50.46	38.55	28.50	9270.38	0.17	0.76
V. lagopus	MZUF-1474	2.47	33237.35	5908.90	53.10	49.01	38.40	25.25	13456.42	0.18	0.78
V. vulpes	161_C_RFOX	5.30	50656.69	8295.91	60.82	54.86	43.92	32.95	9557.87	0.16	0.80
	161_C2_RFOX	4.90	52877.63	9368.56	63.61	58.42	46.70	35.13	10791.35	0.18	0.80
	MZUF-5882	5.38	44873.48	7988.63	58.97	53.67	42.18	30.65	8340.80	0.18	0.79
	BLOC1	5.54	46280.42	8200.61	59.67	52.44	42.72	31.10	8353.87	0.18	0.81
V. zerda	159_C_FFOX	1.01	19023.60	4225.76	44.80	34.63	34.77	24.33	18835.25	0.22	1.00

this *sulcus* is not always well-developed. In *Ce. thous* (Fig. 10F), it is present only on the right side of the brain. Another feature that is more clearly linked to the tribe is the development of the *sulcus proreus*, because it is clearly more developed in the Canini tribe than in the Vulpini. Boch et al. (2024) mentioned this *sulcus* not being present in Vulpini species; however, in our studied sample, foxes also possess this feature, even if underdeveloped. In the Jradzor specimen, the development of its *sulcus proreus* is comparable to that of the Vulpini, particularly with that of *N. procyonoides* (Fig. 10A) and *O. megalotis* (Fig. 10B). It should be noted that *V. vulpes* (Fig. 10C) shows the most developed *sulcus proreus* within the analysed Vulpini. The development of the *sulcus pseudosylvius* in JRD–20/03 is, on the contrary, greater than any other extant Vulpini and is more comparable to the development in Canini species, in particular *C. lupus* (Fig. 10E) and *Ce. thous* (Fig. 10F). The *sulcus pseudosylvius* of *Ce. thous* (Fig. 10F), though, is different from that of the Jradzor specimen, because it also possesses a rostral portion that is connected to the *pars posterior praesylvi sulci*, completely enclosing the *pars anterior compositi gyri*. This feature is seen only in a few other species, i.e. *V. vulpes* (Fig. 10C) and *L. mesomelas* (Fig. 10G), but not in *N. procyonoides* (Fig. 10A), to which previously *Ce. thous* had been phylogenetically associated with brain morphology (Lyras and Van der Geer 2003; Lyras 2009). The phylogenetic relationship between these two species was inferred in particular on the basis of the *gyrus sigmoideus* morphology, because they both share a heart-shaped outline. However, in our sample, we have observed that not all *Nyctereutes* fossil species show this morphology (e.g. *N. sinensis* probably possessed a parenthesis-like outline of this *gyrus*; Fig. 9E–H). It is also clear that the heart-shaped outline of the *gyrus sigmoideus* in *N. procyonoides*

(Fig. 10A) is different from that of *Ce. thous* (Fig. 10F) (i.e. it is more rostrocaudally elongated), which is in contrast more comparable to the heart-shaped outline of the *gyrus sigmoideus* in *O. megalotis* (Fig. 10B). The morphology of the *gyrus sigmoideus* of the fossil specimen from Jradzor is instead more comparable to that of *L. mesomelas* (Fig. 10G), which is the only Canini species possessing a parenthesis-like outline of the *gyrus sigmoideus*. On the contrary, in two species of the genus *Canis*, the *gyrus* has an orthogonal outline (Fig. 10D, E). The *sulcus cruciatus* is also similar to that of *L. mesomelas* rather than to the other Vulpini species (it is also comparable to that of *C. lupus* (Fig. 10E), because also in this species the *sulcus cruciatus* is flat). The *sulcus ectosylvius* of the Jradzor specimen is instead comparable in development to that of the Vulpini species, in particular to *V. vulpes* (Fig. 10C). This *sulcus* is much different in the Canini tribe (excluding *Ce. thous*, which, however, resembles the Vulpini species, especially *V. vulpes*, for this feature) because in this group the *sulcus ectosylvius* is rostrally elongated and merged with the dorsal region of the *sulcus suprasylvius*.

Endocast morphometric analyses

Firstly, the correlation between the body mass and the volume of the brain was investigated in Canidae. In this study, the olfactory bulbs have not been considered due to the impossibility of observing this character. As already noted by other authors (e.g. Gittleman 1986), a clear, strong, positive linear correlation (p-value << 0.001) between the body size of the species and the volume of the brain can be observed (Fig. 11). The plot clearly separates the largest species of canids (e.g. *C. lupus*), which fall at the top right of the graph, from the smaller species, which instead fall at the bottom left part of the biplot (Fig. 11). The analysed dataset also highlights a significant grade shift between the subtribe Canina and all other canids: among all analysed morphometric parameters, this is the only case where the ANCOVA yielded significant results; on the contrary, in the other cases, only a single regression line without the division of the dataset into two groups could be revealed, since no significant covariation results were obtained. The analysis highlights that the two regression lines do not show a significant

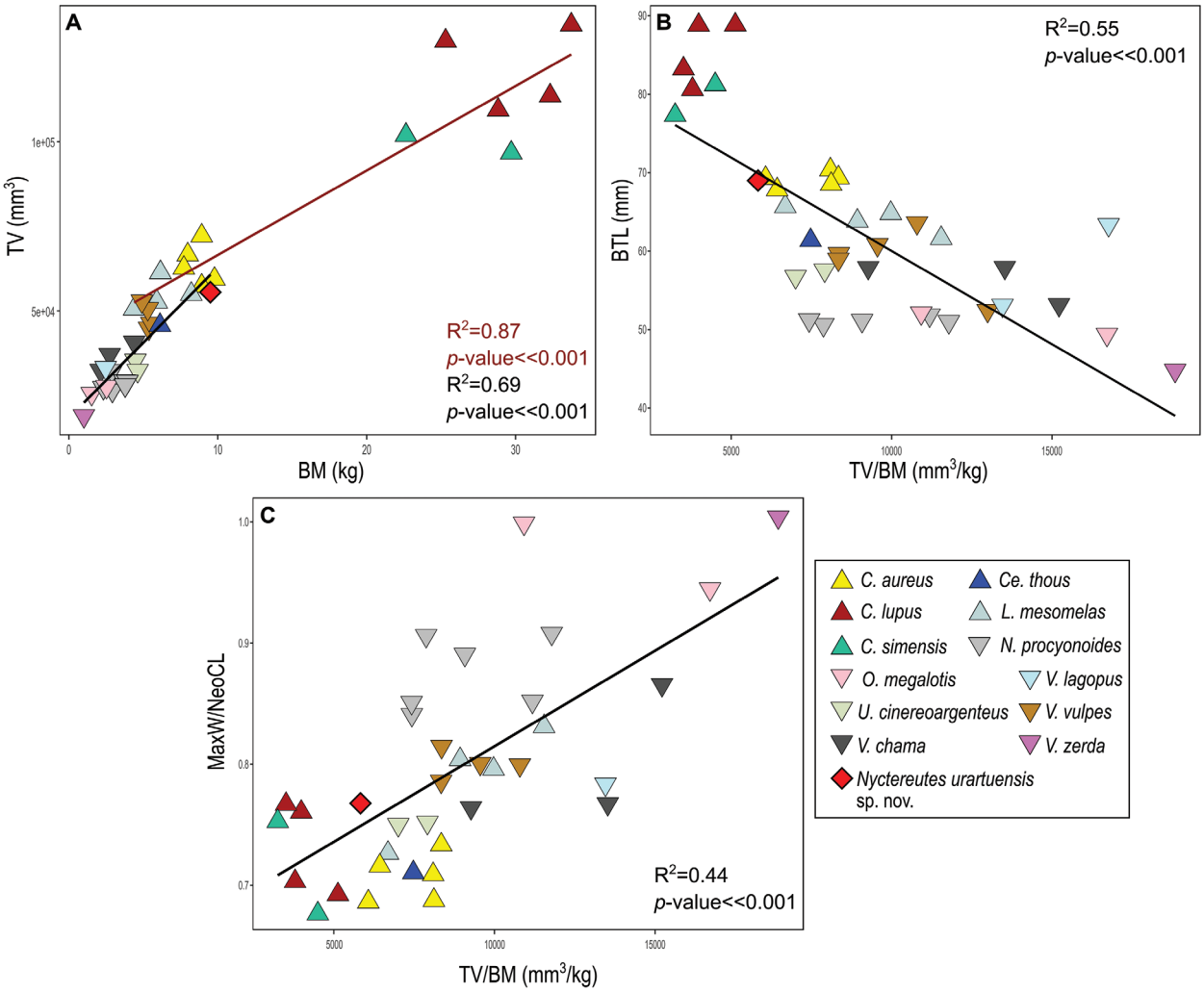

Figure 11. A. Bivariate plot on metric parameters of the endocasts: total volume (TV) and body mass (BM). **B.** Bivariate plot of total length of the brain (TL) and body mass (BM). **C.** Bivariate plot of the ratio between the maximum neocortical width and its length (MaxW/NeoCL) and the relative brain size (TV/BM).

difference between the slopes of the two regression lines (F = 1.146 and *p*-value = 0.050085), but a significant difference among the intercepts of the regression lines (F = 458.605 and $p << 0.001$). The fossil specimen JRD–20/03 places outside the variability of the extant species of the same genus and falls close to the regression line of the non-Canina group (black regression line; Fig. 11A). To evaluate the rostrocaudal elongation of the brain, the comparison between the TL and relative brain size (measured as the ratio between TV and BM) has been used (Fig. 11B).

The correlation, even if not so strong as that one between the BM and TV ($R^2 = 0.54$), is still highly significant (*p*-value << 0.001) and highlights how the species of the tribe Canini show elongated brains in comparison to the tribe Vulpini (Fig. 11B). In this case, the fossil species falls closer to the variability of the Canini tribe than to the variability of the extant species of the genus *Nyctereutes* (Fig. 11B). This relationship is characterised by a negative allometry (slope TL–TV/BM = –0.0024), meaning that the length of the brain increases less than the relative brain size. Thus, species with a higher relative brain size, such as *V. zerda*, show a less rostro-caudally elongated brain than expected. The negative correlation between these two parameters underlines that as the relative brain size increases, the total length of the brain diminishes; thus, species with smaller body mass possess shorter brains than species with larger body mass. When the relationship between the relative brain size (TV/BM) and the ratio between the maximum width of the neocortex and its length is considered, a strong negative allometry is instead highlighted (slope MaxW/NeoCL–TV/BM = 1.58×10^{-5}), meaning that as the relative brain size increases, the brain is less mediolaterally enlarged than expected (Fig. 11C). In this case, we observe the smallest species of the tribe Vulpini on the top right corner of the plot, while the species of the Canini tribe fall at the opposite corner of the graph (Fig. 11C). The correlation between these parameters is not strong ($R^2 < 0.50$), yet it is highly significant (*p*-value << 0.001). The relationship between two parameters underlines the fact that the smaller species of Vulpini tend to possess a more rounded brain in comparison to the larger species of the tribe Canini. In this context JRD–20/03 does not fall particularly close to the extant species and just above the regression line (Fig. 11C).

We further analysed the relative development of the AC region of the brain (Fig. 12). We can observe higher values of this ratio are found in the social canids, which are here represented by the wolf and jackal-like canids (*L. mesomelas*, *C. aureus*, *C. simensis*). They also tend to have a higher value of relative AC development. They can form transitory packs and show more complex social structures than the foxes in periods with a paucity of resources. Regarding various species of the tribe Vulpini, in contrast, it is observable instead that the values of relative AC development are significantly lower, with the negative extreme values represented by *V. chama* (Fig. 12). The relative AC volume of the *Nyctereutes urartuensis* from Jradzor is rather comparable to that of the jackal-like canids, meaning that this species presented a higher value for this parameter than the extant congeneric or other extant foxes (Fig. 12).

Endocast geometric morphometrics analysis

The GPA performed on the set of 14 landmarks placed on the surface of the brain was used to create a PCA: the first three PCs explain 54.0% of total variance (PC1 = 27.4%, PC2 = 17.6%, PC3 = 9.0%) (Fig. 13). Table 4 instead

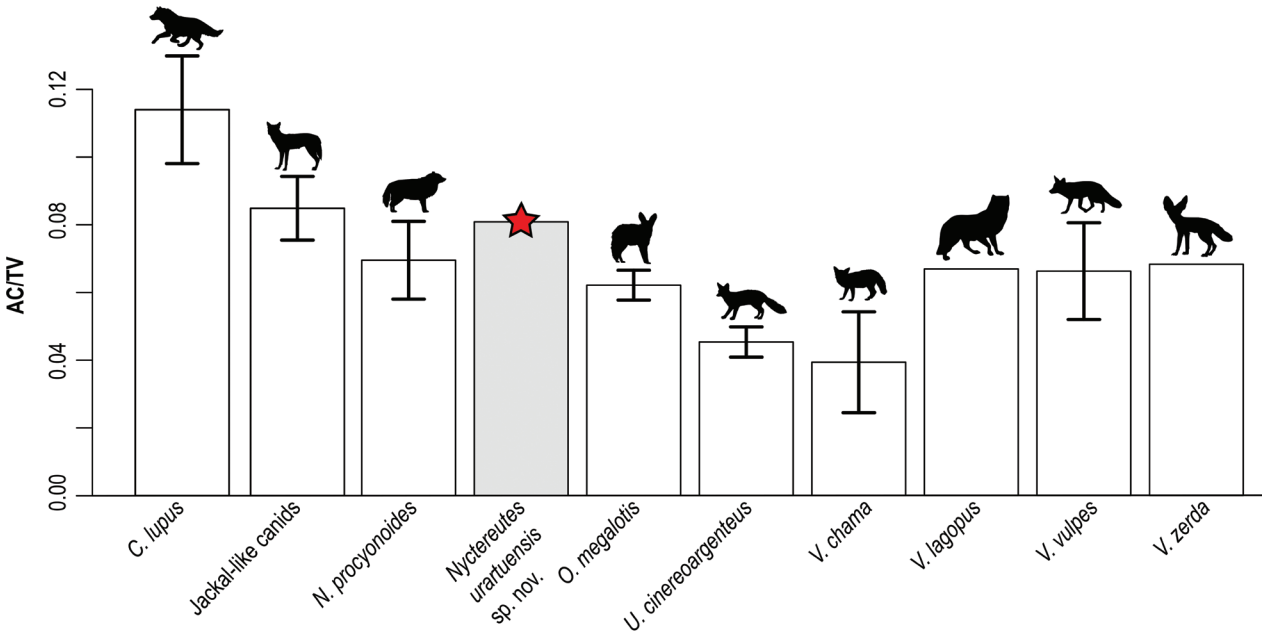

Figure 12. Relative frontal cortex (AC) volume in different species of the tribe Vulpini and two ecological groups of Canini. Error bars indicate the 95% confidence intervals.

Table 4. Results of the correlation analysis between the first three PCs of the PCA and the main morphometric parameters of the brain (significant correlations highlighted in bold).

	R^2	*p*-value	Slope
PC1 vs BM	**0.47**	**<<0.001**	**0.0040**
PC1 vs TV	**0.65**	**<<0.001**	**1.4×10^{-6}**
PC1 vs TV/BM	**0.34**	**0.00010**	**-9×10^{-6}**
PC1 vs NeoCL	**0.75**	**<<0.001**	**0.0041**
PC1 vs MaxW/NeoCL	**0.56**	**<<0.001**	**-0.48**
PC2 vs BM	-0.019	0.55	-0.00047
PC2vs TV	-0.0050	0.37	-2.2×10^{-7}
PC2 vs TV/BM	-0.029	0.94	-1.5×10^{-7}
PC2 vs NeoCL	-0.016	0.51	-0.00043
PC2 vs MaxW/NeoCL	-0.023	0.65	0.041
PC3 vs BM	0.017	0.21	0.00070
PC3vs TV	0.0098	0.25	1.98×10^{-7}
PC3 vs TV/BM	**0.13**	**0.016**	**-3.4×10^{-6}**
PC3 vs NeoCL	0.017	0.21	0.00057
PC3 vs MaxW/NeoCL	0.049	0.10	-0.10

shows the correlation between the main morphometric variables investigated in the previous paragraph and the first three PCs. Among them, only the PC1 is influenced by these parameters, while the other two PCs do not show any significant correlation with the morphometric parameters. The only exception is represented by the correlation between PC3 and the relative brain size, which is significant but weakly supported. Of the five parameters considered in the correlation analysis, only three (i.e. TV, NeoCL and MaxW/NeoCL) show a strong correlation ($R^2 > 0.50$) with the PC1, while the other two parameters (i.e. BM and TV/BM) present a weak correlation ($R^2 < 0.50$). TV, BM and NeoCL all show a positive slope of the correlation, meaning that the higher the value of these parameters, the higher the PC1 values. At the same time, the last two morphometric parameters (TV/BM, MaxW/NeoCL) show a negative slope (i.e. the higher the value of the parameter, the lower the value of PC1). The results are coherent with the previously performed morphometric analyses. There, alongside the PC1, we have on the right side the species of the subtribe Canina (i.e. more voluminous brains, greater body mass, more elongated brains), while on the left side, other canid species are grouped (i.e. higher relative brain dimensions, more rounded brains) (Fig. 13). The most positive values of the PC1 are shown by *C. lupus*, while the most negative ones are presented by *N. procyonoides*. The extreme positive values of this axis are associated with a convoluted brain morphology with a domed structure of the neocortex and a reduced development of the cerebellum, which does not strongly emerge out of the neocortex (Fig. 13C). On the other hand, the rostral region of the brain possesses

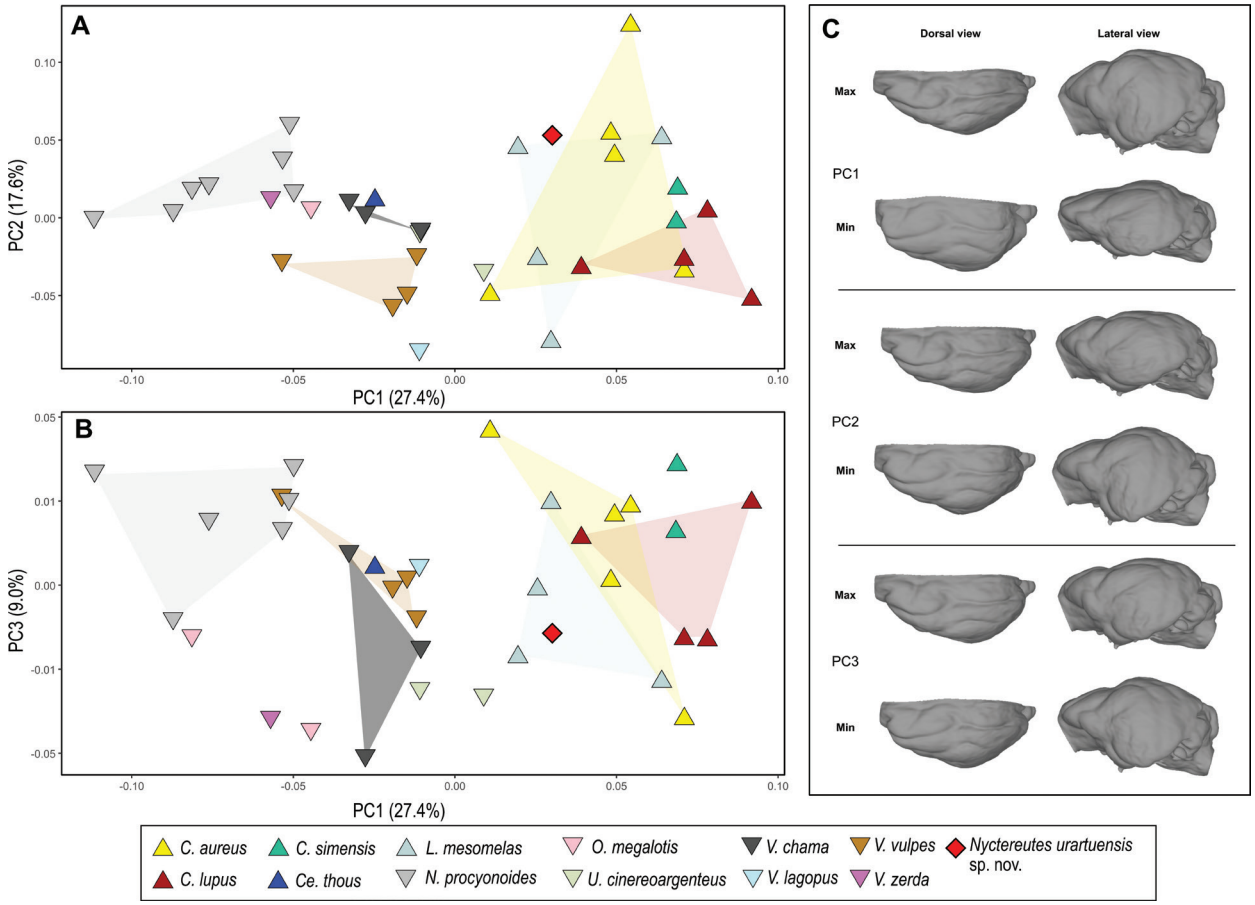

Figure 13. Principal component analysis resulting from the geometric morphometric analyses on the 14 landmarks positioned on the endocast of *Nyctereutes urartuensis* sp. nov. from Jradzor and selected extant Caninae. **A.** Shows the PC1–PC2 scatterplot. **B.** Biplot of PC1–PC3 scatterplot. **C.** Shows the extreme conformations per PCs showing the shape variation of the first three PCs of the PCA.

a more developed and elongated *gyrus proreus*. The pars posterior *gyri sigmoidei* is more developed than the pars anterior, giving the *gyrus sigmoideus* an orthogonal shape (Fig. 13C). The brain morphology associated with negative values of PC1 is instead characterised by a less domed brain, with a predominantly medio-lateral development of the neocortex and a more protruding cerebellum (Fig. 13C). The rostral region of this conformation is instead characterised by a more developed pars anterior *gyri sigmoidei* that gives the *gyrus sigmoideus* a heart-shaped outline and an underdevelopment of the *gyrus proreus* (Fig. 13C). Alongside the PC2, the groups are less well-separated, and the species of the tribe Canini present more variable values for this PC (only *C. lupus* presents only negative values; Fig. 13A). Among the tribe Vulpini, it can be noticed that from all analysed species, *V. lagopus* shows the lowest values for this PC, and further, other species of the genus *Vulpes* tend to have negative values of this PC (Fig. 13A). Among Vulpini, only *N. procyonoides* possesses more positive values of this PC (Fig. 13A). The extreme positive values of the PC2 are associated with a U-shaped *sulcus ectosylvius* and an underdeveloped pars posterior *gyri compositi* (Fig. 13C). Furthermore, the pars posterior *suprasylvii sulci* points towards the caudal region of the brain, giving the *ectosylvius gyrus* a wide, rounded morphology (Fig. 13C). The minimum values of the PC2 are instead associated with a pointier *sulcus suprasylvius* and *sulcus ectosylvius*, with an overall triangular-like neocortex morphology in lateral view (Fig. 13C). Furthermore, the *sulcus pseudosylvius* is deeper in the brain morphology associated with negative values of the PC2. When the PC3 is considered, a clear pattern is not visible either; here all the species are evenly distributed along this axis (Fig. 13B). When the first two PCs are taken into account, the Jradzor specimen (JRD–20/03) falls close to the variability of two jackal-like species, *C. aureus* and *L. mesomelas*, while when PC1 and PC3 are considered, it falls within the variability of *L. mesomelas* (Fig. 13A, B). The extreme positive values of the PC3 are associated with a short rostrocaudal development of the *gyrus sigmoideus* and a *gyrus suprasylvius* that shows the dorsal portion directed towards the caudal region of the brain (Fig. 13C). The negative values of PC3 are instead associated with a longer rostrocaudal development of the *gyrus sigmoideus* and a *gyrus suprasylvius* that shows the dorsal region pointed towards the rostral portion of the brain (Fig. 13C).

Bony labyrinth comparison

The bony labyrinth of *N. urartuensis* sp. nov. is not well preserved. It is filled with sediment and broken at several places (Fig. 14). Some general remarks can still be made, and a comparison to the bony labyrinth of the extant *N. procyonoides* is possible to some extent (Fig. 14). The cochlea of *N. urartuensis* sp. nov. is high and bulky and completes probably about three turns, such as that of *N. procyonoides*. Its position is ventromedially tilted, somewhat masking the spherical recess in medial view, such as in *N. procyonoides*, where the tilt is even stronger. Its overall shape is tubular. It shows a keel on the top part of each turn, which is a character found in *N. procyonoides* as well as in other canids (Ekdale 2013; Schweizer et al. 2017). However, this character is absent in felids or other members of Carnivora (see also Grohé et al. 2016 for musteloids). The basal turn is massive compared to the others and has a marked secondary bony lamina in *N. procyonoides*, unfortunately not visible on *N. urartuensis* sp. nov. because of the bad preservation of the available specimen. On *N. procyonoides*, it further presents a strong and irregular radial expansion of its dorsalmost part (the scala tympani), which recalls to a certain extent the tympanal recess of cetaceans, although being much more reduced. This feature is not visible on *N. urartuensis* sp. nov. because of its preservation, but its basal turn looks similar in shape to that of its extant relative, including the presence of a radial thickening. The cochlear aqueduct is very similar in both species, elongate and thin, very straight and laterally oriented.

The anterior semicircular canal projects slightly above the level of the common crus, less so than in *N. procyonoides*, and is as high as the posterior semicircular canal. The latter is less dorsally expanded than its anterior counterpart in *N. procyonoides*. Both the anterior and posterior semicircular canals have a circular shape in both the extinct and extant *Nyctereutes*. The lateral semicircular canal also has a circular shape in *N. urartuensis* sp. nov., as opposed to a more triangular shape in *N. procyonoides*. Its insertion in the vestibule is not preserved on the fossil *Nyctereutes*, but it seems to be similar to that of *N. procyonoides*, which occurs dorsally in the posterior ampulla, producing a common area (a somewhat secondary common crus) between the lateral and posterior semicircular canals. The angle between the lateral and posterior semicircular canals is very different between both species, reaching 85° in *N. urartuensis* sp. nov. and being larger in *N. procyonoides*, with 95°. The elliptical recess is not particularly marked in either species, while the spherical recess is slightly more bulbous in *N. procyonoides* as well as in *N. urartuensis* sp. nov. The vestibular aqueduct diverges laterally from the axis of the common crus. It is longer in *N. urartuensis* sp. nov. than in *N. procyonoides*. The endolymphatic sac is also different between both taxa: thinner in *N. urartuensis* sp. nov. and wider and more medially bent in *N. procyonoides*.

Discussion

Systematic attribution of the raccoon dog from Jradzor

The morphological and morphometric analyses of the sample of Jradzor reveal a complex pattern of features. The development of the cranial and dentognathic characteristics

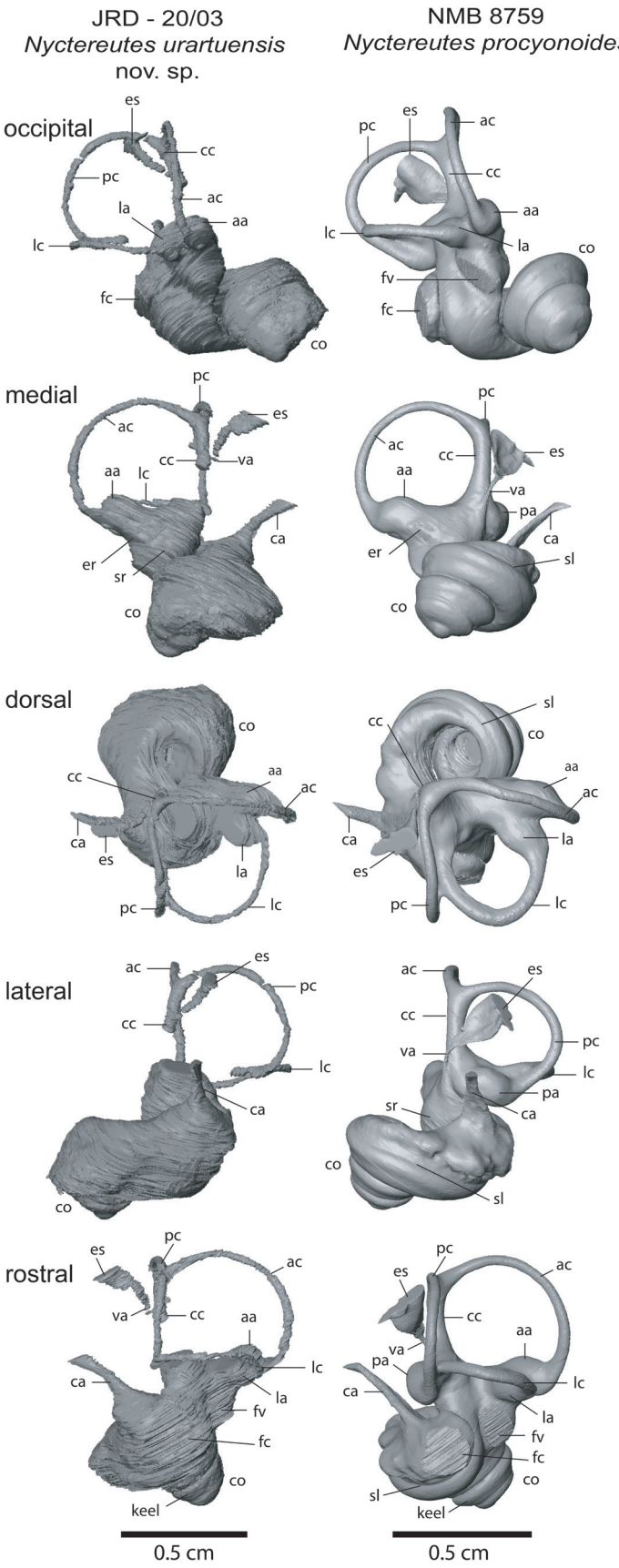

Figure 14. Morphology of the inner ear of *Nyctereutes urartuensis* sp. nov. from Jradzor (JRD–20/03) in comparison to the extant *Nyctereutes procyonoides*. Abbreviations: aa = ac ampulla; ac = anterior semicircular canal; ca = cochlear aqueduct; cc = common crus; co = cochlea; er = elliptical recess; es = endolymphatic sac; fc = fenestra cochleae; fv = fenestra vestibuli; la = lc ampulla; lc = lateral semicircular canal; pa = pc ampulla; pc = posterior semicircular canal; sl = secondary lamina; sr = spherical recess; va = vestibular aqueduct.

shown by the sample from Jradzor is intermediate between primitive raccoon dogs such as *Nyctereutes tingi* and more derived forms, such as *Nyctereutes sinensis*. The presence of a rostrocaudally elongated cranium, large size, poorly developed subangular lobe, but enlarged crushing surface of the first upper molar, with developed cingula and cuspules, combined with a relatively slender occlusal shape of the first and second lower molars, reveals an outstanding combination of features unlike any known species. It is a fact that the cranial morphology and size are close to *N. tingi* (Figs 5–6, 8), and so is the subangular lobe lateral outline, but teeth proportions are different (Fig. 8B, C). This mosaic combination of features contrasts with previously described taxa, but it is shared with *Nyctereutes* recovered from other Eurasian localities, e.g. Çalta-1. We propose that the combination of unusual and mosaic features suggests that the specimens from Jradzor represent a new species which was probably already present in western Asia around 4 Ma (as suggested by the metric and morphological similarities with the specimens from Çalta-1), distinct from both the eastern populations of *N. tingi* and the western one of *N. donnezani*. Ginsburg (1998) referred the specimens from Çalta-1 to *N. donnezani*, and such an attribution was confirmed by Daguenet and Sen (2019). There is compelling evidence that suggests a taxonomic distinction between the specimen from Çalta-1 and those of classic *N. donnezani* from Roussillon Basin and Layna, as already remarked by Bartolini-Lucenti et al. (2018) and Tamvakis et al. (2023). To accommodate the differences, Daguenet and Sen (2019) suggest sexual dimorphism within the populations of *N. donnezani*, although acknowledging that the limited number of specimens hinders a true evaluation of this parameter. Nevertheless, it should be noted that no sexual dimorphism was retrieved in either skull or teeth of the extant *N. procyonoides* or *N. viverrinus* when size or morphology was considered (Kauhala et al. 1998). The morphology-based cladistic analysis in Daguenet and Sen (2019) supported the taxonomic assignment of Çalta-1 as *N. donnezani*. Interestingly, the phylogenetic relationships between fossil *Nyctereutes* spp. were not fully resolved and result in polytomies between most of the fossil species. A better-resolved phylogeny would benefit from a *Nyctereutes*-based data matrix. Daguenet and Sen (2019) used the matrix of Tedford et al. (1995, 2009), which was constructed to understand subfamily-level phylogenetic relationships within Caninae. The use of characters from such pivotal works is no certainty of success for the intrageneric variability, as the characters of Tedford et al. (1995, 2009) do not represent phylogenetically reliable features for *Nyctereutes* species (since they were selected for a wider scope). A profound analysis and discussion on appropriate features to be selected for a specific-level phylogeny of *Nyctereutes* would be necessary, which is, utterly, beyond the scope of this work.

Our results, based on the morphological and morphometric comparison of the fossil raccoon dogs of Eurasia, suggest a stronger affinity of the specimen from Jradzor and that from Çalta-1 than with *N. donnezani* or *N. tingi*. Considering the difference that this taxon possesses, we ascribe the two forms to the new taxon *Nyctereutes urartuensis* sp. nov.

Palaeoneurological variability and phylogeny

The morphological comparison of the analysed samples highlights a clear difference in the development and morphology of the brain in two Caninae tribes. The species of the Canini usually possess a rostrocaudally elongated brain, with a clearly developed *sulcus proreus*. On the contrary, within Vulpini, it is possible to describe two different conditions: some species (e.g. *V. vulpes*) show a rostrocaudally elongated brain, while other species (e.g. *N. procyonoides* and *O. megalotis*) show a more rounded brain (i.e. mediolaterally enlarged) with a width–length of the neocortex ratio close to one. These results are confirmed by all the morphometric analyses we performed, particularly by the geometric morphometric analysis. The latter allowed placing each species in a different portion of the morphospace with just a few overlaps of the morphospaces of different species (Fig. 13). These two different brain morphologies might be linked to different ecologies of the species since the development of different areas of the neocortex is associated with the development of different senses (e.g. Butler and Hodos 2005; Hendelman 2006). A more rounded brain is linked to an expansion of the parietal area of the brain, which corresponds to the *gyri ectosylvius* and *suprasylvius*. It is responsible for primary and higher-order auditory regions (Boch et al. 2024). Thus, a more rounded brain might be linked to a higher auditory capability. This is compatible with the known ecology of the extant species that we took into consideration. Therefore, the most prominent sense in *O. megalotis* for the detection of prey is the hearing sense (Renda and Roux 2017). A high development of hearing has also been noted in *V. chama* and *V. zerda* (Kingdon and Hoffmann 2013). No study is available for *N. procyonoides* on the development of its auditory capabilities. However, it is known that this species is mainly nocturnal (Ward and Wurster-Hill 1990), like all other mentioned species. Thus, it is possible to hypothesise fine auditory capability also in this species, as its brain shape would also support this hypothesis. The cochlea is quite long, with about three turns, as in other canids (Ekdale 2015; Schweizer et al. 2017). A secondary bony lamina, well visible on *N. procyonoides* and usually associated with good ultrasound hearing such as in dogs (Heffner 1983), is not visible, so further considerations are not possible here. On the contrary, the occipital region of the brain in canids is associated with the visual cortex. The development of a *sulcus endomarginalis* in the Canini tribe might be associated with a more developed sight in comparison to the Vulpini species (Boch et al. 2024). In contrast, within the Vulpini, it can be noticed that *V. vulpes* shows a "V-shaped" *sulcus marginalis*, which

might be a case of convergent evolution with the *sulcus endomarginalis* of the Canini tribe. It has to be noted that the *sulcus endomarginalis* seems to be much more variable in our dataset than demonstrated in previous works (e.g. Boch et al. 2024). It is probably visible not only in Canini but also in some Vulpini (e.g. *V. vulpes*). The idea that this *sulcus* is a specific trait present only in the Canini tribe (Lyras and Van Der Geer 2003) might not be entirely correct. This *sulcus* may simply represent a secondary *sulcus* that is sometimes present in species with a highly developed occipital region of the brain. This might imply that the sulcal and gyral morphologies of the *V. vulpes* brain might be linked to a more developed vision capability. The external morphologies and development of different regions of the endocast are then plausibly linked to different ecological adaptations and sensory abilities. The outer morphology of the endocasts can also be used for taxonomic attribution (e.g. Dozo et al. 2023): the differences in the *gyri* and *sulci* of the brain are characteristic of different species. The geometric morphometric analysis (Fig. 13) also seems to distinguish different morphologies of the *gyrus sigmoideus*. So, the species with a heart-shaped outline of this *gyrus* are placed more on the left side of the PCA, while the species with an orthogonal outline are placed on the right side. The *gyrus sigmoideus* morphology in particular is typical in the different species of canids, as already noted in Lyras and Van Der Geer (2003). In particular, the latter paper noted how all the species of the genus *Canis*, *Lycaon* Brookes, 1825 and *Cuon* Hodgson, 1838 show an orthogonal outline of the *gyrus sigmoideus*. In the tribe Vulpini, all the species presented a pentagonal outline of this brain structure, whereas in *N. procyonoides*, it has a heart-shaped one, closely resembling that of *Ce. thous*. In the present study, we noticed some differences compared to previous studies: the species *Lu. mesomelas* (which was previously ascribed to the genus *Canis*) shows a different morphology of the *gyrus sigmoideus* from the other species of the genus *Canis* because it shows a parenthesis-like outline rather than an orthogonal one. It can still be noted, though, that all the *Canis* species present an orthogonal outline of the *gyrus sigmoideus*. The fact that *N. procyonoides* and *Ce. thous* both possess a heart-shaped *gyrus sigmoideus* brought Lyras and Van Der Geer (2003) to a conclusion about a close relationship between these two species, given also the uncertain phylogenetic position of the raccoon dog at the time (Tedford et al. 1995; Wayne et al. 1997). Nevertheless, many recent phylogenies suggest *Nyctereutes* is a Vulpini (Lindblad-Toh et al. 2005; Wayne and Ostrander 2007; Westbury et al. 2017). Moreover, as noticed above, also closely related taxa can present different shapes of the *gyrus sigmoideus* (e.g. *Lu. mesomelas* shows a parenthesis-like outline of the *gyrus*, while the other species of the subtribe Canina have an orthogonal outline of this same *gyrus*), and distantly related species can present the same morphology of this *gyrus* (e.g. *Lu. mesomelas* and fossil specimens of *Nyctereutes*, such as *N. sinensis* from Yushe and the one from Jradzor). The other features of *N. procyonoides* and *Ce. thous* brains do not support a close relationship between these two species and instead support *N. procyonoides* being a Vulpini (e.g. the shallow *sulcus pseudosylvius*, the highly underdeveloped *sulcus* and *gyrus proreus*, as well as the different development and morphology of the *sulci ectosylvius* and *suprasylvius*).

The overall morphology of the analysed fossil specimen is characterised by a highly underdeveloped *gyrus proreus* and by the lack of any *sulcus endomarginalis*, thus confirming the hypothesis that JRD–20/03 belongs to the Vulpini tribe (it is noticeable that even if the *sulcus endomarginalis* is highly variable in the sample that we analysed, all the Canini species possess it; thus, the lack of this *sulcus* is seen only in the tribe Vulpini). On the other hand, the morphology of the *gyrus sigmoideus* of this specimen, usually used for taxonomical purposes, shows a clearly different morphology from the extant species of the genus *Nyctereutes* (i.e. parenthesis-like for the fossil specimen and heart-shaped for *N. procyonoides*). However, the comparison of endocasts of other *Nyctereutes* fossil species suggests a more complex picture. In the past, the genus was highly diversified (Bartolini-Lucenti 2018), and our analysis highlighted the fact that some of the other fossil species belonging to this genus and deeply studied actually show a *gyrus sigmoideus* that is not heart-shaped. It is clear that *N. sinensis* possessed a parenthesis-like outline of the *gyrus sigmoideus*. Thus, it is more plausible to suppose a close relationship between this fossil species of *Nyctereutes*, which probably belonged to a lineage within the genus that shared a common ancestor which developed this kind of morphology of the *gyrus sigmoideus*. It is highly improbable to suppose that within the same genus this morphology has been independently developed three different times. On top of that, also the specimens from Çalta-1 seem to possess this type of morphology for the *gyrus sigmoideus*, thus suggesting that they also belong to this lineage. In particular, their overall morphology and characteristics seem to be compatible with that of *N. urartuensis* sp. nov., thus suggesting that also the Çalta-1 specimens belong to this species. On the other hand, *N. tingi*, *N. megamastoides*, *N.* aff. *donnezani* from Wężе-1 and *N. procyonoides peii* seem to have possessed a heart-shaped outline of this same *gyrus*, so they are more similar to that shown in the extant *N. procyonoides*. Thus, it is likely that this species belonged to another lineage of the genus that gave rise to the extant *N. procyonoides*. Also from the ecological point of view, the specimen from Jradzor probably did not resemble the extant *N. procyonoides*, because the development of the *gyri* and *sulci* of the endocast and its overall development show a closer resemblance with the rostrocaudally elongated endocasts of other Vulpini, in particular because the width–length ratio of the neocortex is lower than that of Vulpini with well-developed hearing. This suggests a well-developed sight in this species, even if no bifurcated *sulcus marginalis* or any *sulcus endomarginalis* has been highlighted.

To sum up, endocast morphology of *N. urartuensis* reveals a parenthesis-shaped *gyrus sigmoideus* and a deep *sulcus pseudosylvius*, the latter being the most developed among fossil *Nyctereutes*. These traits, combined with the absence of a bifurcated *sulcus marginalis*, confirm its placement within Vulpini, while indicating a closer resemblance to Canini in some cortical features. Our comparative analysis also demonstrates that characters such as the cerebellar vermis shape and the presence of *sulcus endomarginalis* are more variable than previously assumed, questioning their taxonomic reliability.

Behavioural and ecological inferences

Barton and Harvey (2000) highlighted how natural selection pressures related to social information processing may act on functionally discrete areas of the brain, including the frontal cortex, resulting in changes in the relative size of the brain regions. The analysis of the relative size of the frontal region of the brain was done by Sakai and Arasznov (2017) for felids and hyaenids. However, canids remain not yet investigated in this aspect. The results obtained in this analysis confirm the hypothesis suggested by Burton and Harvey (2000) that the most social species among all herein considered canids is the grey wolf, which shows the largest frontal region. *Canis lupus* can live in packs of up to 36 individuals, especially in winter (during summer they tend to be more solitary), with a dominant breeding pair (Sillero-Zubiri et al. 2004). The second more developed frontal region is shown instead by the jackal-like canids, which possess a much more variable and flexible social structure: the basic social unit consists of a breeding pair, which sometimes can be accompanied by yearlings and the puppies of its current litter, but can also form some kind of small pack during the harsher season (Sillero-Zubiri et al. 2004). On the other hand, all species of the tribe Vulpini have a less-developed frontal region of the brain. The basic social unit of the fox-like canids is a monogamous couple (Sillero-Zubiri et al. 2004); thus, the social structure in this tribe is much simpler than in Canini. The combined craniodental and palaeoneurological evidence points to a hypocarnivorous canid that might have had enhanced social-cognitive potential relative to extant raccoon dogs. Dentognathic specialisations (expanded crushing basins on M1–M2; streamlined m1 talonid) align with an omnivorous diet requiring efficient grinding, whereas the relative enlargement of the anterior cerebrum (AC) falls within the range of jackal-like Canini, which are capable of flexible social systems and seasonal aggregation (Sillero-Zubiri et al. 2004). Although the development of the rostral part of the cerebrum might not be the strongest character, we suggest some considerations: *N. urartuensis* likely formed stable breeding pairs but might have had the capacity to organise into small seasonal packs, similarly to some jackal-like canids, e.g. *C. aureus* (Moehlman and Hayssen 2018).

The endocast proportions further suggest a comparatively elongated, less medio-laterally inflated neocortex than in highly auditory-specialised Vulpini (e.g. *Otocyon megalotis*, *Vulpes zerda*), consistent with a sensory balance not dominated by extreme auditory adaptations and possibly greater reliance on vision and multimodal cues (Renda and Le Roux 2017; Grewal et al. 2020; Boch et al. 2024). Although the inner ear of *N. urartuensis* is imperfectly preserved, the overall cochlear configuration appears broadly comparable to extant *Nyctereutes*, without clear evidence for the extreme specialisations seen in bat-eared foxes (Ekdale 2013; Schweizer et al. 2017). As always, these behavioural inferences should be regarded as probabilistic and contingent on further sampling, but they provide an ecologically coherent framework that integrates cranial function, endocast anatomy, and comparative ethology.

Conclusion

The present study reports the detailed description of the raccoon dog material recovered from the Late Pliocene site of Jradzor. The area and the timeframe of the locality are of pivotal importance for the evolutionary history of this group of canids. The Pliocene, and particularly the Late Pliocene, was a time of great diversification for the genus *Nyctereutes* across the entire Eurasian continent as well as Africa. Several taxa were described, each with peculiar morphologies and adaptations to a meso- to hypocarnivorous diet, typical of the genus itself. In this framework, the specimens from Jradzor are very crucial considering that the South Caucasus is located at the crossroads between Asia, Europe, and Africa. Superficially, dimensions and morphology of the *Nyctereutes* from Jradzor are similar to the group of primitive species, much like *N. tingi*: large size, rostrocaudally elongated cranium, poor subangular lobe in the mandible, and modest enlargement of the dental molar surface. Nevertheless, teeth proportions and morphology are somewhat aberrant if compared to the Asian taxon and to primitive-like forms. Morphological and morphometric affinities are much greater with *Nyctereutes* sp. from Çalta-1, which used to be considered affine to Western European N. donnezani. Considered as a whole, the pattern of cranial and dentognathic features and proportions of *Nyctereutes* from Jradzor differs from that of the known *Nyctereutes*. Even endocranially, its endocast differs from that of other known taxa and instead closely resembles that of the specimens recovered from Çalta-1, supporting the hypothesis that they belonged to the same species. For this reason, we propose here the erection of a new species, *Nyctereutes urartuensis* sp. nov. The analyses on the endocast morphology of *Nyctereutes urartuensis* sp. nov., together with a deep and thorough revision of canids and especially of fossil raccoon dogs' brain morphology, revealed interesting outcomes:

1. The intrageneric variability within *Nyctereutes*. The heart-shaped outline of the *gyrus sigmoideus* is not constant in the genus but probably arose in some of its lineages; the same can be stated for the morphology of other *gyri*, e.g. the *gyri proreus*, *cruciatus*, *ansatus*, and *pseudosylvius*.
2. Some taxonomic traits common in the endocranial literature (Lyras and Van Der Geer 2003; Lyras 2009; Ivanoff et al. 2014) should be reassessed, e.g. the morphology of the cerebellar vermis does not seem to be a reliable diagnostic trait for distinguishing between the genera *Nyctereutes* and *Canis*, as stated in the literature.
3. Furthermore, the presence of the *sulcus endomarginalis* is not exclusive to the tribe Canini, as it is also found in some Vulpini (e.g. *V. vulpes*). Previous phylogenetic affinities inferred on the basis of single traits (e.g. *gyrus sigmoideus* between *N. procyonoides* and *Ce. thous*) require revision in light of greater intraspecific variability and broader comparative analyses. In this new framework, the specimen from Jradzor presents a unique combination of traits, some of which align it with Vulpini (e.g. for the *sulci marginalis* and *ectosylvius* and development of the *sulcus proreus*), while others have been often associated with Canini (e.g. deep *sulcus pseudosylvius*, parenthesis-like *gyrus sigmoideus* such as *L. mesomelas*, and flat *sulcus cruciatus* such as *C. lupus*). This suggests a complex morphological interrelationship within the canid family that deserves further investigation.

The analysis of the relative development of the frontal area reveals interesting correlations with sociality (Boch et al. 2024). Our results support this interpretation and back up the hypothesis that selective pressures related to social information processing influenced the size of brain regions. Surprisingly, as opposed to extant raccoon dogs, the analysis on *Nyctereutes urartuensis* sp. nov. from Jradzor suggests that its social structure was similar to that of modern jackals, forming reproductive pairs with the ability to aggregate into small seasonal packs. This ethological interpretation is further reinforced and confirmed by other morphometric and ecological analyses.

Acknowledgements

The authors are thankful for the kindness and availability of E. Cioppi and P. Agnelli, curators of the IGF and of the MZUF, respectively; M. Bukhsianidze of the GNM; E. Robert of the "Laboratoire de Géologie", Université Claude-Bernard–Lyon 1; D. Berthet of the Musée des Confluences; J. Galkin and J. Meng, for granting access to the collection of fossil mammals of AMNH; M. Gasparik, curator of the Palaeovertebrate Collection of the HMNH; C. Argot, from the Paleovertebrate collection of the MNHN; and S. Fraile and J. Morales from the MNCN-CSIC of Madrid. This research has been partly supported by the SYNTHESYS Project http://www.synthesys.info/ (Project Numbers ES-TAF-6553 and HU-TAF-6520 to SBL), which is financed by the European Community Research Infrastructure Action under the FP7 "Capacities" Programme. The Spanish Research Project CGL201568333-P (MINECO/FEDER-UE) and the Research Groups CSIC 641538 and CAM-UCM 910607 funded aspects of this research. The authors thank Lilit Sahakyan (IGS deputy director, Yerevan, Armenia) for the scientific, administrative, and logistic support of our studies in Armenia. We would also like to thank Renaud Roch (JURASSICA Museum, Porrentruy, Switzerland), who took part in the excavations at Jradzor and performed the preparation of the studied specimen (JURASSICA Museum, Porrentruy, Switzerland). LC thanks Alicia Rich for her help in segmenting the bony labyrinth of *N. procyonoides*. We are grateful to Georg Schulz and Bert Müller (DBE, BMC, University of Basel) for CT-scanning the skull from Jrazdor as well as extant comparative material. We thank the editor of the manuscript (Olivier Maridet, JURASSICA Museum, POrrentruy, Switzerland) and the reviewers: Manuel Salesa and an anonymous reviewer for their insight and constructive revisions that helped improve the preliminary version of the manuscript. SBL thanks the CERCA Programme/Generalitat de Catalunya (Spain).

Additional information

Conflict of interest

The authors have declared that no competing interests exist.

Ethical statement

No ethical statement was reported.

Use of AI

No use of AI was reported.

Funding

No funding was reported.

Author contributions

SBL, SF, and JMM wrote the main manuscript text; MM, WL, LC, DB, and DV revised and improved the first draft of the text; SBL, SF, DV, and LC prepared the figures; SBL and LC did the CT-scanning; and JMM, LC, and SF prepared the files for analysis. SBL and SF performed the analyses. All authors reviewed and approved the final version of the manuscript.

Author ORCIDs

Saverio Bartolini-Lucenti https://orcid.org/0000-0003-1280-5378
Samuele Frosali https://orcid.org/0009-0004-7117-9332
Joan Madurell-Malapeira https://orcid.org/0000-0003-4639-9451
Loïc Costeur https://orcid.org/0000-0001-6213-8556
Davit Vasilyan https://orcid.org/0000-0001-8712-0678

Data availability

No datasets were generated or analysed during the current study.

References

Adams DC, Collyer M, Kaliontzopoulou A, Sherratt E (2016) geomorph: Software for geometric morphometric analyses. [Available from:] https://rune.une.edu.au/web/handle/1959.11/21330 [February 9, 2025]

Alberdi MT, Cerdeño E, López-Martínez N, Morales J, Soria MD (1997) La fauna villafranquiense de El Rincon-1 Albacete. Estudios Geológicos 53: 69–93. https://doi.org/10.3989/egeol.97531-2248

Alcalá L (1994) Macromamíferos Neógenos de la fosa de Alfambra-Teruel. Instituto de Estudios Turolenses y Museo Nacional de Ciencias Naturales, Teruel, Spain, 554 pp.

Allman J (1990) Evolution of Neocortex. In: Jones EG, Peters A (Eds) Comparative Structure and Evolution of Cerebral Cortex, Part I. Springer US, Boston, MA, 269–283. https://doi.org/10.1007/978-1-4757-9622-3_7

Argant A (2004) The Carnivores of the late Pliocene site of Saint-Vallier (Drome, France). Geobios 37: S133–S182. https://doi.org/10.1016/S0016-6995(04)80013-5

Argant A (2024) Chapter 9 - The Carnivores of Senèze (Haute-Loire). In: Delson E, Faure M, Guérin C (Eds) Senèze: Life in Central France Around Two Million Years Ago: Paleontology, Geochronology, Stratigraphy and Taphonomy. Vertebrate Paleobiology and Paleoanthropology. Springer Nature Switzerland, Cham. https://doi.org/10.1007/978-3-031-64415-3

Bardeleben C, Moore RL, Wayne RK (2005) A molecular phylogeny of the Canidae based on six nuclear loci. Molecular Phylogenetics and Evolution 37: 815–831. https://doi.org/10.1016/j.ympev.2005.07.019

Bartolini-Lucenti S (2017) *Nyctereutes megamastoides* (Canidae, Mammalia) from the early and middle Villafranchian (late Pliocene and early Pleistocene) of the Lower Valdarno (Firenze and Pisa, Tuscany, Italy). Rivista Italiana di Paleontologia e Stratigrafia 123: 211–218.

Bartolini-Lucenti S, Rook L, Morales J (2018) *Nyctereutes* (Mammalia, Carnivora, Canidae) from Layna and the Eurasian raccoon-dogs: An updated revision. Rivista Italiana di Paleontologia e Stratigrafia 124: 597–616. https://doi.org/10.13130/2039-4942/10739

Barton RA, Harvey PH (2000) Mosaic evolution of brain structure in mammals. Nature 405: 1055–1058. https://doi.org/10.1038/35016580

Bates DMA (1937) Palaeontology: The fossil fauna of the Wady el-Mughara caves. In: The Stone Age of Mount Carmel. Excavations at the Wady El-Mughara. Clarendon Press, Oxford, UK, 137–233.

Batsch AJGC (1788) Versuch einer Anleitung zur Kenntniss und Geschichte der Thiere und Mineralien: für akademische Vorlesungen entworfen, und mit den nöthigsten Abbildungen versehen. Academischen Buchhandlung, Jena, Germany, 528 pp. [Available from:] https://ia800609.us.archive.org/32/items/versucheineranle11788bats/versucheineranle11788bats.pdf [April 22, 2024]

Berta A (1988) Quaternary evolution and biogeography of the large South American Canidae (Mammalia, Carnivora). Univ. of California Press, Berkeley, Calif., 149 pp.

Boch M, Karadachka K, Loh KK, Benn RA, Roumazeilles L, Bertelsen MF, Manger PR, Wriggelsworth E, Spiro S, Spocter MA, Johnson PJ, Avelino-de-Souza K, Patzke N, Lamm C, Miller KL, Sallet J, Khrapitchev AA, Tendler BC, Mars RB (2024) Comparative neuroimaging of the carnivoran brain: Neocortical sulcal anatomy, 2024.06.03.597118. https://doi.org/10.1101/2024.06.03.597118

Bowdich ET (1821) An analysis of the natural classifications of Mammalia, for the use of students and travellers. J. Smith, Paris, France, 115 pp.

Broom R, Schepers GWH (1946) 2 The South African Fossil Ape-Men, The Australopithecinae. Transvaal Museum, Pretoria, South Africa.

Butler AB, Hodos W (2005) Comparative Vertebrate Neuroanatomy: Evolution and Adaptation. 1st ed. Wiley. https://doi.org/10.1002/0471733849

Chen L, Zhang H (2012) The complete mitochondrial genome and phylogenetic analysis of *Nyctereutes procyonoides*. Acta Ecologica Sinica 32: 232–239. https://doi.org/10.1016/j.chnaes.2012.07.003

Czeibert K, Nagy G, Csörgő T, Donkó T, Petneházy Ö, Csóka Á, Garamszegi LZ, Kolm N, Kubinyi E (2024) High-resolution computed tomographic (HRCT) image series from 413 canid and 18 felid skulls. Scientific Data 11: 753. https://doi.org/10.1038/s41597-024-03572-x

Czyżewska T (1969) *Nyctereutes sinensis* Schlosser (Canidae, Mammalia) from the Pliocene breccia in Węże, Poland. Acta Zoologica Cracoviensia 14: 441–450.

Czyżewska T (1981) Natural Endocranial Casts of the Canidae from Węże I near Działoszyn (Poland). Acta Zoologica Cracoviensia 25: 251–260.

Daguenet T, Sen S (2019) Phylogenetic relationships of *Nyctereutes* Temminck, 1838 (Canidae, Carnivora, Mammalia) from early Pliocene of Çalta, Turkey. Geodiversitas 41: 663. https://doi.org/10.5252/geodiversitas2019v41a18

Datta R, Lee J, Duda J, Avants BB, Vite CH, Tseng B, Gee JC, Aguirre GD, Aguirre GK (2012) A Digital Atlas of the Dog Brain. Paxinos G (Ed.). PLoS ONE 7: e52140. https://doi.org/10.1371/journal.pone.0052140

De Villalta-Comella JF (1952) Contribución al conocimiento de la fauna de mamíferos fósiles del Plioceno de Villaroya. Boletin del Instituto Geologico y Minero de España 64: 1–204.

Del Campana D (1917) Sulla presenza di (*Canis*) *Cerdocyon megamastoides* Pomel, nel Pliocene del Valdarno inferiore. Rivista Italiana di Paleontologia e Stratigrafia 23: 29–36.

Depéret MC (1890) Les Animaux pliocènes du Roussillon. Mémoires de la Société Géologique de France (Paleontologie) 3: 4–194.

Dermitzakis MD, Van der Geer AE, Lyras G (2004) The phylogenetic position of raccoon dogs: implications of their neuroanatomy. Proceedings of 5th International Symposium on Eastern Mediterranean Geology.

Domingo L, Koch PL, Hernández Fernández M, Fox DL, Domingo MS, Alberdi MT (2013) Late Neogene and Early Quaternary Paleoenvironmental and Paleoclimatic Conditions in Southwestern Europe: Isotopic Analyses on Mammalian Taxa. PLoS ONE 8: e63739. https://doi.org/10.1371/journal.pone.0063739

Dong W, Liu J, Fang Y (2013) The large mammals from Tuozidong (eastern China) and the Early Pleistocene environmental availability for early human settlements. Quaternary International 295: 73–82. https://doi.org/10.1016/j.quaint.2012.01.014

Dong W, Zhang L-M, Liu W-H (2017) New material of the Early Pleistocene mammalian fauna from Chutoulang, Chifeng, eastern Nei Mongol, China and binary faunal similarity analyses. Vertebrata PalAsiatica 7: 257–275.

Dozo MT, Paulina-Carabajal A, Macrini TE, Walsh S [Eds] (2023) Paleoneurology of Amniotes: New Directions in the Study of Fossil Endocasts. Springer International Publishing, Cham. https://doi.org/10.1007/978-3-031-13983-3

Ekdale EG (2013) Comparative Anatomy of the Bony Labyrinth (Inner Ear) of Placental Mammals. Soares D (Ed.). PLoS ONE 8: e66624. https://doi.org/10.1371/journal.pone.0066624

Engelman RK (2022) Occipital condyle width (OCW) is a highly accurate predictor of body mass in therian mammals. BMC Biology 20: 37. https://doi.org/10.1186/s12915-021-01224-9

Fedorov A, Beichel R, Kalpathy-Cramer J, Finet J, Fillion-Robin J-C, Pujol S, Bauer C, Jennings D, Fennessy F, Sonka M, Buatti J, Aylward S, Miller JV, Pieper S, Kikinis R (2012) 3D Slicer as an image computing platform for the Quantitative Imaging Network. Magnetic Resonance Imaging 30: 1323–1341. https://doi.org/10.1016/j.mri.2012.05.001

Ficcarelli G, Torre D, Turner A (1984) First evidence for a species of raccoon dog, *Nyctereutes* Temminck 1838, in South African Plio-Pleistocene deposits. Bollettino della Società Paleontologica Italiana 23: 125–130.

Gabunia LK, Mchedlidze GA (1986) Basic features of the brain evolution in some groups of ancient mammals. Metsniereba, Tbilisi, Georgia.

Gaspard M (1964) La region de l'angle mandibulaire chez les canidae. Mammalia 28: 249–329. https://doi.org/10.1515/mamm.1964.28.2.249

Geraads D (1997) Carnivores Du Pliocene Terminal de Ahl Al Oughlam (Casablanca Maroc). Geobios 30: 127–164. https://doi.org/10.1016/S0016-6995(97)80263-X

Geraads D (2011) A revision of the fossil Canidae (Mammalia) of north-western Africa. Palaeontology 54: 429–446. https://doi.org/10.1111/j.1475-4983.2011.01039.x

Geraads D, Alemseged Z, Bobe R, Reed D (2010) *Nyctereutes lockwoodi*, n. sp., a new canid (Carnivora: Mammalia) from the middle Pliocene of Dikika, Lower Awash, Ethiopia. Journal of Vertebrate Paleontology 30: 981–987. https://doi.org/10.1080/02724631003758326

Ginsburg L (1998) Le gisement de vertébrés pliocenes de Çalta, Ankara, Turquie. 5. Carnivores. Sen S (Ed.). Geodiversitas 20: 379–396.

Gittleman JL (1986) Carnivore brain size, behavioral ecology, and phylogeny. Journal of Mammalogy 67: 23–36. https://doi.org/10.2307/1380998

Gliozzi E, Abbazzi L, Argenti P, Azzaroli A, Caloi L, Barbato LC, Stefano GD, Esu D, Ficcarelli G, Girotti O, Kotsakis T, Masini F, Mazza P, Mezzabotta C, Palombo MR, Petronio C, Rook L, Sala B, Sardella R, Zanalda E, Torre D (1997) Biochronology of selected mammals, molluscs and ostracods from the Middle Pliocene to the Late Pleistocene in Italy. the State of the Art. Rivista Italiana di Paleontologia e Stratigrafia 103: 369–388. https://doi.org/10.13130/2039-4942/5299

Gray J (1834) 2 Illustrations of Indian Zoology, chiefly selected from the collection of Major-General Hardwicke. Volume 2. Treuttel, Wurz, Treuttel Jun. and Richter, and Parbury, Allen and Co. Publishers, London, UK, 216 pp.

Grewal JS, Gloe T, Hegedus J, Bitterman K, Billings BK, Chengetanai S, Bentil S, Wang VX, Ng JC, Tang CY, Geletta S, Wicinski B, Bertelson M, Tendler BC, Mars RB, Aguirre GK, Rusbridge C, Hof PR, Sherwood CC, Manger PR, Spocter MA (2020) Brain gyrification in wild and domestic canids: Has domestication changed the gyrification index in domestic dogs? Journal of Comparative Neurology 528: 3209–3228. https://doi.org/10.1002/cne.24972

Grohé C, Tseng ZJ, Lebrun R, Boistel R, Flynn JJ (2016) Bony labyrinth shape variation in extant Carnivora: a case study of Musteloidea. Journal of Anatomy 228: 366–383. https://doi.org/10.1111/joa.12421

Hecht EE, Smaers JB, Dunn WD, Kent M, Preuss TM, Gutman DA (2019) Significant neuroanatomical variation among domestic dog breeds. Journal of Neuroscience 39: 7748–7758. https://doi.org/10.1523/JNEUROSCI.0303-19.2019

Heffner HE (1983) Hearing in large and small dogs: Absolute thresholds and size of the tympanic membrane. Behavioral Neuroscience 97: 310–318. https://doi.org/10.1037/0735-7044.97.2.310

Hemprich WF, Ehrenberg CG (1833) Symbolae physicae, seu icones et descriptiones corporum naturalium novorum aut minus cognitorum quae ex itineribus per Libyam, Aegyptium, Nubiam, Dongalam, Syriam, Arabiam et Habessiniam. Pars zoologica II. Berolini, Ex Officina Academica, Berlin, 81 pp. [Available from:] https://www.biodiversitylibrary.org/item/189238

Hendelman WJ (2006) Atlas of Functional Neuroanatomy. Second Edition. Taylor & Francis Group, Boca Raton, Florida, USA, 253 pp. https://doi.org/10.1201/9780849330841

Hennig W (1966) Phylogenetic Systematics. Illinois University Press, Chicago, 263 pp.

Holekamp KE, Benson-Amram S (2017) The evolution of intelligence in mammalian carnivores. Interface Focus 7: 20160108. https://doi.org/10.1098/rsfs.2016.0108

Horowitz A (1979) The Quaternary of Israel. The Quaternary of Israel 1979: 257–290. https://doi.org/10.1016/B978-0-12-356170-1.50013-1

Ivanoff DV, Wolsan M, Marciszak A (2014) Brainy stuff of long-gone dogs: A reappraisal of the supposed *Canis* endocranial cast from the Pliocene of Poland. Naturwissenschaften 101: 645–651. https://doi.org/10.1007/s00114-014-1200-4

Jiang H, Liu J, Jiangzuo Q, Ning J (2024) The latest ancestor of extant raccoon-dog from Zhoukoudian, Beijing, China, highlights a complex or convoluted transition on the dietary habits. Historical Biology 36: 2739–2761. https://doi.org/10.1080/08912963.2023.2276147

Jin C, Liu J [Eds] (2009) Paleolithic Site - The Renzidong Cave, Fanchang, Anhui Province. Science Press, Beijing, China.

Kelava I, Lewitus E, Huttner WB (2013) The secondary loss of gyrencephaly as an example of evolutionary phenotypical reversal. Frontiers in Neuroanatomy 7: 16. https://doi.org/10.3389/fnana.2013.00016

Kim SI, Oshida T, Lee H, Min MS, Kimura J (2015) Evolutionary and biogeographical implications of variation in skull morphology of raccoon dogs (*Nyctereutes procyonoides*, Mammalia: Carnivora). Biological Journal of the Linnean Society 116: 856–872. https://doi.org/10.1111/bij.12629

Kim SI, Park SK, Lee H, Oshida T, Kimura J, Kim YJ, Nguyen ST, Sashika M, Min MS (2013) Phylogeography of Korean raccoon dogs: Implications of peripheral isolation of a forest mammal in East Asia. Journal of Zoology 290: 225–235. https://doi.org/10.1111/jzo.12031

Kingdon J, Hoffmann M [Eds] (2013) Volumes I–VI Mammals of Africa. Bloomsbury Publishing Plc, London, UK, 3763 pp.

Koufos GD (1993) Late Pliocene carnivores from western Macedonia (Greece). Paläontologische Zeitschrift 67: 357–376. https://doi.org/10.1007/BF02990288

Koufos GD (1997) The canids *Eucyon* and *Nyctereutes* from the Ruscinian of Macedonia, Greece. Paleontologia i Evolucio 30–31: 39–48.

Koufos GD (2014) The Villafranchian carnivoran guild of Greece: implications for the fauna, biochronology and paleoecology. Integrative Zoology 9: 444–460. https://doi.org/10.1111/1749-4877.12061

Kretzoi M (1945) Bemerkungen über das Raubtiersystem. Annales Historico-Naturales Musei Nationalis Hungarici 38: 59–83.

Kurtén B (1965) The Carnivora of the Palestine Caves. Acta Zoologica Fennica 107: 3–74.

Kurtén B, Crusafont-Pairó M (1977) Villafranchian carnivores (Mammalia) from La Puebla de Valverde (Teruel, Spain). Commentationes Biologicae 85: 1–39.

Lazarev S, Maul LC, Kuiper K, Becker D, Bukhsianidze M, Hovakimyan H, Sahakyan L, Vasilyan D (2023) Pliocene volcanic terrain of the South Caucasus as a missing link in Eurasian palaeobiogeography: Dating and palaeoenvironments of vertebrate assemblages of the Jradzor locality, Armenia. Palaeogeography, Palaeoclimatology, Palaeoecology 625: 111685. https://doi.org/10.1016/j.palaeo.2023.111685

Li Q, Wang X, Qiu Z (2003) Pliocene mammalian fauna of Gaotege in Nei Mongol (Inner Mongolia), China. Vertebrata PalAsiatica 41: 104–114.

Lindblad-Toh K, Wade CM, Mikkelsen TS, Karlsson EK, Jaffe DB, Kamal M, Clamp M, Chang JL, Kulbokas EJ, Zody MC, Mauceli E, Xie X, Breen M, Wayne RK, Ostrander EA, Ponting CP, Galibert F, Smith DR, DeJong PJ, Kirkness E, Alvarez P, Biagi T, Brockman W, Butler J, Chin C-W, Cook A, Cuff J, Daly MJ, DeCaprio D, Gnerre S, Grabherr M, Kellis M, Kleber M, Bardeleben C, Goodstadt L, Heger A, Hitte C, Kim L, Koepfli K-P, Parker HG, Pollinger JP, Searle SMJ, Sutter NB, Thomas R, Webber C, Baldwin J, Abebe A, Abouelleil A, Aftuck L, Ait-Zahra M, Aldredge T, Allen N, An P, Anderson S, Antoine C, Arachchi H, Aslam A, Ayotte L, Bachantsang P, Barry A, Bayul T, Benamara M, Berlin A, Bessette D, Blitshteyn B, Bloom T, Blye J, Boguslavskiy L, Bonnet C, Boukhgalter B, Brown A, Cahill P, Calixte N, Camarata J, Cheshatsang Y, Chu J, Citroen M, Collymore A, Cooke P, Dawoe T, Daza R, Decktor K, DeGray S, Dhargay N, Dooley KKK, Dooley KKK, Dorje P, Dorjee K, Dorris L, Duffey N, Dupes A, Egbiremolen O, Elong R, Falk J, Farina A, Faro S, Ferguson D, Ferreira P, Fisher S, FitzGerald M, Foley K, Foley C, Franke A, Friedrich D, Gage D, Garber M, Gearin G, Giannoukos G, Goode T, Goyette A, Graham J, Grandbois E, Gyaltsen K, Hafez N, Hagopian D, Hagos B, Hall J, Healy C, Hegarty R, Honan T, Horn A, Houde N, Hughes L, Hunnicutt L, Husby M, Jester B, Jones C, Kamat A, Kanga B, Kells C, Khazanovich D, Kieu AC, Kisner P, Kumar M, Lance K, Landers T, Lara M, Lee W, Leger J-P, Lennon N, Leuper L, LeVine S, Liu J, Liu X, Lokyitsang Y, Lokyitsang T, Lui A, Macdonald J, Major J, Marabella R, Maru K, Matthews C, McDonough S, Mehta T, Meldrim J, Melnikov A, Meneus L, Mihalev A, Mihova T, Miller K, Mittelman R, Mlenga V, Mulrain L, Munson G, Navidi A, Naylor J, Nguyen TT, Nguyen N, Nguyen C, Nguyen TT, Nicol R, Norbu N, Norbu C, Novod N, Nyima T, Olandt P, O'Neill B, O'Neill K, Osman S, Oyono L, Patti C, Perrin D, Phunkhang P, Pierre F, Priest M, Rachupka A, Raghuraman S, Rameau R, Ray V, Raymond C, Rege F, Rise C, Rogers J, Rogov P, Sahalie J, Settipalli S, Sharpe T, Shea T, Sheehan M, Sherpa N, Shi J, Shih D, Sloan J, Smith C, Sparrow T, Stalker J, Stange-Thomann N, Stavropoulos S, Stone C, Stone S, Sykes S, Tchuinga P, Tenzing P, Tesfaye S, Thoulutsang D, Thoulutsang Y, Topham K, Topping I, Tsamla T, Vassiliev H, Venkataraman V, Vo A, Wangchuk T, Wangdi T, Weiand M, Wilkinson J, Wilson A, Yadav S, Yang S, Yang X, Young G, Yu Q, Zainoun J, Zembek L, Zimmer A, Lander ES, Clubs B, Bac B, Resource B, Bac T, Biosciences A, Lindblad-Toh K, Wade CM, Mikkelsen TS, Karlsson EK, Jaffe DB, Kamal M, Clamp M, Chang JL, Kulbokas EJ, Zody MC, Mauceli E, Xie X, Breen M, Wayne RK, Ostrander EA, Ponting CP, Galibert F, Smith DR, DeJong PJ, Kirkness E, Alvarez P, Biagi T, Brockman W, Butler J, Chin C-W, Cook A, Cuff J, Daly MJ, DeCaprio D, Gnerre S, Grabherr M, Kellis M, Kleber M, Bardeleben C, Goodstadt L, Heger A, Hitte C, Kim L, Koepfli K-P, Parker HG, Pollinger JP, Searle SMJ, Sutter NB, Thomas R, Webber C, Baldwin J, Abebe A, Abouelleil A, Aftuck L, Ait-Zahra M, Aldredge T, Allen N, An P, Anderson S, Antoine C, Arachchi H, Aslam A, Ayotte L, Bachantsang P, Barry A, Bayul T, Benamara M, Berlin A, Bessette D, Blitshteyn B, Bloom T, Blye J, Boguslavskiy L, Bonnet C, Boukhgalter B, Brown A, Cahill P, Calixte N, Camarata J, Cheshatsang Y, Chu J, Citroen M, Collymore A, Cooke P, Dawoe T, Daza R, Decktor K, DeGray S, Dhargay N, Dooley KKK, Dooley KKK, Dorje P, Dorjee K, Dorris L, Duffey N, Dupes A, Egbiremolen O, Elong R, Falk J, Farina A, Faro S, Ferguson D, Ferreira P, Fisher S, FitzGerald M, Foley K, Foley C, Franke A, Friedrich D, Gage D, Garber M, Gearin G, Giannoukos G, Goode T, Goyette A, Graham J, Grandbois E, Gyaltsen K, Hafez N, Hagopian D, Hagos B, Hall J, Healy C, Hegarty R, Honan T, Horn A, Houde N, Hughes L, Hunnicutt L, Husby M, Jester B, Jones C, Kamat A, Kanga B, Kells C, Khazanovich D, Kieu AC, Kisner P, Kumar M, Lance K, Landers T, Lara M, Lee W, Leger J-P, Lennon N, Leuper L, LeVine S, Liu J, Liu X, Lokyitsang Y, Lokyitsang T, Lui A, Macdonald J, Major J, Marabella R, Maru K, Matthews C, McDonough S, Mehta T, Meldrim J, Melnikov A, Meneus L, Mihalev A, Mihova T, Miller K, Mittelman R, Mlenga V, Mulrain L, Munson G, Navidi A, Naylor J, Nguyen TT, Nguyen N, Nguyen C, Nguyen TT, Nicol R, Norbu N, Norbu C, Novod N, Nyima T, Olandt P, O'Neill B, O'Neill K, Osman S, Oyono L, Patti C, Perrin D, Phunkhang P, Pierre F, Priest M, Rachupka A, Raghuraman S, Rameau R, Ray V, Raymond C, Rege F, Rise C, Rogers J, Rogov P, Sahalie J, Settipalli S, Sharpe T, Shea T, Sheehan M, Sherpa N, Shi J, Shih D, Sloan J, Smith C, Sparrow T, Stalker J, Stange-Thomann N, Stavropoulos S, Stone C, Stone S, Sykes S, Tchuinga P, Tenzing P, Tesfaye S, Thoulutsang D, Thoulutsang Y, Topham K, Topping I, Tsamla T, Vassiliev H, Venkataraman V, Vo A, Wangchuk T, Wangdi T, Weiand M, Wilkinson J, Wilson A, Yadav S, Yang S, Yang X, Young G, Yu Q, Zainoun J, Zembek L, Zimmer A, Lander ES (2005) Genome sequence, comparative analysis and haplotype structure of the domestic dog. Nature 438: 803–819. https://doi.org/10.1038/nature04338

Linnaeus C von (1758) Tomus I Systema Naturae per Regna Tria Naturae secundum Classes, Ordines, Genera, Species, cum Characteribus, Differentiis, Synonymis, Locis. Editio Decima. Laurentii Salvii, Stockholm, Sweden, 823 pp. https://doi.org/10.5962/bhl.title.542

Liu P, Qin H, Li S, Yuan B (2021) Magnetostratigraphic dating of the Danangou and Dongyaozitou mammalian faunas in the Nihewan Basin, North China. Quaternary Science Reviews 257: 106855. https://doi.org/10.1016/j.quascirev.2021.106855

Liu W (2019) *Nyctereutes* from Hongya Yangshuizhan Locality at Nihewan Basin, and the Systematic Revision on the Genus *Nyctereutes*. Unpublished Ph.D. Thesis. Institute of Vertebrate Paleontology and Paleoanthropology, Chinese Academy of Science.

Lyras GA (2009) The evolution of the brain in Canidae (Mammalia: Carnivora). Scripta Geologica 139: 1–39.

Lyras GA, Van Der Geer AAE (2003) External brain anatomy in relation to the phylogeny of Caninae (Carnivora: Canidae). Zoological Journal of the Linnean Society 138: 505–522. https://doi.org/10.1046/j.1096-3642.2003.00067.x

Marciszak A, Kropczyk A, Gornig W, Kot M, Nadachowski A (2023) History of Polish Canidae (Carnivora, Mammalia) and Their Biochronological Implications on the Eurasian Background. Genes 14: 1–27. https://doi.org/10.3390/genes14030539

Martin R (1971) Les affinités de *Nyctereutes megamastoides* (Pomel), Canidae du gisement villafranchien de Saint-Vallier (Drôme, France). Palaeovertebrata 4: 39–58. https://doi.org/10.18563/pv.4.2.39-58

Matsumoto H (1930) Report of the mammalian remains obtained from the sited at Aoshima and Hibiku, Province fo Rikuzen. Science reports of the Tohoku Imperial University. 2nd series, Geology 13: 59–93.

Michaud M, Toussaint SLD, Gilissen E (2022) The impact of environmental factors on the evolution of brain size in carnivorans. Communications Biology 5: 998. https://doi.org/10.1038/s42003-022-03748-4

Moehlman PD, Hayssen V (2018) *Canis aureus*. Mammalian Species 50: 14–25. https://doi.org/10.1093/mspecies/sey002

Monguillon A, Spassov N, Argant A, Kauhala K, Viranta S (2004) *Nyctereutes vulpinus* comb. et stat. nov. (Mammalia, Carnivora, Canidae) from the late Pliocene of Saint-Vallier (Drôme, France). Geobios 37: S183–S188. https://doi.org/10.1016/S0016-6995(04)80014-7

Morales J (2016) 6. Los carnivoros de Villaroya. In: Alberdi MT, Azanza B, Cervantes E (Eds) Villaroya, yacimiento llave de la paleotologia Riojana. Instituto de Estudios Riojanos, Logroño, 119–142.

Müller S (1836) Jahresbericht tiber die Fortschritte der anatomisch-physiologischen Wissenschaften im Jahre 1834. Archiv fur Anatomie und Physiologie 1835: 1–151, 225–243.

Pei W (1934) On the Carnivora from Locality 1 of Choukoutien. Palaeontologia Sinica Series C 8: 1–216.

Penrose F, Kemp GJ, Jeffery N (2016) Scaling and accommodation of jaw adductor muscles in Canidae. The Anatomical Record 299: 951–966. https://doi.org/10.1002/ar.23355

Penrose F, Cox P, Kemp G, Jeffery N (2020) Functional morphology of the jaw adductor muscles in the Canidae. The Anatomical Record 303: 2878–2903. https://doi.org/10.1002/ar.24391

Poe S, Wiens JJ (2000) Character selection and the methodology of morphological phylogenetics. Phylogenetic analysis of morphological data: 20–36.

Pomel A (1842) Nouvelle espèce de Chien fossile dècouverte dans les alluvions volcaniques de l'Auvergne. Bulletin de la Société Géologique de France 14: 38–41.

Qiu Z, Wang X, Li Q (2013) Neogene Faunal Succession and Biochronology of Central Nei Mongol (Inner Mongolia). In: Wang X, Flynn L, Fortelius M (Eds) Fossil Mammals of Asia. Columbia University Press, New York, USA, 155–186. https://doi.org/10.7312/columbia/9780231150125.003.0005

R Core Team (2024) R: A language and environment for statistical computing, Vienna, Austria. [Available from:] https://www.R-project.org/

Radinsky LB (1973) Evolution of the Canid Brain. Brain, Behavior and Evolution 7: 169–202. https://doi.org/10.1159/000124409

Renda S, Roux A le (2017) The sensory ecology of prey detection in the bat-eared fox (*Otocyon megalotis*). https://doi.org/10.1163/1568539X-00003419

Reynolds SC (2012) *Nyctereutes terblanchei*: The raccoon dog that never was. South African Journal of Science 108: 1–10. https://doi.org/10.4102/sajs.v108i1/2.589

Rook L, Bartolini-Lucenti S, Bukhsianidze M, Lordkipanidze D (2017) The Kvabebi Canidae record revisited (late Pliocene, Sighnaghi, eastern Georgia). Journal of Paleontology 91: 1–14. https://doi.org/10.1017/jpa.2017.73

RStudio Team (2024) RStudio: integrated development environment for R. Boston, MA. [Available from:] http://www.rstudio.com/

Sakai ST, Arsznov BM (2017) Carnivoran Brains: Effects of Sociality on Inter- and Intraspecific Comparisons of Regional Brain Volumes. In: Evolution of Nervous Systems. Elsevier, 413–428. https://doi.org/10.1016/B978-0-12-804042-3.00054-3

Savvidou A, Kostopoulos DS (2025) New and revised middle Villafranchian canid material from Dafnero-3 (Greece): Implications to *Nyctereutes* systematics and zoogeography. Palaeoworld: 201011. https://doi.org/10.1016/j.palwor.2025.201011

Schlosser M (1903) Die fossilen Säugethiere Chinas nebst einer Odontographie der recenten Antilopen. Abhandlungen der Bayerischen Akademie der Wissenschaften 22: 1–222.

Schweizer AV, Lebrun R, Wilson LAB, Costeur L, Schmelzle T, Sánchez-Villagra MR (2017) Size Variation under Domestication: Conservatism in the inner ear shape of wolves, dogs and dingoes. Scientific Reports 7: 13330. https://doi.org/10.1038/s41598-017-13523-9

Shikama T (1949) The Kuzuü ossuaries: geological and palaeontological studies of the limestone fissure deposits in Kuzuü, Tochigi Prefecture. Scientific Report of the Tohoku University 23.

Sillero-Zubiri C, Hoffmann M, Macdonald DW (2004) Canids: Foxes, Wolves, Jackals and Dogs Canids: Foxes, Wolves, Jackals and Dogs. Status Survey and Conservation Action Plan, 1–443.

Simões TR, Vernygora O, Paparella I, Jimenez-Huidobro P, Caldwell MW (2017) Mosasauroid phylogeny under multiple phylogenetic methods provides new insights on the evolution of aquatic adaptations in the group. PLoS ONE 12: e0176773. https://doi.org/10.1371/journal.pone.0176773

Soria D, Aguirre E (1976) El cánido de Layna: revisión de los *Nyctereutes* fósiles. Trabajos sobre Neogeno y Cuaternario 5: 83–116.

Sotnikova M (2004) The Middle Pliocene assemblage of Carnivore from Shamar locality (Northern Mongolia). In: The International Conference on the Paleontology of the Central Asia. Paleontological Institute, Moscow, Russia, 54–56.

Sotnikova MV, Baigusheva VS, Titov VV (2002) Carnivores of the Khapry faunal assemblage and their stratigraphic implications. Stratigraphy and Geological Correlation 10: 375–390.

Spassov N (2000) Biochronology and zoogeographic affinities of the Villafranchian faunas of Bulgaria and south Europe. Historia naturalis Bulgarica 12: 89–128.

Storr GCC (1780) Prodromvs methodi mammalivm. Litteris Reissianis, Tvbingæ, Germany, 43 pp.

Tamvakis A, Savvidou A, Spassov N, Youlatos D, Merceron G, Kostopoulos DS (2023) New insights on Early Pleistocene *Nyctereutes* from the Balkans based on material from Dafnero-3 (Greece) and Varshets (Bulgaria). Palaeoworld 32: 555–572. https://doi.org/10.1016/j.palwor.2022.09.006

Tedford RH, Qiu Z (1991) Pliocene *Nyctereutes* (Carnivora: Canidae) from Yushe, Shanxi, with comments on chinese fossil racoon-dogs. Vertebrata PalAsiatica 29: 176–189.

Tedford RH, Taylor BE, Wang Xiaoming (1995) Phylogeny of the Caninae (Carnivora: Canidae): the living taxa. American Museum Novitates 3146: 1–40.

Tedford RH, Wang X, Taylor BE (2009) Phylogenetic Systematics of the North American Fossil Caninae (Carnivora: Canidae). Bulletin of the American Museum of Natural History 2009: 1–218. https://doi.org/10.1206/574.1

Teilhard de Chardin P, Piveteau J (1930) Les mammifères fossiles de Nihowan (Chine). Annales de Paleontologie 19: 1–134.

Temminck C (1838) Over de kennis en de Verbreiding der Zoogdieren van Japan. Tijdschrift Natuurlijke Geschiedeins en Physiologie 5: 273–293.

Torre D (1979) The Ruscinian and the Villafranchian dogs of Europe. Bollettino della Società Paleontologica Italiana 18: 162–165.

Vekua A (1972) Kvabebi Fauna of Akchagylian Vertebrates. Moscow, Russia, 258 pp.

Viret J (1954) Le lœss à bancs durcis de Saint-Vallier (Drôme), et sa faune de mammifères villafranchiens (avec une analyse granulométrique et une analyse pollinique). Nouvelle Archives du Musèum d'Histoide Naturelle de Lyon 4: 1–258. https://doi.org/10.3406/mhnly.1954.986

Wada MY, Imai HT (1991) On the robertsonian polymorphism found in the Japanese raccoon dog (*Nyctereutes procyonoides viverrinus*). Idengaku Zasshi 66: 1–11. https://doi.org/10.1266/jjg.66.1

Wada MY, Lim Y, Wurster-Hill DH (1991) Banded karyotype of a wild-caught male Korean raccoon dog, *Nyctereutes procyonoides koreensis*. Genome 34: 302–306. https://doi.org/10.1139/g91-049

Wang X, Flynn LJ, Fortelius M [Eds] (2013) Fossil Mammals of Asia Fossil Mammals of Asia. Columbia University Press, New York, 759 pp. https://doi.org/10.7312/columbia/9780231150125.001.0001

Ward OG, Wurster-Hill DH (1990) *Nyctereutes procyonoides*. Mammalian Species 358: 1–5. https://doi.org/10.2307/3504213

Ward OG, Wurster-Hill DH, Ratty FJ, Song Y (1987) Comparative cytogenetics of Chinese and Japanese raccoon dogs, *Nyctereutes procyonoides*. Cytogenetics and Cell Genetics 45: 177–186. https://doi.org/10.1159/000132451

Wayne RK, Ostrander EA (2007) Lessons learned from the dog genome. Trends in Genetics 23: 557–567. https://doi.org/10.1016/j.tig.2007.08.013

Wayne RK, Lau LM, Geffen E, Girman DJ, Koepfli KP, Marshall CR (1997) Molecular systematics of the Canidae. Systematic Biology 46: 622–653. https://doi.org/10.1093/sysbio/46.4.622

Werdelin L, Peigné S (2010) Carnivora. In: Werdelin L, Sanders W (Eds) Cenozoic Mammals of Africa. University of California Press, Berkeley, California, USA, 609–633. https://doi.org/10.1525/california/9780520257214.003.0032

Werdelin L, Dehghani R (2011) Carnivora. In: Harrison T (Ed.) Paleontology and Geology of Laetoli: Human Evolution in Context. Volume 2: Fossil Hominins and the Associated Fauna. Vertebrate Paleobiology and Paleoanthropology. Springer International Publishing, New York, 189–232. https://doi.org/10.1007/978-90-481-9962-4

Westbury M, Dalerum F, Norén K, Hofreiter M (2017) Complete mitochondrial genome of a bat-eared fox (*Otocyon megalotis*), along with phylogenetic considerations. Mitochondrial DNA, Part B, Resources 2: 298–299. https://doi.org/10.1080/23802359.2017.1331325

Wickham H, Chang W, Wickham MH (2016) Package 'ggplot2'. Create elegant data visualisations using the grammar of graphics. Version 2: 1–189. https://doi.org/10.1007/978-3-319-24277-4_9

Wiley EO, Siegel-Causey D, Brooks DR, Funk VA (1991) The Compleat Cladist - A Primer of Phylogenetic Procedures. University of Kansas Museum of Natural History Special Publication 19: 1–12. https://doi.org/10.5962/bhl.title.4069

Zhao C, Zhang H, Liu G, Yang X, Zhang J (2016) The complete mitochondrial genome of the Tibetan fox (*Vulpes ferrilata*) and implications for the phylogeny of Canidae. Comptes Rendus - Biologies 339: 68–77. https://doi.org/10.1016/j.crvi.2015.11.005

Zimmermann EAW von (1780) Geographische Geschichte des Menschen und der allgemein verbreiteten vierfüßigen Tiere. Zweiter Band. Weygandschen Buchhandlung, Liepzig. [Available from:] https://cir.nii.ac.jp/crid/1130848327417958144 [January 8, 2024]

Zrzavý J, Duda P, Robovský J, Okřinová I, Pavelková Řičánková V (2018) Phylogeny of the Caninae (Carnivora): Combining morphology, behaviour, genes and fossils. Zoologica Scripta 47: 373–389. https://doi.org/10.1111/zsc.12293

Supplementary material 1

Suppl. tables S1–S5

Authors: Saverio Bartolini-Lucenti
Data type: docx
Explanation note: **table S1.** List of extant species used as comparative material with catalogue numbers. **table S2.** Metadata associated with the specimens downloaded from MorphoSource (https://www.morphosource.org). **table S3.** Loadings of the PCA on cranial variables (see Fig. 7A). **table S4.** Loadings of the PCA on upper variables (see Fig. 7B). **table S5.** Loadings of the PCA on lower variables (see Fig. 7C).

Link: https://doi.org/10.3897/sjp.145.180388.suppl1